NTNU – Trondheim
Norwegian University of
Science and Technology

Impact Loading on Parts made of Injection-moulded PP

John Fredrick Berntsen

Civil and Environmental Engineering
Submission date: July 2015
Supervisor: Arild Holm Clausen, KT
Co-supervisor: David Morin, KT
Yann Claude Ngueveu, Toyota Motors Europe
Ernesto Mottola, Toyota Motors Europe

Norwegian University of Science and Technology
Department of Structural Engineering

Department of Structural Engineering
Faculty of Engineering Science and Technology
NTNU- Norwegian University of Science and Technology

ACCESSIBILITY

OPEN

MASTER THESIS 2015

SUBJECT AREA:	DATE:	NO. OF PAGES:
Polymer engineering	27. jul. 2015	85

TITLE:

Impact loading on parts made of injection-moulded PP

Støtbelastning på sprøytestøpte komponenter av PP

BY:

John Fredrick Berntsen

SUMMARY:
This project is set as a part of the ongoing development of the constitutive model the SIMLab Polymer Model (SPM) developed at SIMLab, NTNU. The goal with this thesis is to explore the capabilities of this model using two validation cases set up in cooperation with Toyota Motor Europe (TME). The validation cases are designed with the purpose to reproducing similar loading conditions and deformations as observed in pedestrian protection tests on full cars.

The experimental part of this thesis was performed with a standard drop tower. The test components are both made of a PP material provided by Toyota. The test specimen for the first validation case is a generic test box with a simple geometry. The test results show generally low test variability. However there are some problems with imperfections on the boxes. The test specimen for the second validation case is a lower absorber provided by TME. The tests results show significant test variability in the first series of tests as the fixtures were not properly handled, the second series of tests show very consistent results.

The majority of the work done during this thesis is in the two numerical studies performed on the box and the lower absorber respectively. The overall results of the box study show that high accuracy is achieved prior to fracture occurring. The box study highlights some key properties of this type of problems. Firstly that it is very sensitive to geometry, and secondly that fracture is in its current state unreliable. Fracture is seen to be very mesh dependent and to require heavy models.

The results of the lower absorber study show good accuracy using the SPM and a significant improvement compared to a standard material model. This improvement is due to how the SPM is able to better capture key physical properties of the ductile polymer like viscoelasticity and pressure sensitivity. The added complexity of the SPM comes at a significant cost in terms CPU. It is also observed that for complex geometries as the lower absorber a solid model may be needed to fully capture all the critical events.

RESPONSIBLE TEACHER: Professor Arild H. Clausen

SUPERVISOR(S): Arild H. Clausen, David Morin, Ernesto Mottola

CARRIED OUT AT: Toyota technical centre, Zaventem, Belgium

MASTER THESIS 2015

John Fredrick Berntsen

Impact loading on parts made of injection-moulded PP

(Støtbelastning på sprøytestøpte komponenter av PP)

As a part of the development of the finite element method, significant effort has been devoted to propose new material models which are able to represent the material behaviour at different conditions. Relevant parameters involve strain level, strain rate, temperature, and the material at hand may also exhibit pressure sensitivity, anisotropy, viscoelasticity etc. The material properties may also be dependent on the production process.

The intention with this master thesis is to explore the capability of a constitutive model developed at SIMLab, Department of Structural Engineering, NTNU. The work is carried out in close cooperation with Toyota Motors Europe, who plans to apply the material model in their ongoing product development. Two validation cases, both involving parts made of injection-moulded polypropylene (PP), are treated in this project. Firstly, the impact on a generic crash box will be investigated experimentally and numerically. Secondly, the candidate shall investigate the response of a lower energy absorber part which is applied in the front in one of Toyota's models. In both cases, the experimental work is carried out in a test rig (drop tower) at SIMLab, while all activities related to the numerical modelling will be performed at Toyota Motors Europe's research centre in Zaventem close to Brussels. The required parameters of the material model will be determined from test results obtained in previous studies.

Possible keywords for activities in this master thesis research work may include:

- Literature: Material models, energy absorption
- Experimental work: Tests on crash box and stiffener. Presentation of test results
- Numerical work: Modelling and simulation of experimental tests
- Validation: Comparison of experimental and numerical results. Evaluation of the model

The candidate may agree with the supervisors to pay particular attention to specific parts of the investigation, or include other aspects than those already mentioned.

The thesis is to be organized as a research report, recognising the guidelines provided by Department of Structural Engineering.

Supervisors at NTNU: David Morin and Arild Holm Clausen
Supervisors at Toyota: Yann Claude Ngueveu and Ernesto Mottola

The report is to be handed in not later than 27 July 2015.

NTNU, 2 January 2015

Arild Holm Clausen

Acknowledgements

There are many people who have been critical for the completion of this project. A special thanks to Professor Arild H. Clausen and researcher Ph.D. David Morin for the continued support throughout the project, especially David for answering the many phone calls and the plethora of e-mails I've sent. I would also like to thank senior engineer Trond Auestad for spending two wonderful weeks at the SIMLab Laboratory with me, and staff engineer Tore Wisth fixing the fixtures. Also thanks to Magnus Landseth and Torodd Berstad for their input to the project.

The majority of the thesis work was done at the Toyota Motors Europe in Brussels. A special thanks to Ph.D. Ernesto Mottola for valuable feedback throughout the whole thesis, and inspiring me to fully explore "the pig" as the box later was known as. Thanks to Yann Claude Ngueveu for all the assistance and the interesting conversations during my stay in Brussels. Also thanks to Vincent, Matsumoto-san, Ozge, Pedro and the rest of the team at TME for making the un-Norwegian amount of hours spent at work pleasant.

Finally thanks to NTNU and TME for giving me this opportunity. Looking forward to continue working with both in the coming four years as a PhD candidate for the new research centre CASA.

Abstract

This project is set as a part of the ongoing development of the constitutive model the SIMLab Polymer Model (SPM) developed at SIMLab, NTNU. The goal with this thesis is to explore the capabilities of this model using two validation cases set up in cooperation with Toyota Motor Europe (TME). The validation cases are designed with the purpose to reproducing similar loading conditions and deformations as observed in pedestrian protection tests on full cars.

The experimental part of this thesis was performed at SIMLab, NTNU with a standard drop tower. The test components are both made of a ductile polypropylene material provided by Toyota. The test specimen for the first validation case is a generic test box with a simple geometry. It was run three test series with different impact locations, the test results show generally low test variability considering the material. However there are some problems with imperfections on the boxes. The test specimen for the second validation case is a lower absorber provided by TME. The tests results show significant test variability in the first series of tests as the fixtures were not properly handled, the second series of tests show very consistent results.

The majority of the work done during this thesis is in the two numerical studies performed on the box and the lower absorber respectively. The numerical study on the box impacts were performed with the purpose of obtaining knowledge of the behaviour of the SPM such that it could be applied to the second numerical study on the lower absorber. There were significant issues with the geometry of the box model leading to several iterations of the geometry. The overall results of the box study show that high accuracy is achieved prior to fracture occurring especially considering the issues with the geometry. The box study highlights some key properties of this type of problems. Firstly that it is very sensitive to geometry, and secondly that fracture is in its current state unreliable. Fracture is seen to be very mesh dependent and to require heavy models.

The numerical study on the lower absorber has the purpose of performing validation on an industry component, and to observe the benefits and costs of going from a standard material model to a research based material model. It is observed during the project that it is possible to obtain accurate results using the SPM, proving that it is a significant improvement in accuracy compared to a standard material model. This improvement is due to how the SPM is able to better capture key physical properties of the ductile polymer like viscoelasticity and pressure sensitivity. The added complexity of the SPM comes at a significant cost in terms CPU, going from MAT81 (LS-Dyna) to the SPM with viscoelasticity is roughly an increase in CPU time by a factor of 50. It is also observed that for complex geometries as the lower absorber a solid model may be needed to fully capture all the critical events.

Sammendrag

Dette prosjektet er en del av en pågående utvikling av den konstitutive material modellen SIMLab Polymer Model (SPM) utviklet av SIMLab, NTNU. Målet med oppgaven er å utforske egenskapene til denne material modellen ved å bruke to validerings tilfeller satt opp i samarbeid med Toyota Motor Europe (TME). Disse validasjonstilfellene er utviklet med hensikt på å reprodusere liknende lastvirkninger og deformasjoner som observert i simuleringer av fotgjenger beskyttelse.

Den eksperimentelle delen av oppgaven var utført på SIMLab ved NTNU med et standard «drop tower». Test komponentene er begge laget av et duktilt polypropylen materiale som er levert av Toyota. Test objektene for den første valideringstilfellet er en generisk test boks med en enkel geometri. Det var kjørt tre test serier med forskjellige treff punkter, testresultatene viser generelt lav varians spesielt med tanke på materialet som er brukt. Det er derimot noen problemer med imperfeksjoner på boksene. Testobjektene for det andre valideringstilfellet er en nedre absorbsjons komponent som er levert av TME. Testresultatene viser stor testvarians i den første serien av tester ettersom innfestningene ikke var ordentlig gjennomført, den andre serien av tester hvor dette ble tatt hånd om viste derimot liten testvariasjon.

Mesteparten av arbeidet utført på oppgaven er utført på de to numeriske studiene av testboksen og den nedre absorbsjonskomponenten. Det numeriske studiet på bokstestene var utført med hensikt å oppnå kunnskap om oppførselen til SPM slik at det senere kan benyttes på studiet av den nedre absorbsjonskomponenten. Det var markante feil med geometrien av boksmodellen, slik at det måtte lages flere iterasjoner av geometrien. Overordnet sett så gir de numeriske modellene av bokstesten høy nøyaktighet inntil brudd inntreffer, spesielt med tanke på problemene med geometrien. Studiet av boksene viser noen av nøkkel egenskapene til denne typen tester. For det første så er denne typen tester svært sensitiv til geometri, og for det andre så er bruddmodellen som er implementert for øyeblikket ikke konsistent. Brudd ser ut til å være svært avhengig av oppløsningen til modellen i tillegg til at det generelt ser ut til å kreves tyngre modeller.

Det numeriske studiet på den nedre absorbsjonskomponenten har som formål å gjennomføre en validering av en industrikomponent, i tillegg til å observe fordelene og kostnadene ved å gå fra en standard material modell til en forskningsbasert materialmodell. Det er observert i løpet av prosjektet at det er mulig å oppnå gode resulteter ved bruk av SPM, som igjen viser en betydelig forbedring i forhold til en standard materialmodell. Denne forbedringen skyldes at SPM klarer å representere nøkkelegenskaper i polymerer som trykksensitivitet og viskoelastisitet. Den økte kompleksiteten i SPM kommer med en høy kostnad i form av CPU tid. Å gå fra MAT81 (LS-Dyna) til SPM med viskoelastisitet medfører en økning i CPU tid med en faktor på rundt 50. Det er også observert at for en kompleks geometri som den nedre absorbsjonskomponenten har så kan det bli behov for en «solid model» for å fange opp alle hendelser.

Table of Contents

1 Introduction

This project is set as a part of the ongoing development of the constitutive model SIMLab Polymer Model (SPM) developed at SIMLab, NTNU. The goal with this thesis is to explore the capabilities of this model using two validation cases set up in cooperation with Toyota Motor Europe (TME). The validation cases are designed with the purpose to reproducing similar loading conditions and deformations as observed in pedestrian protection tests on full cars.

The first validation case is impact on a generic test box with a simple geometry. The second case is impact on a lower absorber (LA) used in the Toyota Yaris currently in production. Both components are made of an injection moulded ductile polypropylene material which has been studied previously in Heine Røstum's master thesis [1]. The laboratory tests have been performed at SIMLab, while the numerical studies have been performed at TME technical centre in Zaventem, Belgium.

This structure of this thesis is to first to briefly cover the basic theoretical background needed to understand the rest of the thesis. The two laboratory sessions used for the experimental part of the project is covered in detail in chapter three. The numerical studies are split into two chapters. The first chapter is spent on the generic test box with the purpose to obtain a better understanding of the behaviour of the SPM, such that the results can be applied to the numerical study of the more complex lower absorber. The chapter spent on the lower absorber is to do a final validation with an industry perspective. The last two chapters will cover the conclusions and the recommendations for further work.

2 Theoretical Background

This chapter will cover the basic material needed to understand the content of this thesis. That means an overview of SIMLab Polymer Model and the properties of that model on a qualitative level. For a detailed mathematical description see the SPM theory manual [1]. For details on the ductile polypropylene material used see Røstum's master thesis [2].

2.1 Overview of SIMLab Polymer Model

The SIMLab Polymer Model is a complicated research based material model with many options. The options used during this thesis and that will be covered in this chapter is:

- Elastic domain
  - Elasticity
  - Viscoelasticity
- Plastic domain
  - Raghava yield criteria
  - Non-associated plastic potential
  - Isotropic hardening
  - Viscoplasticity
- Fracture
  - Damage based fracture
  - Effective stress based fracture

The calibration of the material parameters except for the viscoelastic ones were calibrated in a previous project [3], the viscoelastic parameters are calibrated by Toyota. For more details on the calibration process see Røstum's master thesis [1].

2.2 Elastic Properties

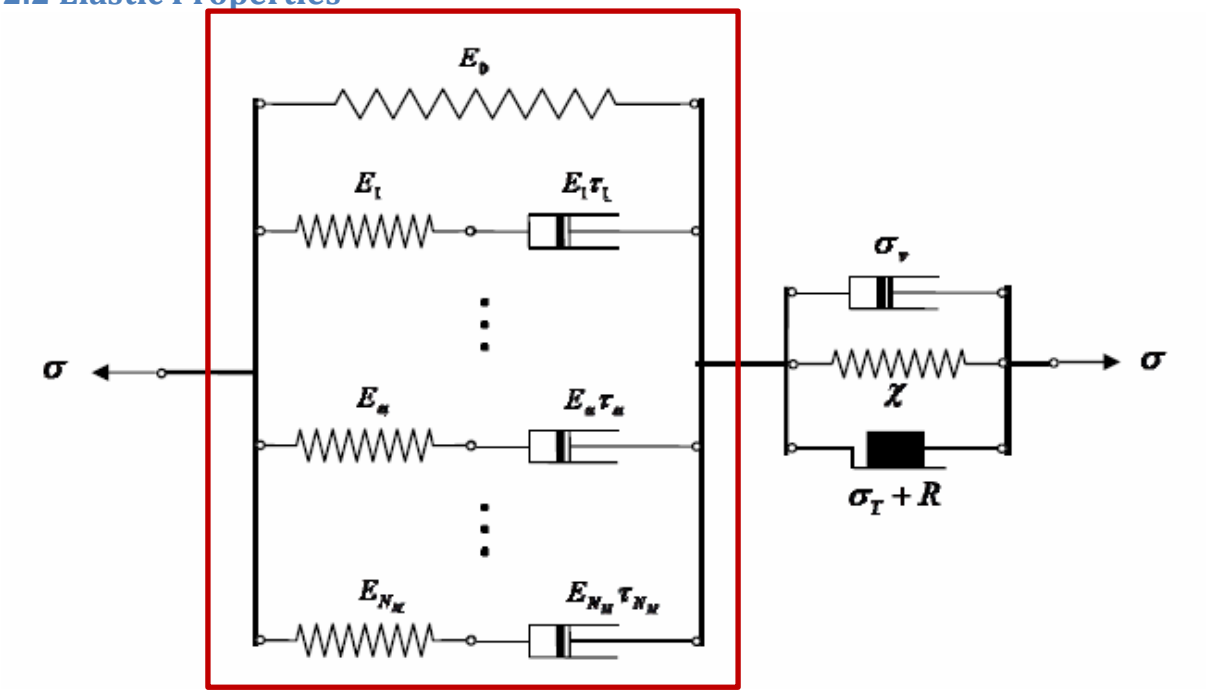

Figure 2-1: Rheological model SPM, focus elastic region [1]

The elastic region is described in the rheological model by a spring and up to 9 Maxwell elements in parallel. The spring describes pure elastic behaviour while the Maxwell elements describe the viscoelastic behaviour.

The viscoelastic behaviour is generated by the dashpots in the Maxwell elements, as the response of them are determined by the strain rate and not the actual strain. The dashpots are also dissipating energy instead of storing it. The reason for having multiple Maxwell elements is to describe rate sensitivity of a large spectre of strain rates.

2.3 Plastic Properties

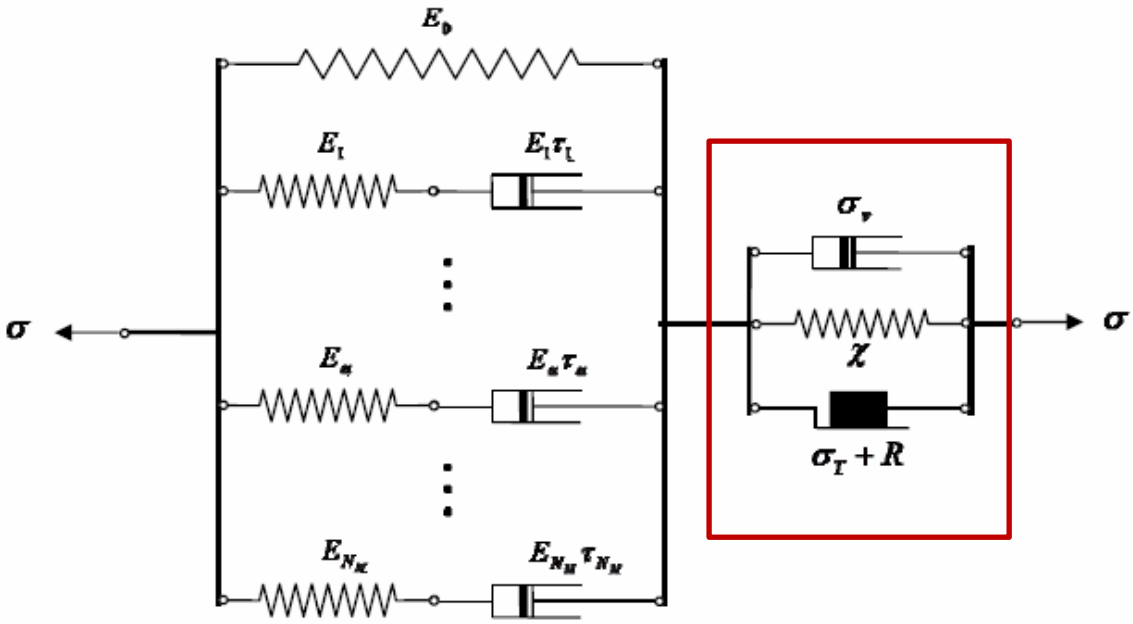

Figure 2-2: Rheological model SPM, focus plastic region [1]

The plastic region is described in the rheological model by a dashpot, a spring and a friction element. The response of the dashpot is determined by the plastic strain rate and it is dissipative and gives the viscoplastic behaviour. The spring is used for a backstress formulation and is not utilized during this thesis. The friction element sets a requirement in terms of a yield function to allow plastic deformation. The friction element also dissipates energy.

The yield function used in the SPM is the Raghava yield function. The Raghava yield function makes yielding dependent on the first stress invariant in addition to the second deviatoric stress invariant, this makes yielding pressure sensitive. As figure 2-3 show, yielding occurs earlier with a positive first stress invariant which represents tension and yielding is delayed in compression.

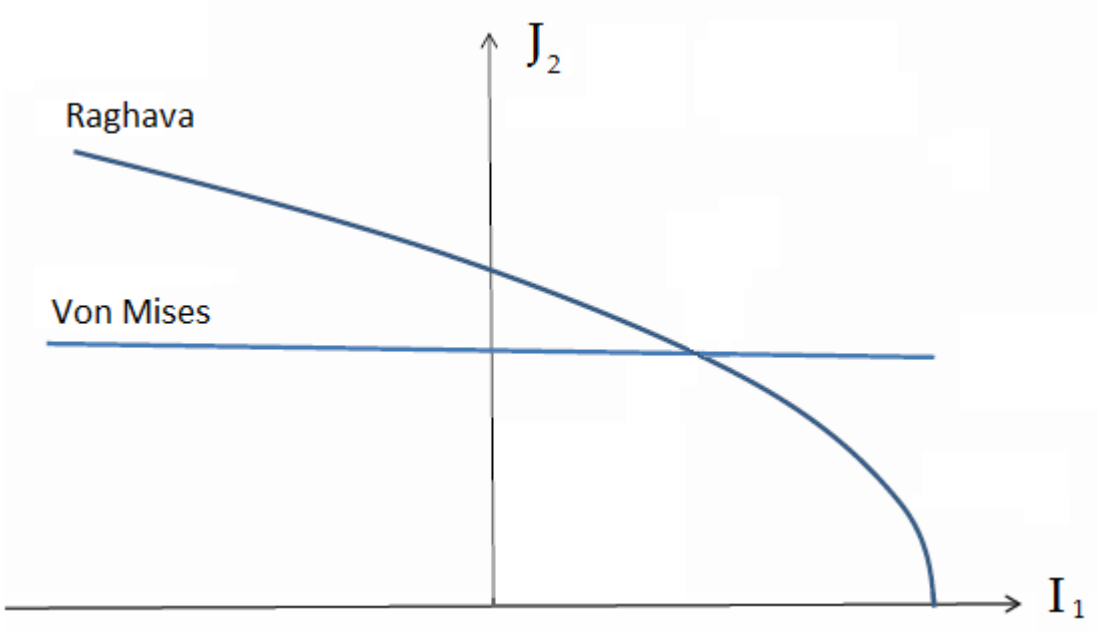

Figure 2-3: Illustration of Raghava yield surface compared to Von Mises yield surface

Another feature of the plastic region in the SPM is a non-associated flow rule. The plastic potential used for this flow rule allows for volumetric strains in the plastic region and to calibrate this volumetric strain separately. As the damage evolution is directly linked to the plastic volumetric strain this allows for proper calibration of the damage evolution in the material.

2.4 Fracture Models

The way fracture is implemented in the SPM currently is that when a fracture parameter reaches a critical value in an integration point that element is deleted. In the SPM it is possible to choose between the fracture parameters damage and effective stress or to initiate fracture when either one of the parameters reaches the critical value.

The damage parameter is described mathematically in equation (1). In the equation σ^{comp} is the compressible stress, and σ^{inc} is the incompressible stress. Initially without any deformations these two stresses will be equal to each other such that the damage is equal to zero. As the voids grow the incompressible stress will increase more than the compressible stress, because the incompressible stress represents the stresses on the effective surface. This leads to ratio between the two becomes smaller and thus increasing the damage.

$$D = 1 - \frac{\sigma^{comp}}{\sigma^{inc}} \tag{1}$$

The effective stress is defined in equation (2) where σ_1 is the first principal stress and D is the damage as defined in equation (1). Using the effective stress as a fracture parameter indirectly introduces rate sensitivity to the fracture model. This is because increased strain rate leads to increased stresses and thus increasing σ_1 leading to a higher effective stress and earlier fracture.

$$\sigma^{eff} = \frac{\sigma_1}{1 - D} \tag{2}$$

3 Laboratory Tests

3.1 Tests on Simple Geometry: Box

3.1.1 Background for Tests

The background for the box tests is an interest from Toyota Motor Europe (TME) point of view to see the performance and behaviour of SIMLab Polymer Model (SPM) for loading conditions where their current material model (MAT81 in LS-Dyna) has poor performance. These loading conditions are results of simulations performed for pedestrian protection, meaning that the tests would have to be fully dynamic impact tests.

The Nutini Box was chosen as a test specimen as it has been used for similar purpose before in addition to being easily available. In addition the geometry of the Nutini Box is considered simple compared to a typical component from the industry like the lower absorber. There were also performed an initial analysis by Yann Claude Ngueveu (TME) to determine the impact locations and impact velocities needed to achieve the conditions of interest. The tests are performed with a standard drop tower built by Instron as it was easily available in addition to being able to provide the intended velocities and mass.

3.1.2 Test Setup

3.1.2.1 Overview

Below is an overview of the test setup.

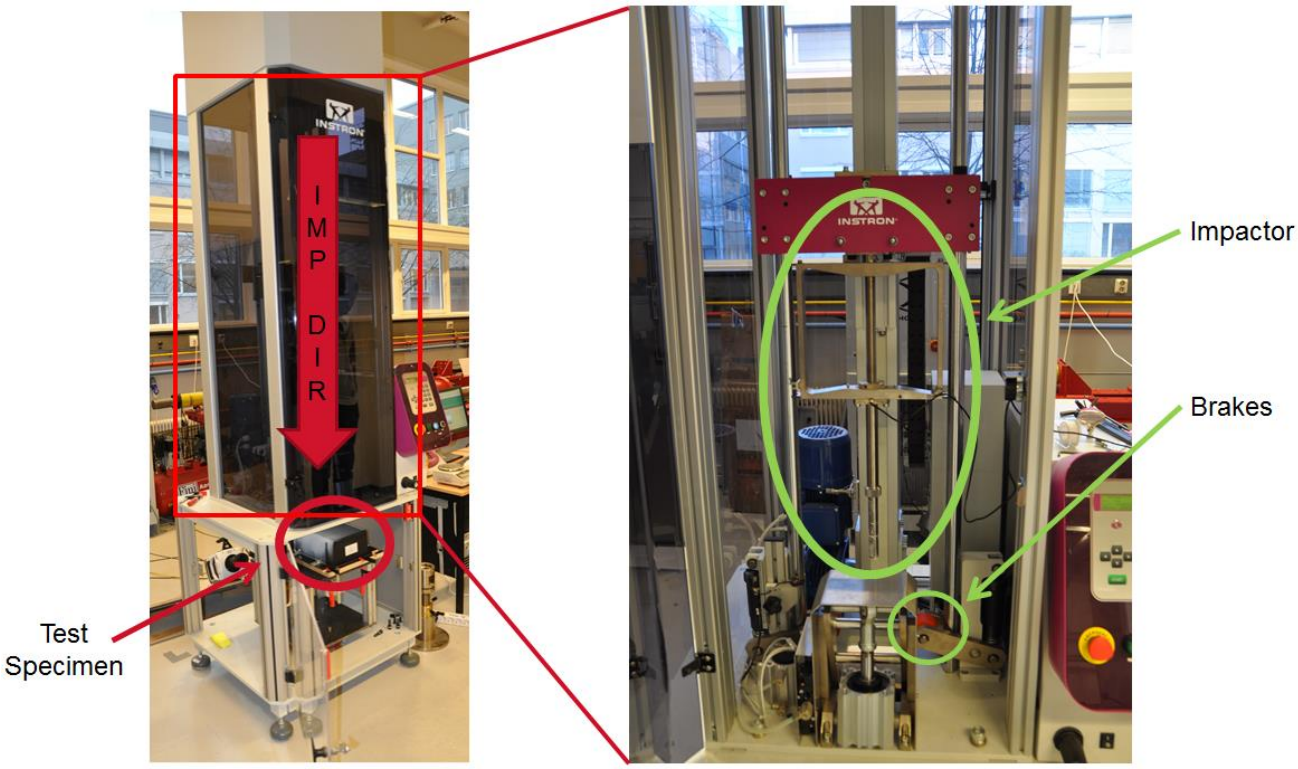

Figure 3-1: Overview of box test setup

The test machine is a standard drop tower made by Instron. The test machine features a spring system in the top enabling a range of impact velocities. One important feature to notice with this machine is that the brakes which limits the displacement of the impactor and invalidates the force output upon initial contact. This will be covered in more detail in section 3.1.3.1.

Data collected from the tests is a force measured in the load cell on the impactor which is used to integrate up velocity and displacement given a mass of the impactor. The load cell sample the force at a rate of 500 000 Hz. The tests are also filmed from two angles with high speed cameras (Phantom v1610) with a framerate of 20 000 Hz.

3.1.2.2 Test Specimen

Below is a picture of a model of the Nutini box with key features marked:

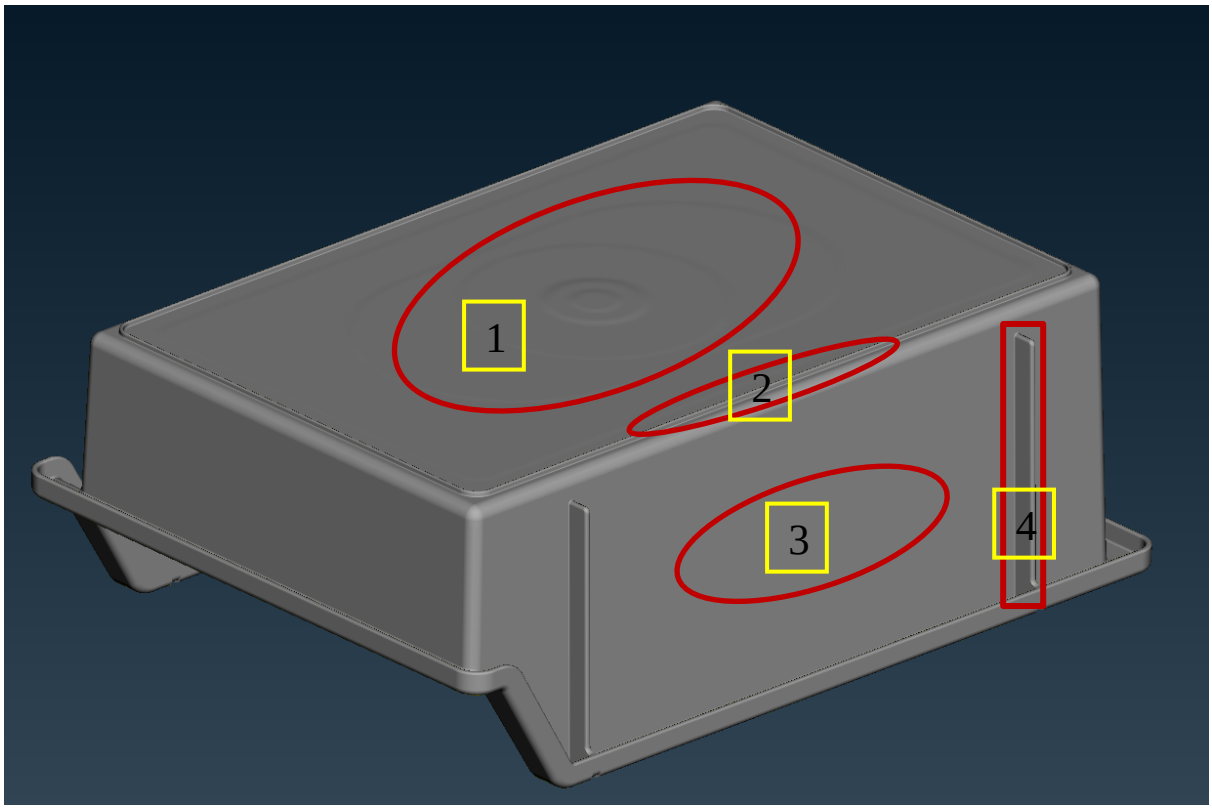

Figure 3-2: Test specimen

Feature number	Feature name
1	Impact surface
2	Impact surface rib
3	Sidewall
4	Sidewall rib

Table 3-1: Box feature names

The test specimen is a standard Nutini box made out of an injection moulded ductile polypropylene material provided by TME. It is worth noting that the sidewalls are at a slight angle, and that there is a thickness variation. The thickness varies from 2.6mm at the injection point in the centre of the impact surface to 1.8mm close to the impact surface ribs and the sidewalls have a thickness of roughly 2.4mm with a slight variation as well. The sidewall ribs are 2.6mm thick.

There are some key imperfections on this test box. Most notably is the imperfection at the injection point as seen in figure 3-3. The surface details of this imperfection vary from significantly from test specimen to test specimen and is one likely reason to the variability in fracture timing for the centre impact.

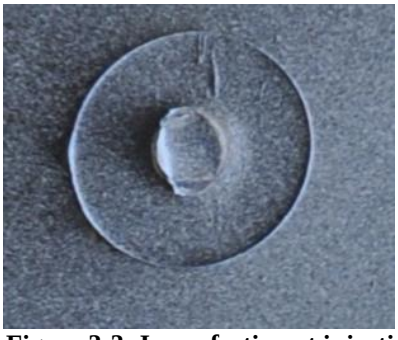

Figure 3-3: Imperfection at injection point

Another imperfection worth noting is damage done to the test specimens during transport. Especially the second batch of test specimens was deformed during transportation as seen in figure 3-4. As seen in the figure, one of the sidewalls is significantly bent in towards the centre in addition to not being completely straight.

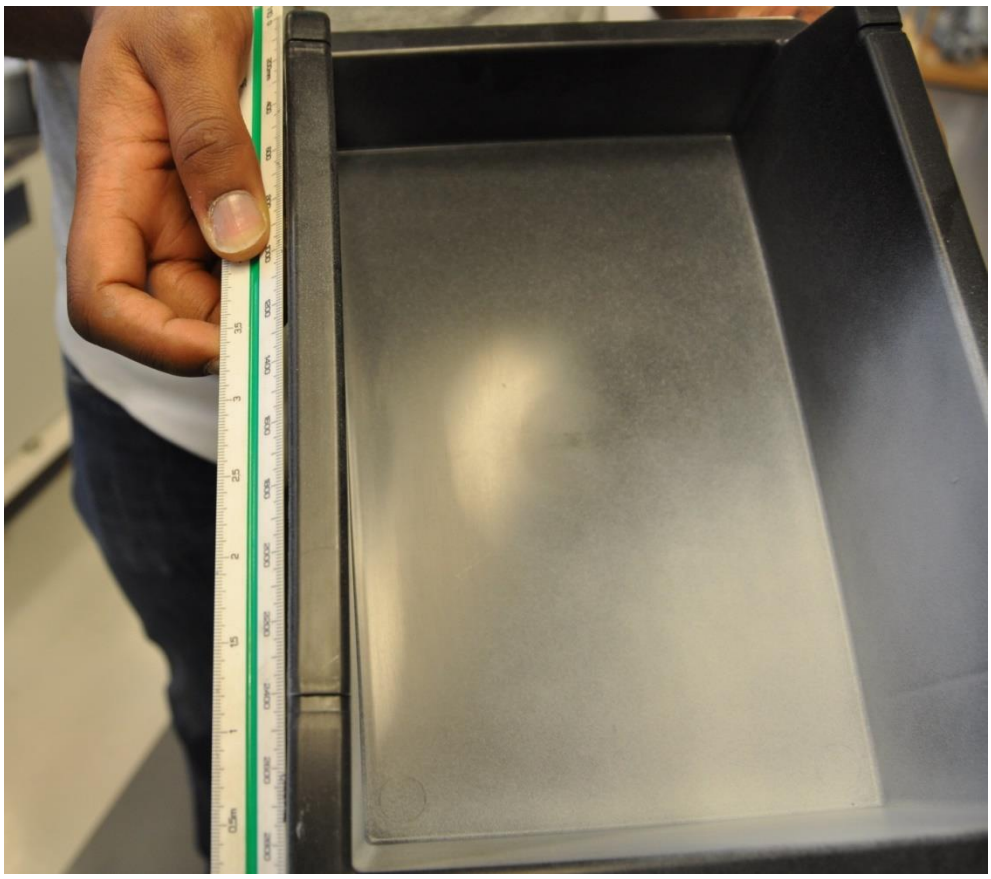

Figure 3-4: Imperfection due to damage during transport.

Impact Locations

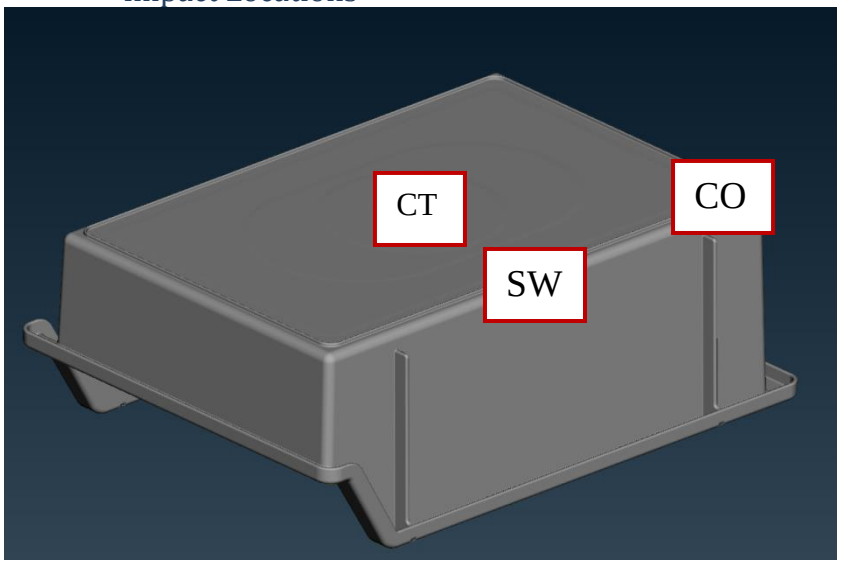

SW	Sidewall Impact
CT	Centre Impact
CO	Corner Impact

Figure 3-5: Impact locations

3.1.2.3 Impactor

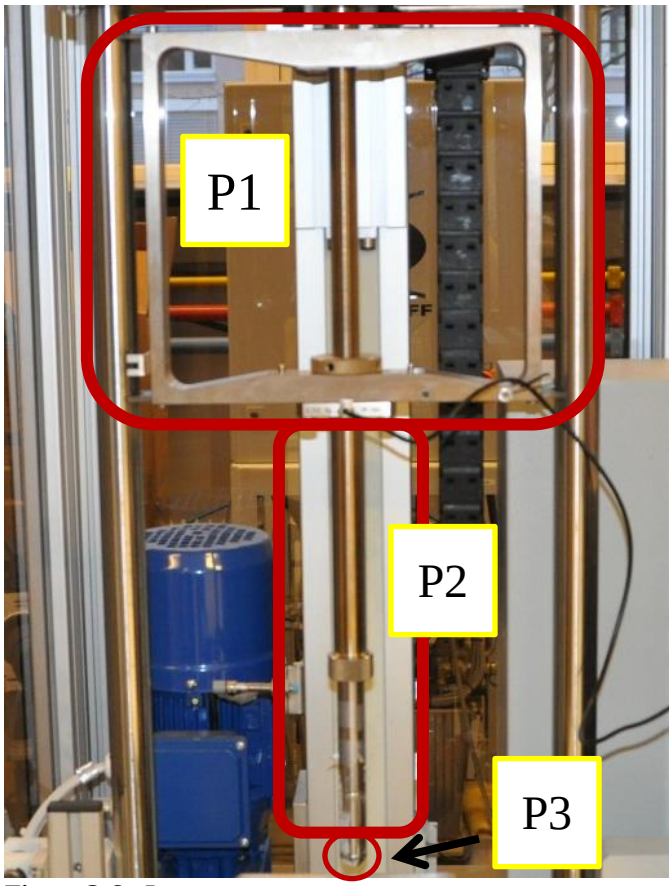

Figure 3-6: Impactor

The impactor can be separated into 3 parts. The upper part marked as p1 in figure 3-6, the impactor rod marked as p2 and the impactor nose marked as p3.

The upper part is a simple steel frame and the only part that is supported by the two large rails on each side of the impactor. There is no initial contact between the guides and the rails, but any movement in the horizontal plane will initiate contact. Meaning the only resistance against out of plane movement is a soft connection on the upper part of the impactor.

The impactor rod is sufficiently long to bend under the forces observed during these tests, this is both a source of error and noise which will be studied more in detail later chapters.

The impactor nose is an interchangeable piece at the end of the impactor rod. For the box impacts a spherical nose with a diameter of 20mm is used leaving the total weight of the impactor at 5.8kg.

3.1.2.4 Fixture

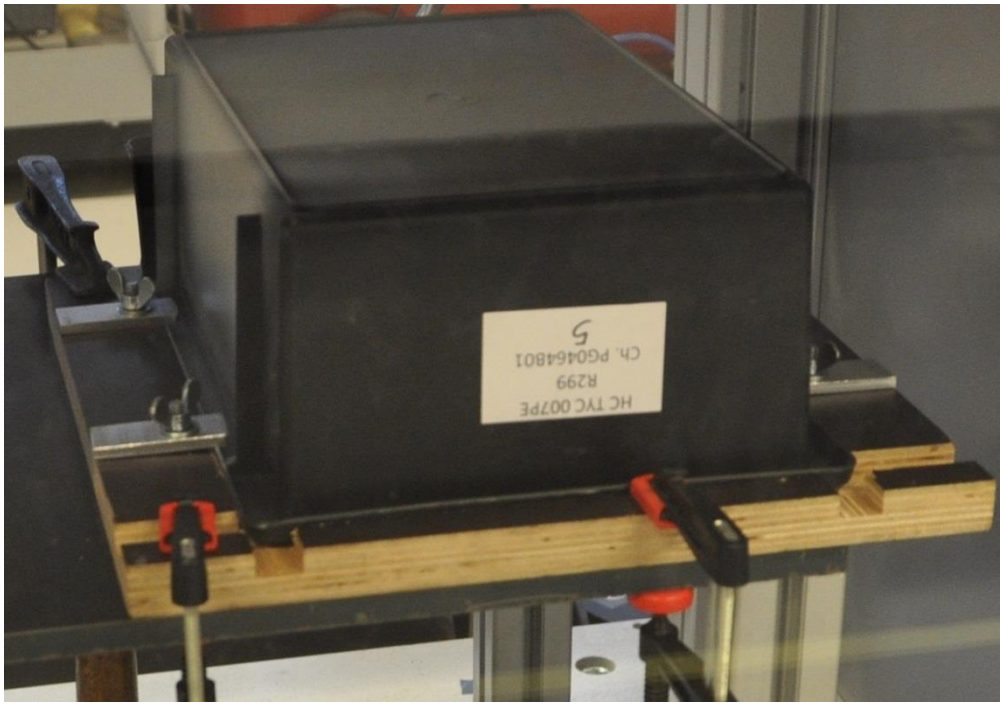

Figure 3-7: Fixtures for box tests.

The box itself is fixed to a wooden plate which has a hole in the centre cut out to give access to the bottom camera, and tracks cut out for the flanges of the box. In addition to a tight fit in the tracks, there are 4 small steel plates that lock the box in place for every run. The wooden plate itself is fastened to a rigid steel frame connected to the whole drop tower machine. During the tests it is seen that the fixtures themselves have no noticeable displacement.

3.1.2.5 Impact Setups

Full Test Matrix

Impact Location	Test Name	Impact Velocity [m/s]
SW	SW1	12.95
	~~SW2~~	~~12.05~~
	SW3	13.05
	SW4	12.92
	SW5	13.02
	SW6	12.90
CT	~~CT1~~	~~12.96~~
	CT2	9.97
	CT3	9.99
	CT4	9.97
	CT5	9.94
	CT6	9.97
	CT7	9.99
CO	CO1	9.93
	CO2	10.01
	CO3	10.03
	CO4	10.02
	CO5	10.00

Table 3-2: Full test matrix for box impacts

The goal was to run 5 repetitions of each impact location. There are two tests that have the wrong impact velocity for the corresponding impact location (SW2 and CT1). There was run one additional test in for the CT impact location as there was a large variability in terms of fracture.

Sidewall Impact

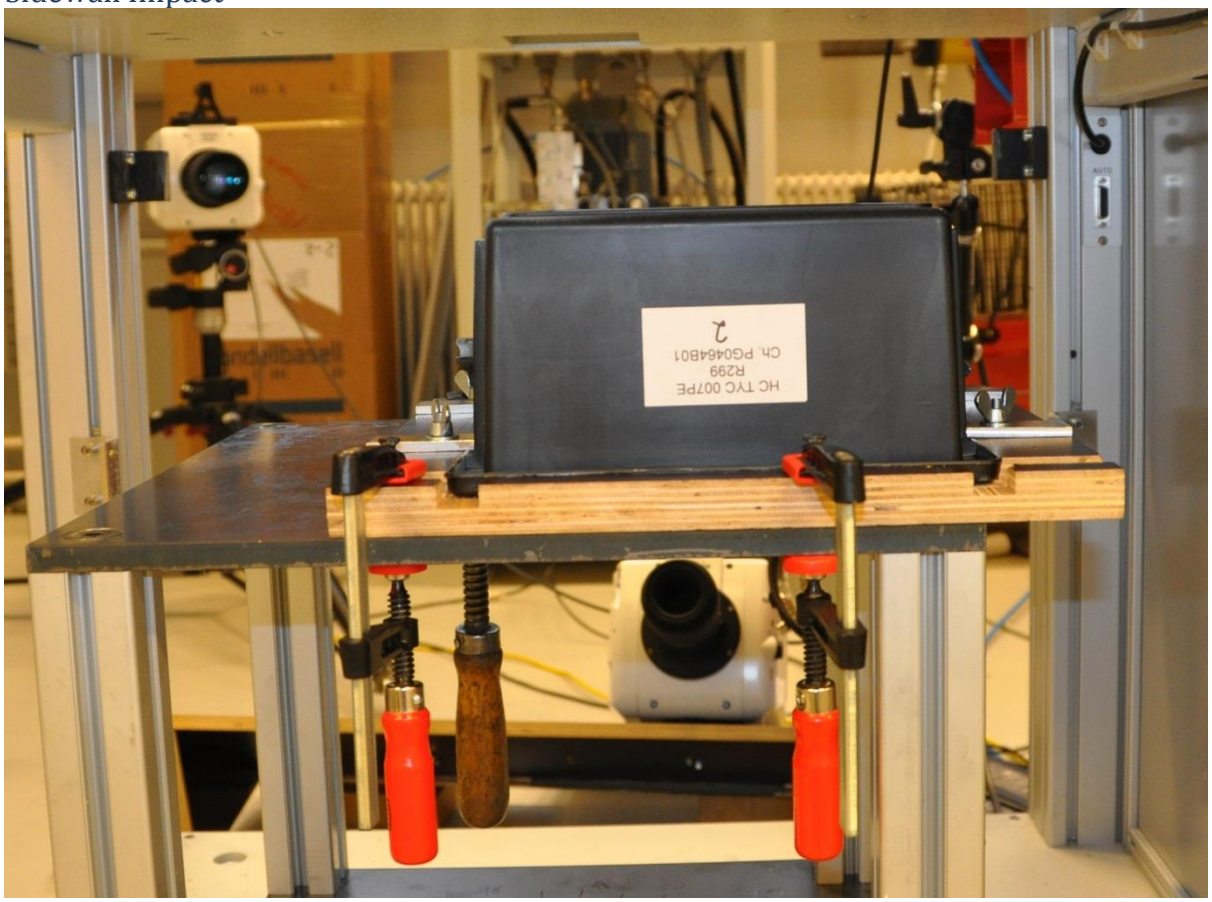

Figure 3-8: Test configuration: SW

Figure 3-9: Camera views: SW

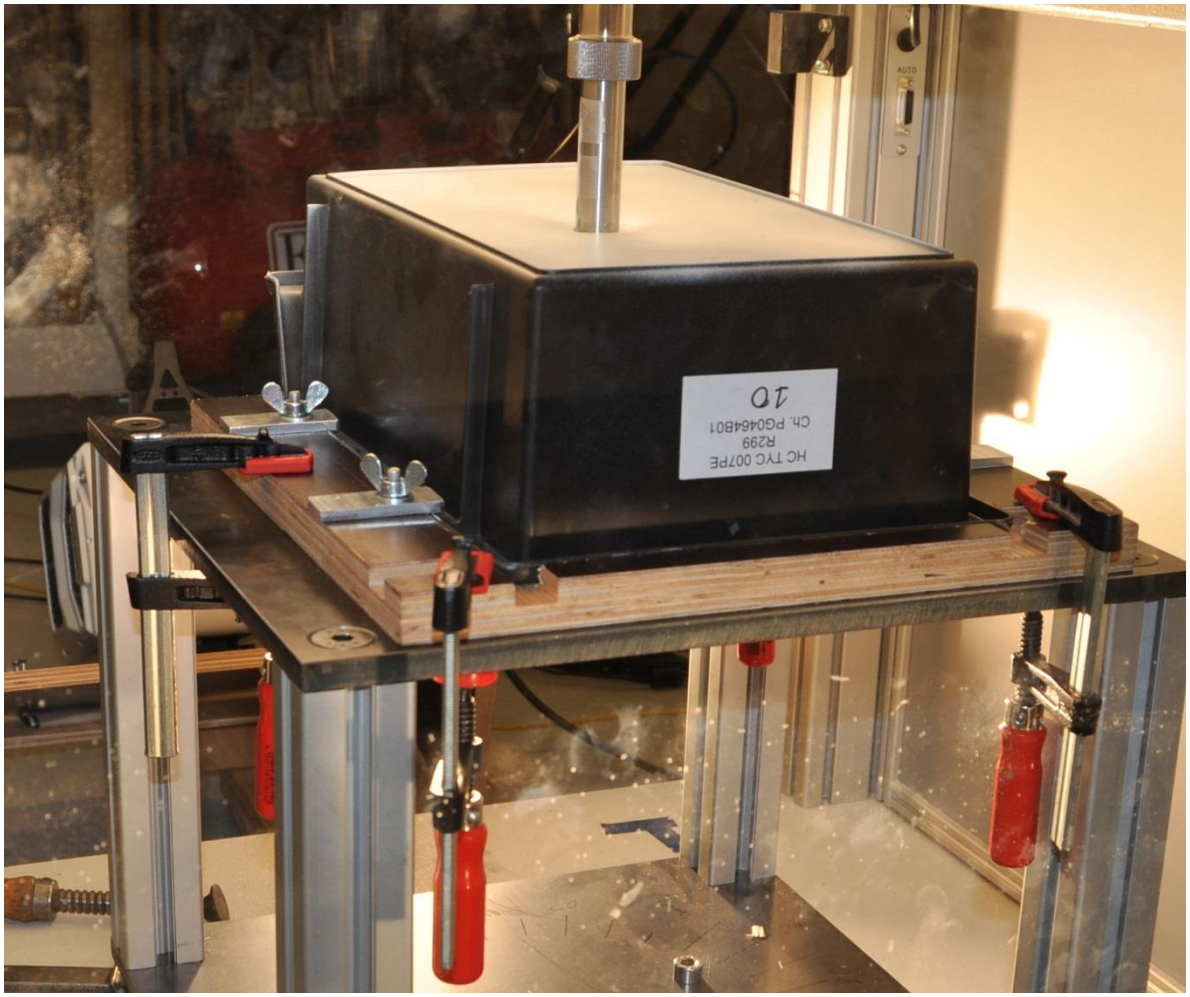

Figure 3-10: Test configuration: CT

Figure 3-11: Camera views: CT

Corner Impact

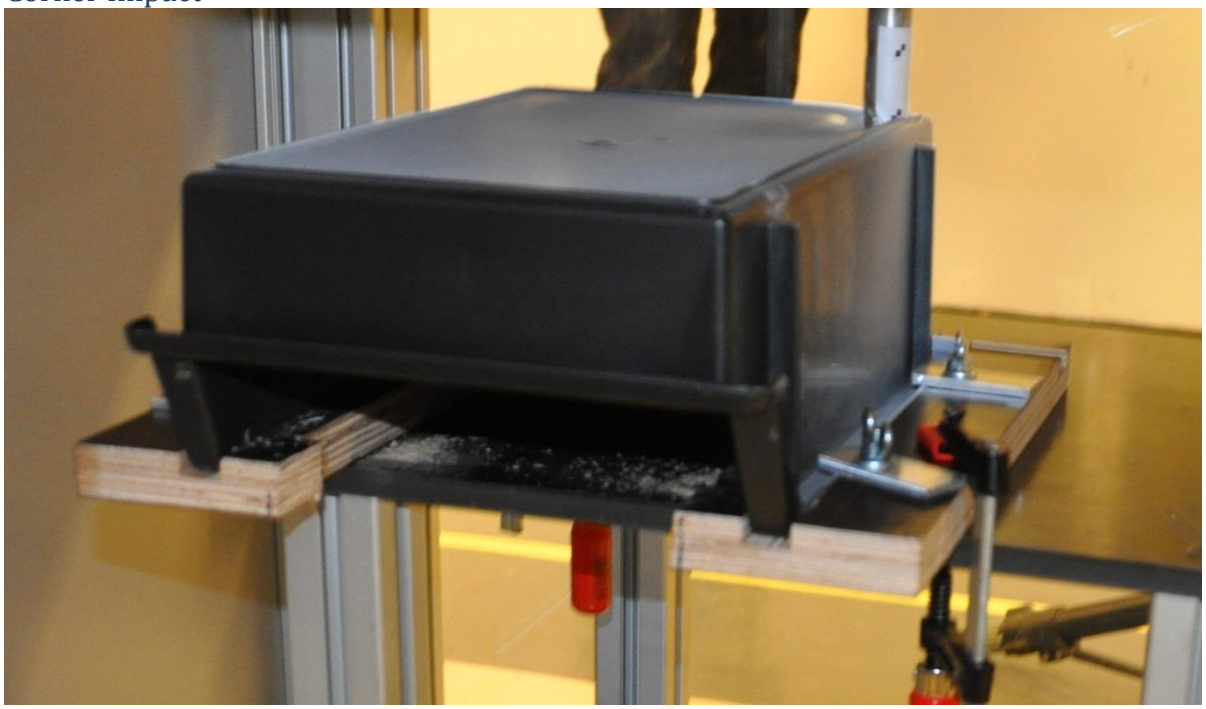

Figure 3-12: Test configuration: CO

Figure 3-13: Camera views: CO

3.1.3 Results

3.1.3.1 Sidewall Impact

Response Curves

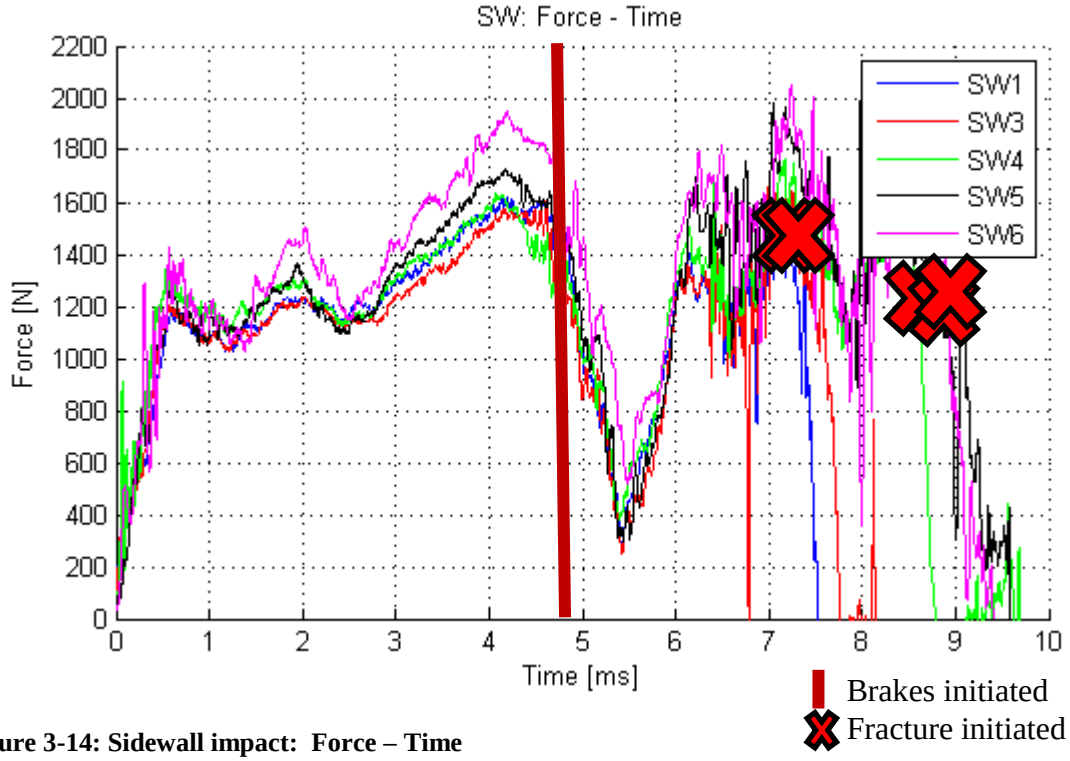

Figure 3-14: Sidewall impact: Force – Time

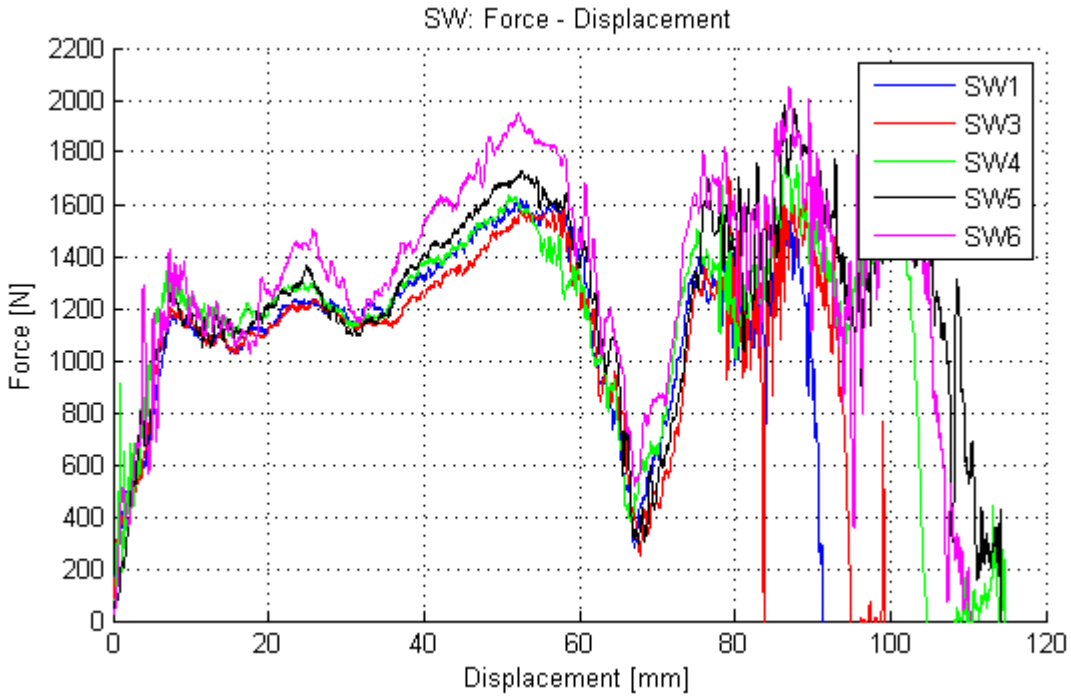

Figure 3-15: Sidewall impact: Force – Displacement

Comments

The key event to highlight for all the box impacts are the brakes initiated at around 60mm displacement. The brakes make contact with the upper part of the impactor such that the load cell in the lower part of the impactor registers a significantly reduced force. This makes all data past that point worthless without detailed knowledge of the brakes which is unavailable.

The tests display some variance, which is likely to be caused by the imperfection seen in figure 3-4. During the test series the fixture was in a fixed location, so that the mentioned imperfection could influence the impact location. The numerical study for the sidewall impact clearly shows that it is very sensitive to impact location further suggesting that the imperfection this imperfection is the cause of the variance. Considering the material being used to variance is not unreasonable however, see Røstum's master thesis [1] for further information on material.

Another observation is that the response of the box is not large enough to significantly slow the impactor such that the FT and FD curves are more or less similar for the box tests. The rest of the box study will be based on only FD curves.

3.1.3.2 Centre Impact

Response Curve

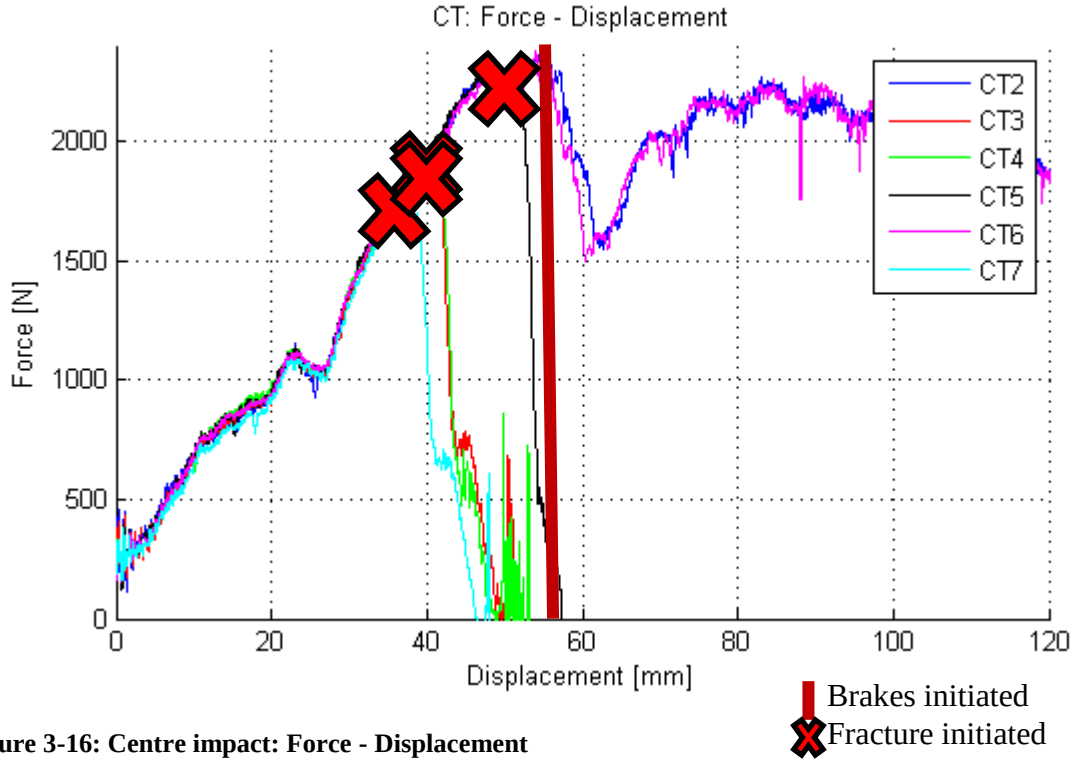

Figure 3-16: Centre impact: Force - Displacement

Comments

Key observations here are that the variation is significantly less than for the sidewall impact. One reason to that is that the box carries the load in a significantly different way for centre impact than sidewall impact making it much less sensitive to impact location. There is a very large spread in terms of fracture initiation with 2 out of 6 tests without fracture, this is very likely due to the imperfection in the centre at the point of injection as shown in figure 3-3.

3.1.3.3 Corner Impact

Response Curve

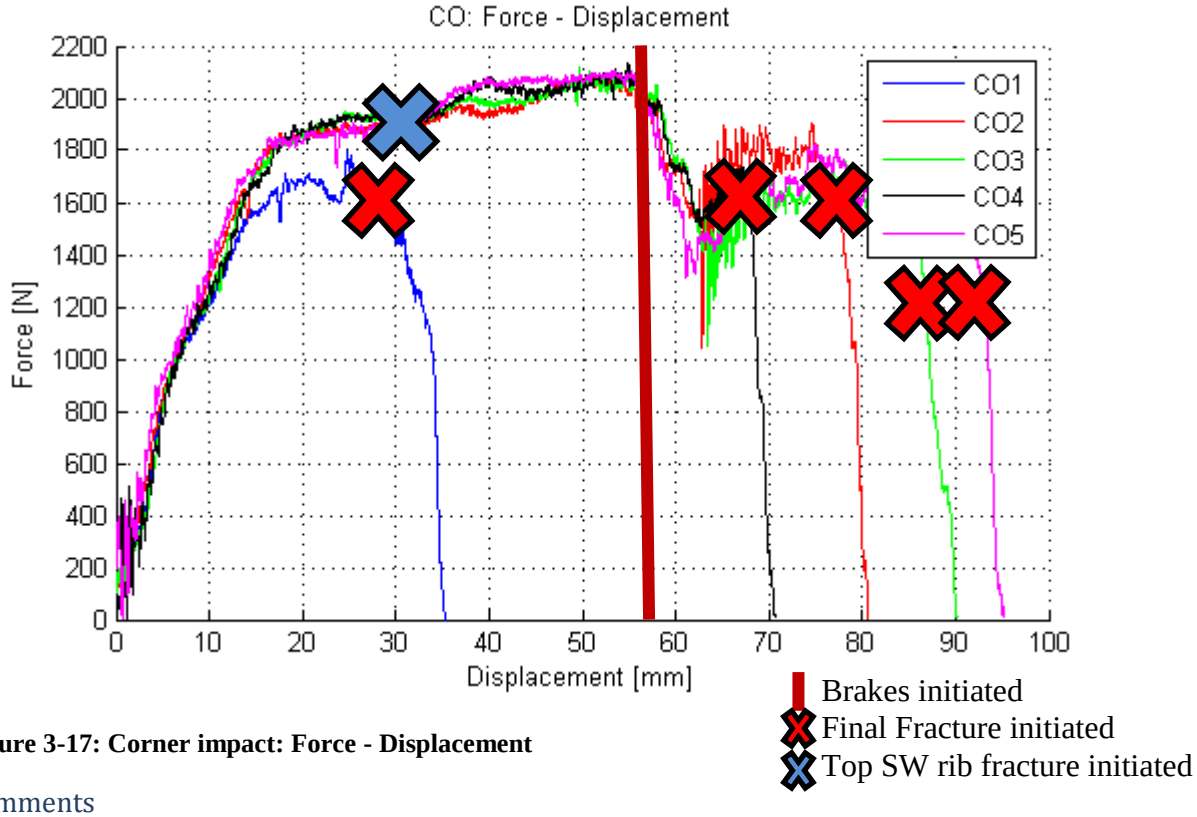

Figure 3-17: Corner impact: Force - Displacement

Comments

Corner impact is in general very consistent, except for CO1. There are two likely causes of this very different behaviour between CO1 and the rest. Most notably is the difference in impact location which means the contact between the impactor and the impact surface rib is different. This can be seen in figure 3-18, CO1 barely has any contact with the rib making it carry the load different manner from the rest and thus more critical in terms of local fracture. There is also a small defect on the inside of the box right beneath the corner impact location which could also influence the initiation of fracture.

Figure 3-18: CO1 on the left with a different impact location and fracture compared to CO2 on the right.

3.2 Tests on Complex Geometry: Lower Absorber

3.2.1 Background for Tests

The background for the lower absorber tests is to perform tests on an industry component with the complexity it brings. The lower absorber used for the tests is a previous model of a lower absorber in a Toyota Yaris. Performing the tests will gather data to do correlation and evaluation on the performance and behaviour of SIMLab Polymer model in an industrial environment.

A preliminary analysis was performed on a simplified model before the tests were run. This preliminary analysis was used to ensure a test setup that gave a comparable deformation pattern and strain rate as observed in a pedestrian protection simulation. A full set of fixtures, impact velocities, impactor shape and mass was decided based on these analyses. In addition out of plane displacement was discovered as a concern for the tests.

3.2.2 Test Setup

3.2.2.1 Overview

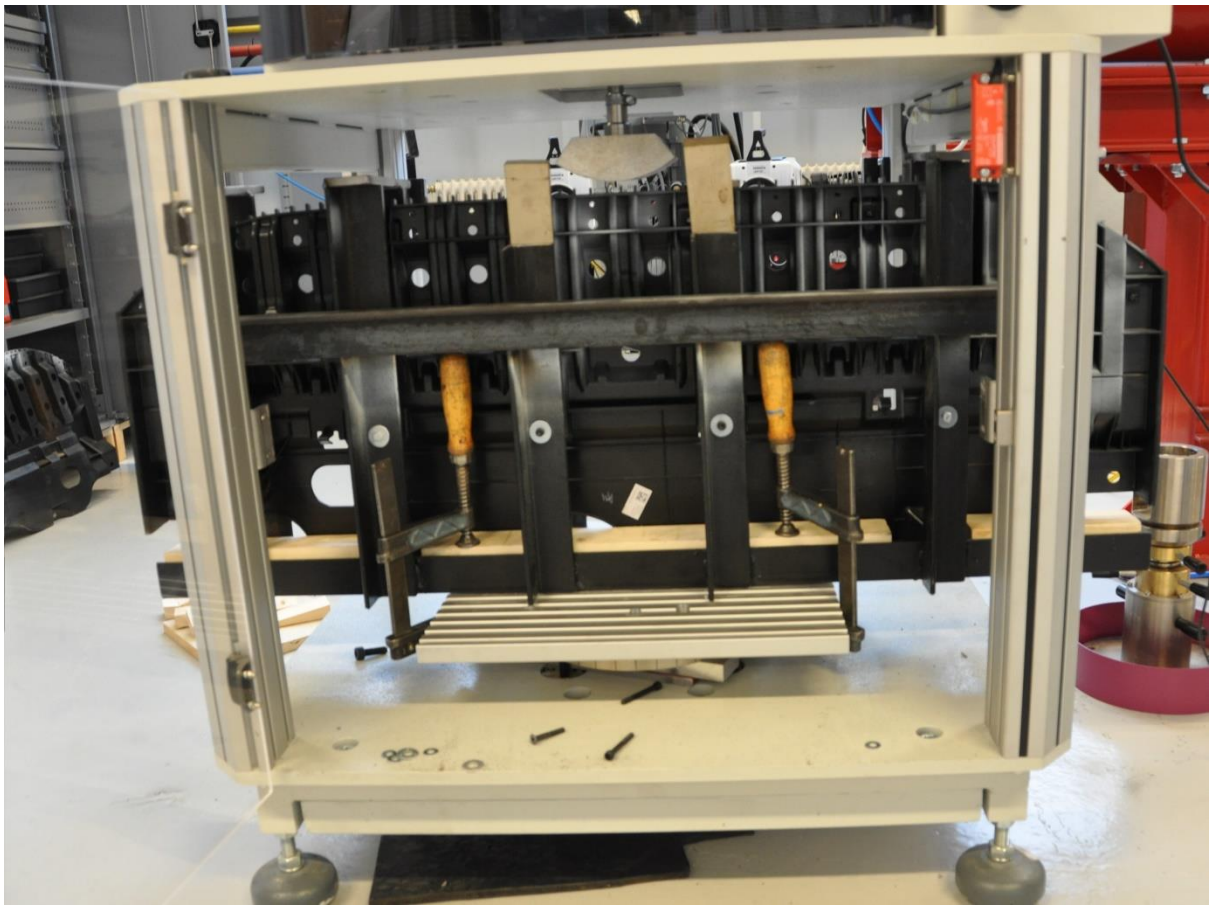

Figure 3-19: Overview of lower absorber test setup

In the above picture the test setup used for the primary test series is shown. This is the same drop tower as used for the box tests, the brakes are not initiated in the lower absorber test series making the whole response valid. This is seen from the back side of the lower absorber (LA), the front side is the side that is facing the cameras which can be seen in the back.

Primary data collection is again the 500 000 Hz load cell. In the initial test series it was used two high speed cameras (Phantom v1610) recording at 30 000 Hz focused on the area closest to impact. It was also an additional camera recording at 1000 Hz from the side to monitor out of plane displacement.

3.2.2.2 Test Specimen

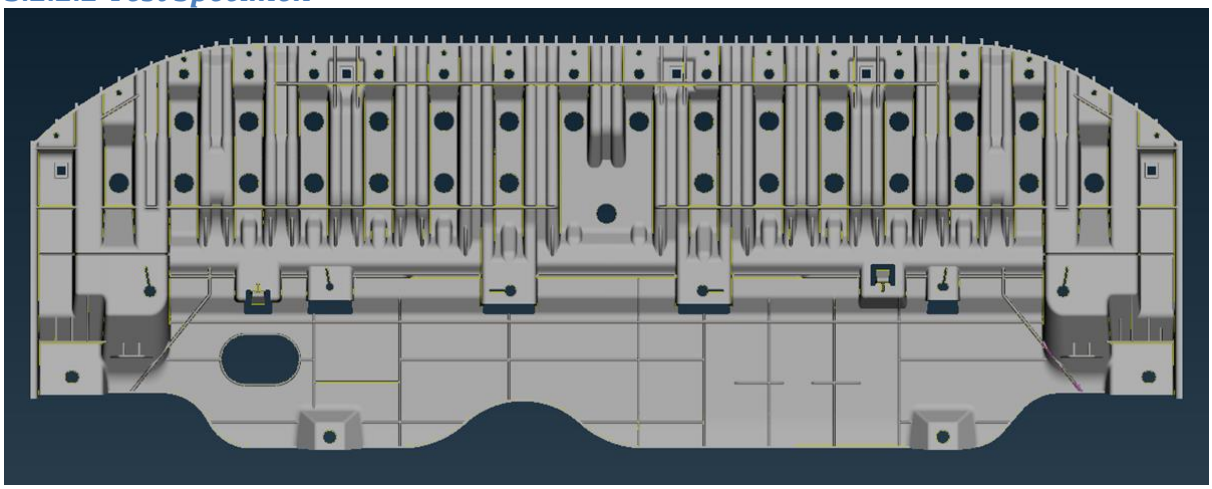

Figure 3-20: CAD geometry of the lower absorber

Figure 3-20 shows the CAD geometry of the test specimen which is a lower absorber of an old version of the Toyota Yaris. It is made of the same ductile polypropylene material as the boxes, but with a significantly more complex geometry. In figure 3-21 below are the key features in the impact area seen from the front side marked and named.

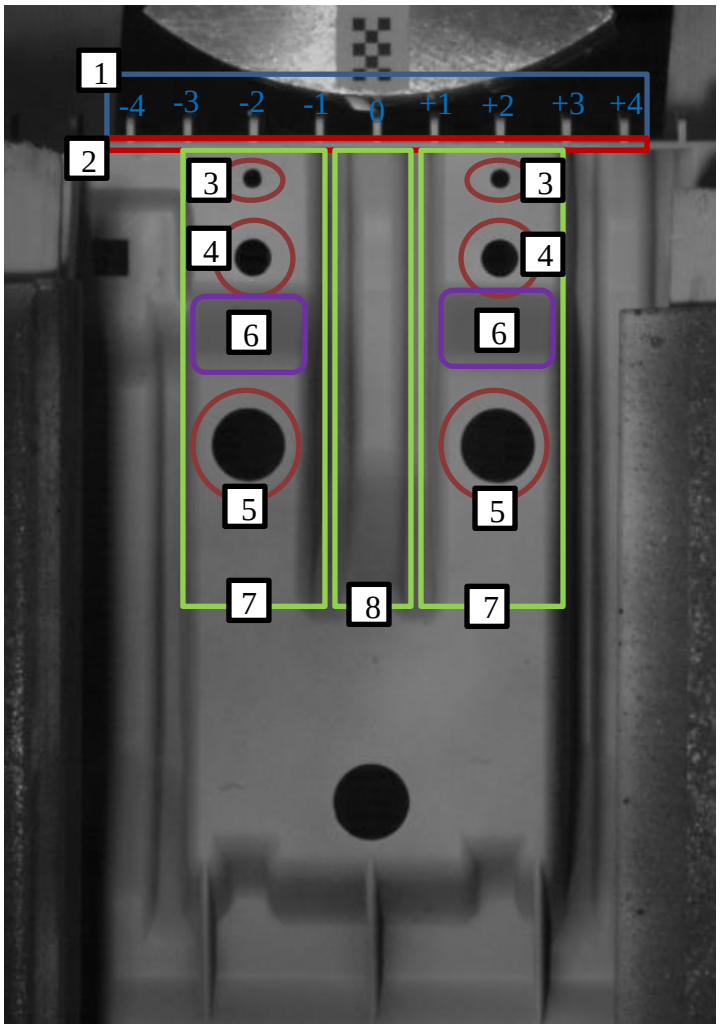

Figure 3-21: Overview of LA features

Feature #	Feature name
1	Ribs (-4 → +4)
2	Front wall
3	Left/right top hole
4	Left/right middle hole
5	Left/right bottom hole
6	Left/right bend
7	Left/right primary
8	Centre primary

Table 3-3: LA feature names

It was initially planned to have 2 impact locations, centre as seen here and off centre (200mm offset). The offset impact location will not be a part of this thesis as the response was dominated by noise, in addition to large out of plane displacements endangering the rig at a low impact velocity.

3.2.2.3 Fixture

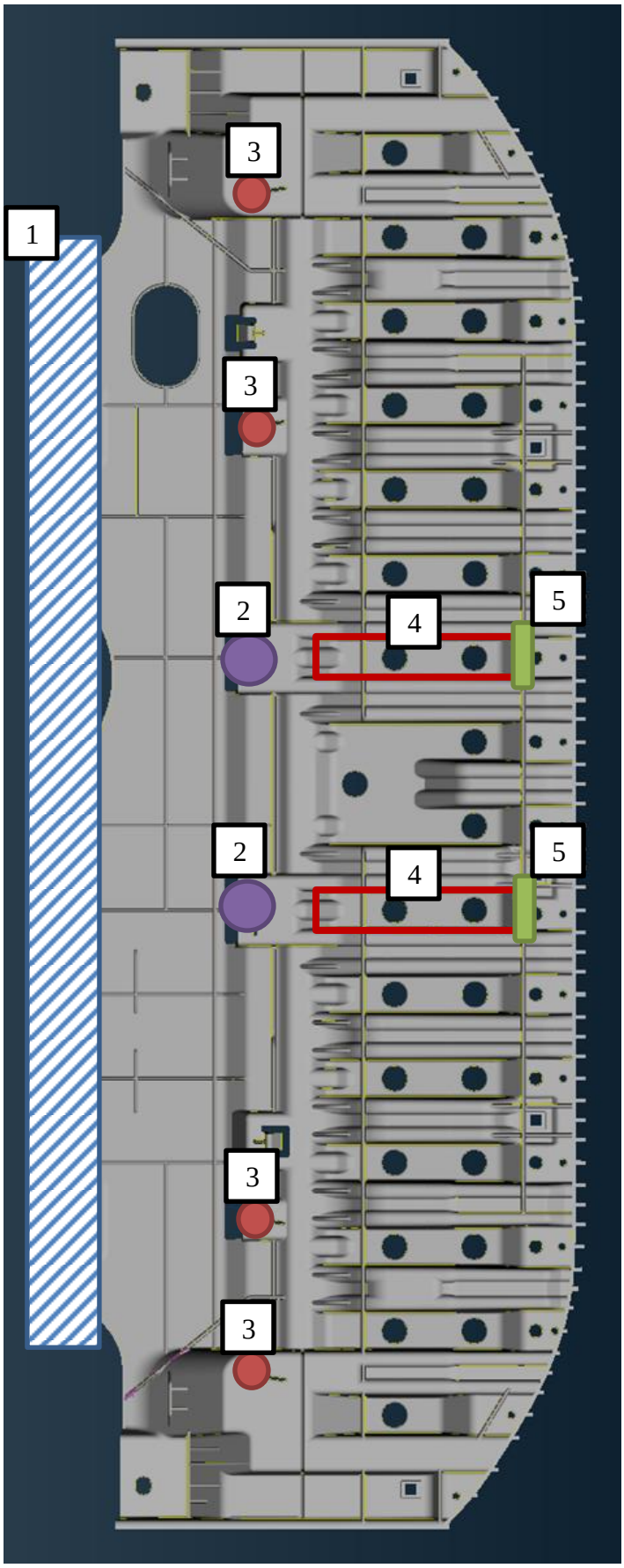

Figure 3-22: Fixture overview, seen from back side

Fixture #	Fixture name
1	Bottom fixture
2	Primary bolts
3	Secondary bolts
4	Front wooden fixture
5	Back wooden fixture

Table 3-4: Fixture names

The areas marked as fixtures in figure 3-22 represent the area restricted by said fixture.

The bottom fixture (see figure 3-23) is a loose guide to reduce vibrations in the lower part of the lower absorber, it has a low influence on the response of the component.

The primary bolts (see figure 3-24) will carry most of the load from the impact. As the bolt holes are modelled as rigid boundary conditions in the numerical model it is critical that these bolts are securely fastened and do not deform during impact.

The secondary bolts (see figure 3-24) carry a small part of the load but aid in fixing the LA into position for each test.

The front and back wooden fixture (see figure 3-24 and 3-23) were added after the initial trial runs in order to reduce out of plane displacements. The front wooden fixture is supposed to be parallel to LA surface in the area marked on figure 3-22 for modelling purposes. The back wooden fixture is only supposed to support two points on the wall which is clearly seen in figure 3-23.

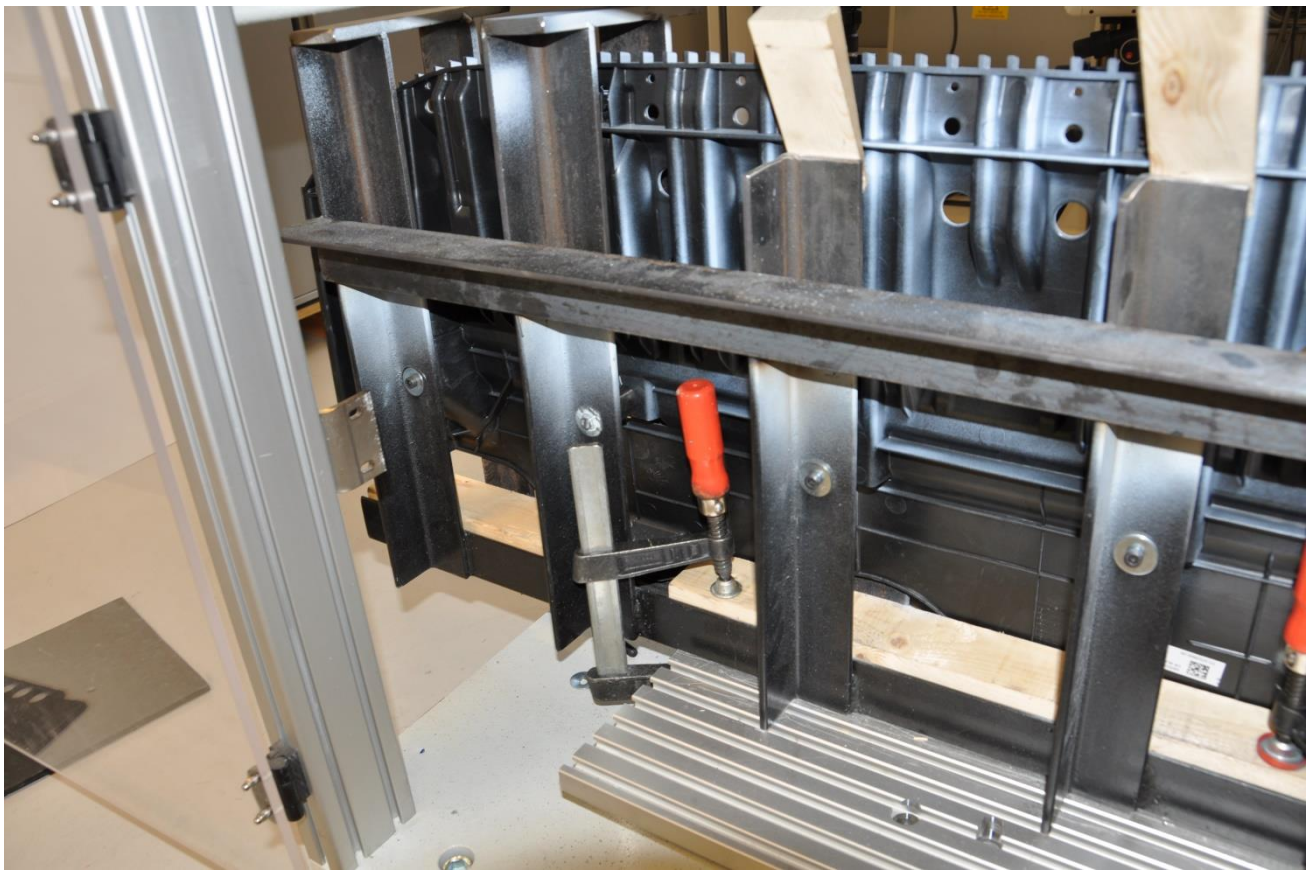

Figure 3-23: Back side fixtures

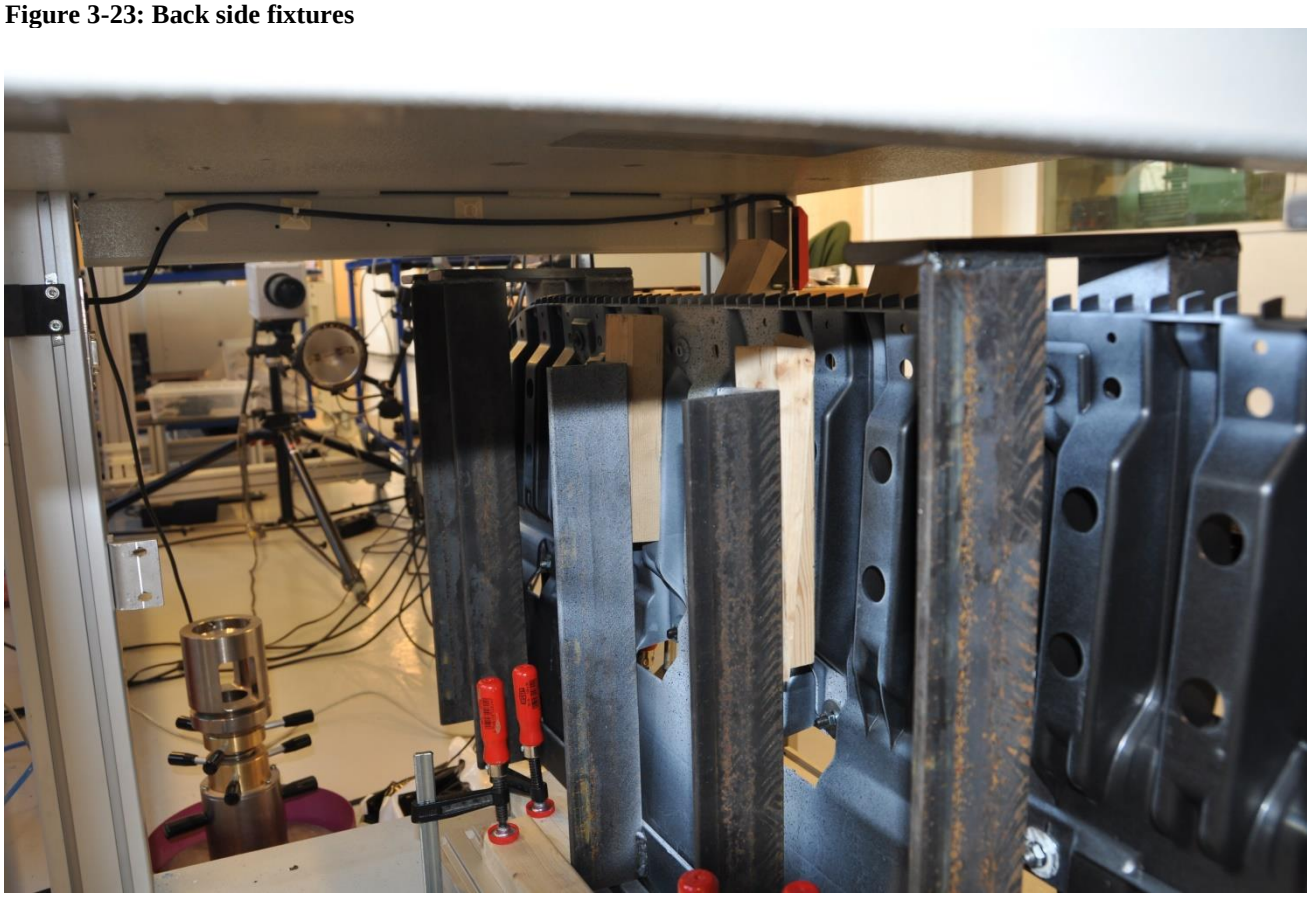

Figure 3-24: Front side fixtures

Figure 3-24 show how the front wooden fixture is implemented in the first round of testing. It can be seen that the fixtures are not parallel with the LA which deviates from the numerical model. As the wooden fixtures have to be removed and reapplied between each run they introduce significant variance in the test results. It was also discovered during the initial round of post-processing that the primary bolts deformed significantly during the impact even at lower speeds. These two problems are the reason behind performing a second round of testing where these issues are under control, and use the results from those tests as a basis for correlation.

3.2.2.4 Impactor

Figure 3-25: Impactor: Top view

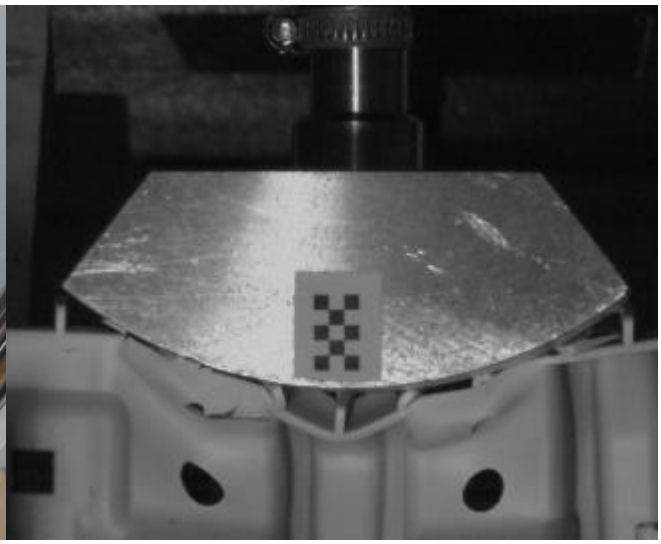

Figure 3-26: Impactor: Front view

The majority of the impactor is exactly the same as described in chapter 3.1.2.3 except for the impactor nose, which is custom made to obtain the intended deformation pattern. The total mass of the impactor is increased to 7.395kg. The impactor nose in this setup is nearly free to rotate on the axis of the impactor rod.

3.2.2.4 Test Matrix and Views

Full Test Matrix

Test series	Test name	Impact velocity [m/s]
CI45	CI4501	4.34
	CI4502	4.38
	CI4503	4.39
	CI4504	4.42
	CI4505	4.40
CI80 (Round 1)	CI8001	7.74
	CI8002	7.73
	CI8003	7.73
	CI8004	7.71
	CI8005	7.71
CI80 (Round 2)	CI8006	7.75
	~~CI8007~~	~~7.75~~
	CI8008	7.75

Table 3-5: Full test matric for LA

The tests were run in two rounds because of the issues mentioned in chapter 3.2.2.3. Due to limited time for the second round of tests the priority was put on CI80 as it deforms significantly more generating more data for correlation. There was also a mistake in the run CI8007 such that the two primary test results are CI8006 and CI8008 as they best satisfy the assumptions made in the numerical model.

In addition to the listed tests it was run 6 initial trial runs to ensure that there was no risk of damaging the drop tower rig. There were also run 4 trial runs with an offset impact location where it was added additional fixtures between each try. The offset impact location tests were not completed as it yielded too large out of plane displacements in addition to the response being dominated by oscillations at 4.5m/s impact velocity.

Camera Views

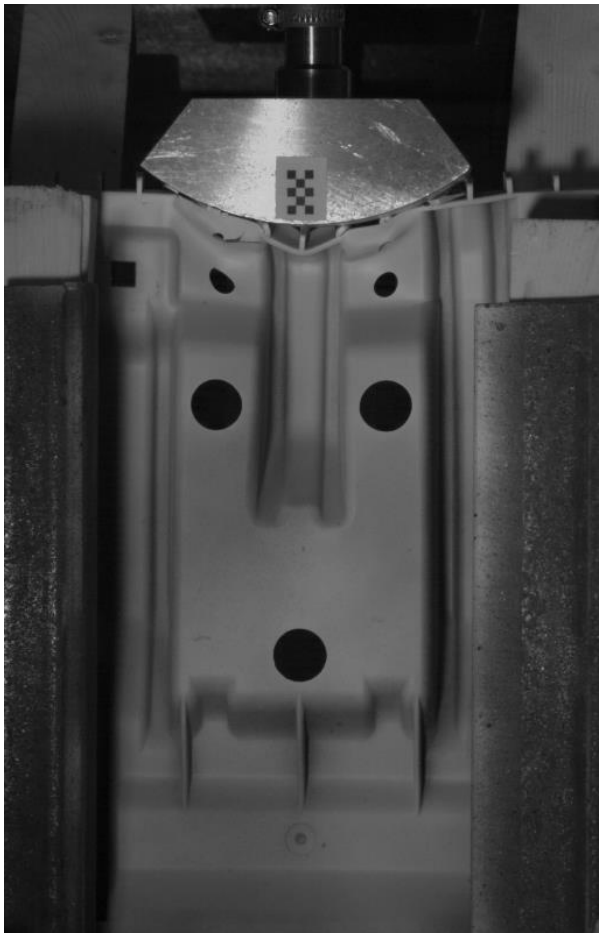

Figure 3-27: Primary view

Figure 3-28: Side view

The primary camera records the front part of the lower absorber with a resolution of 512x800. This camera view is used together with frame number to determine all the events and the timing of them. The side view is used to monitor out of plane displacement and movement of fixtures.

3.2.3 Results

3.2.3.1 Unfiltered Results

Results CI45

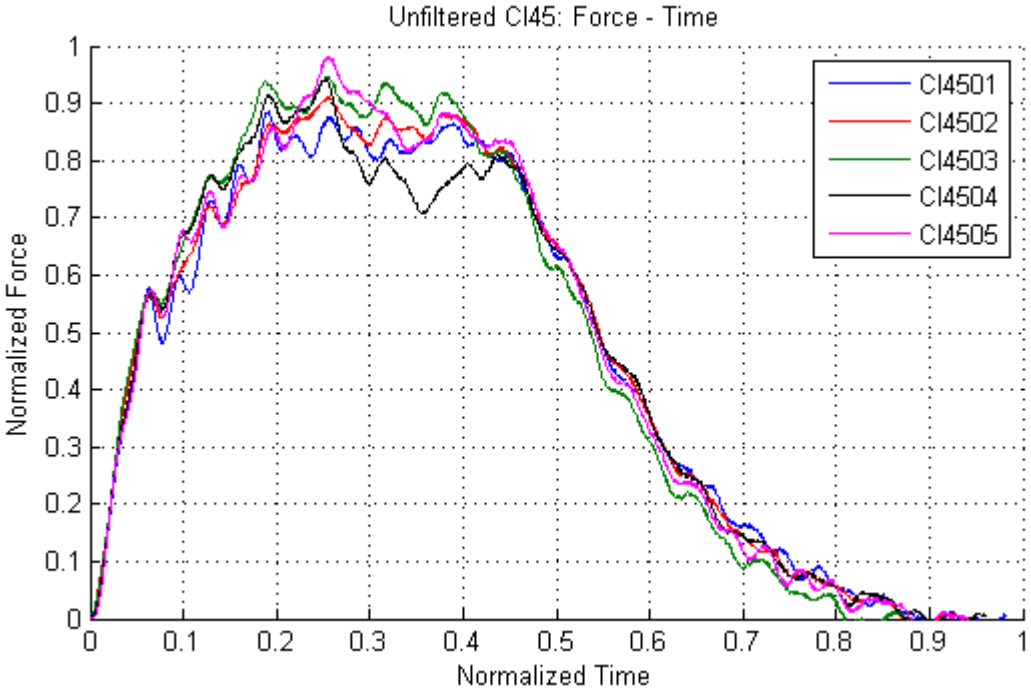

Figure 3-29: Unfiltered response: CI45

Results CI80

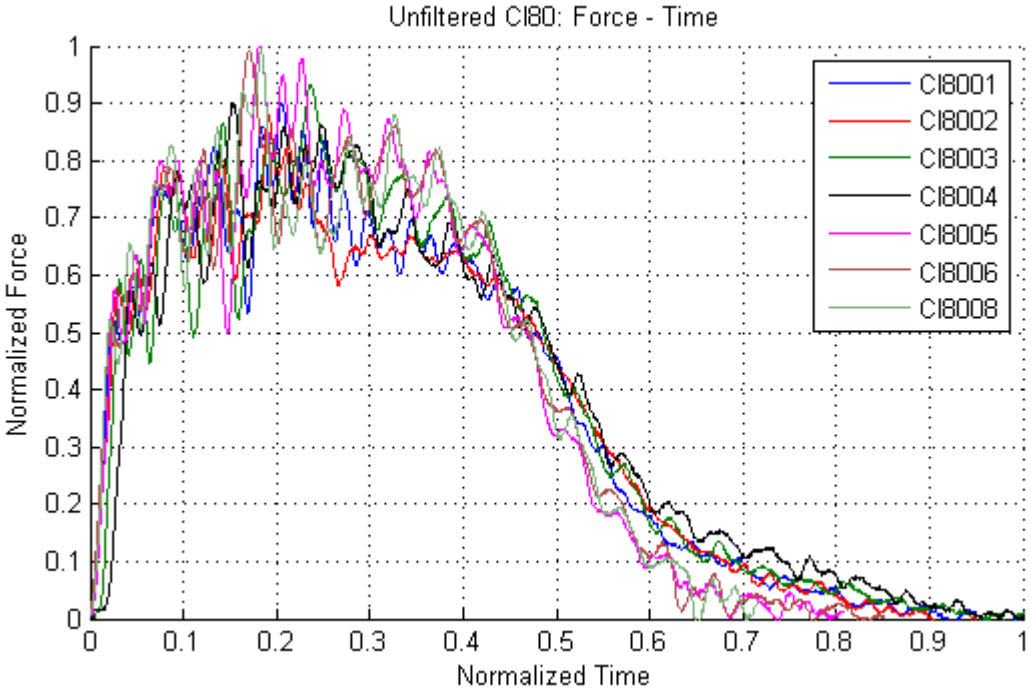

Figure 3-30: Unfiltered Response: CI80

Comments

The unfiltered results are polluted by large oscillations in the response making it difficult to correlate response to the physical phenomena. A Fourier analysis has been performed on the test data to discover the source of the oscillations and to find a solution in terms of post-processing the data.

The Fourier analysis found two frequencies that are the source of the oscillations. Analysing the footage from the high speed cameras it was not observed any vibrations with similar frequencies. These two frequencies were found on test data for both velocities as well as in the initial trial run which did not have the wooden fixtures, only the amplitude of the oscillations changed. Adding the additional fixtures to the test setup makes it stiffer such that any vibrations should have a higher frequency, this strongly suggest that the oscillations in the response are not caused by vibrations in the test specimen but rather by vibrations on the impactor influencing the load cell. This is further verified by the numerical study, as one of the two frequencies was found on a simplified impactor model.

Based on the results of the Fourier analysis it was decided to filter the response curves of the LA before performing result analysis and correlation. For filtering a CFC180 filter was chosen as it is a standard filter in the automotive industry, in addition to being strong enough to remove the oscillations. The test results are filtered with a sae180 filter which is similar to CFC180 except for the initial conditions.

3.2.3.2 Filtered Results

CI45 (sae180)

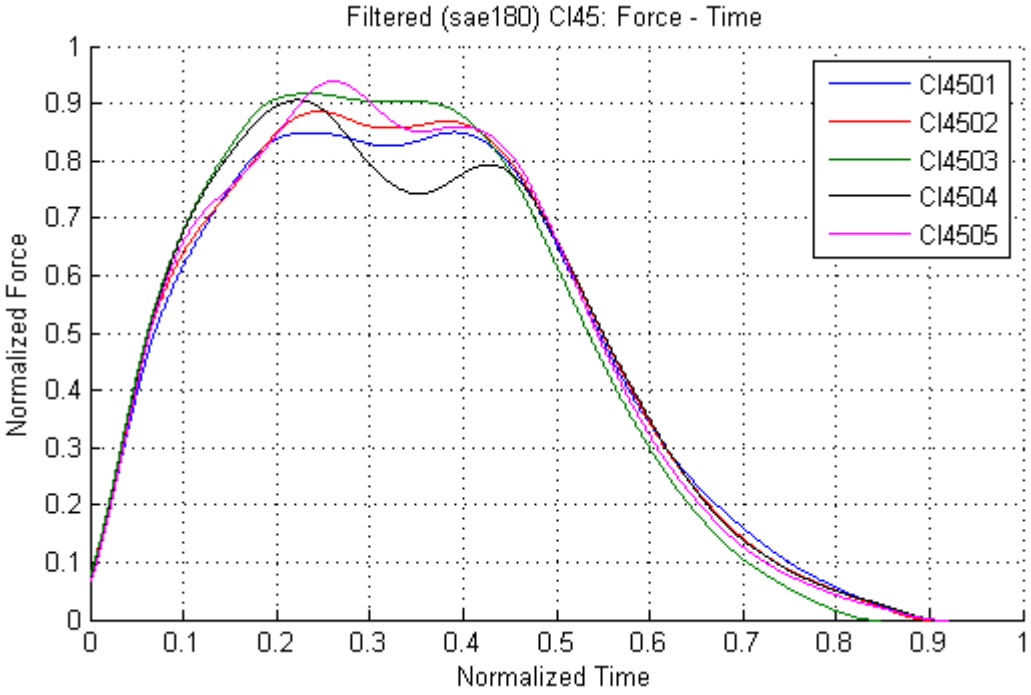

Figure 3-31: Normalized and filtered (sae180) FT curve for CI45

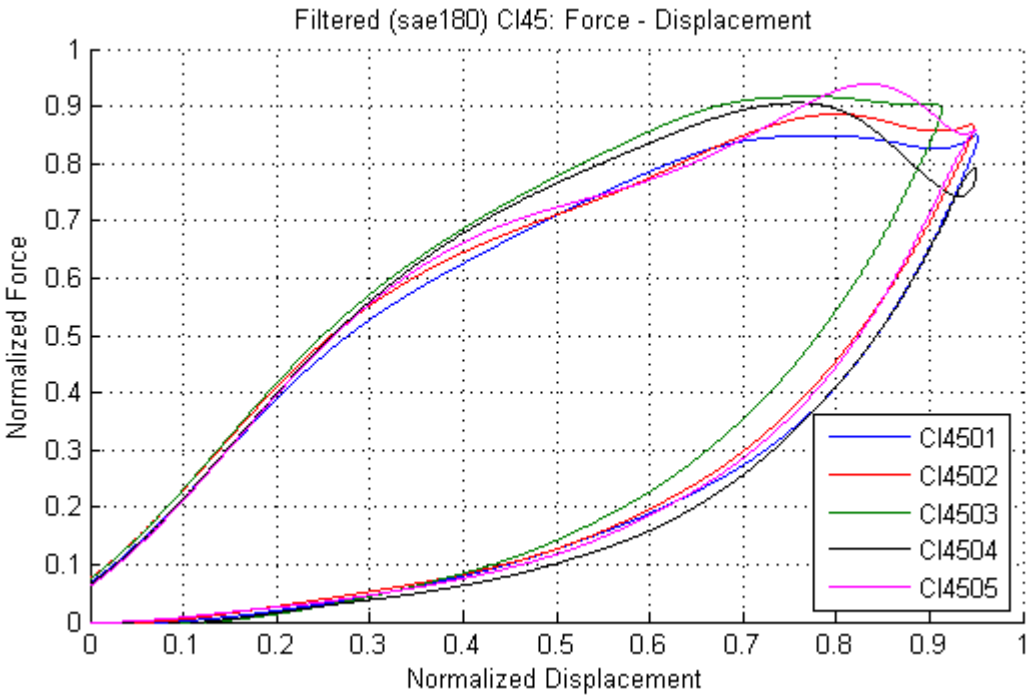

Figure 3-32: Normalized and filtered (sae180) FD curve for CI45

CI80 (sae180)

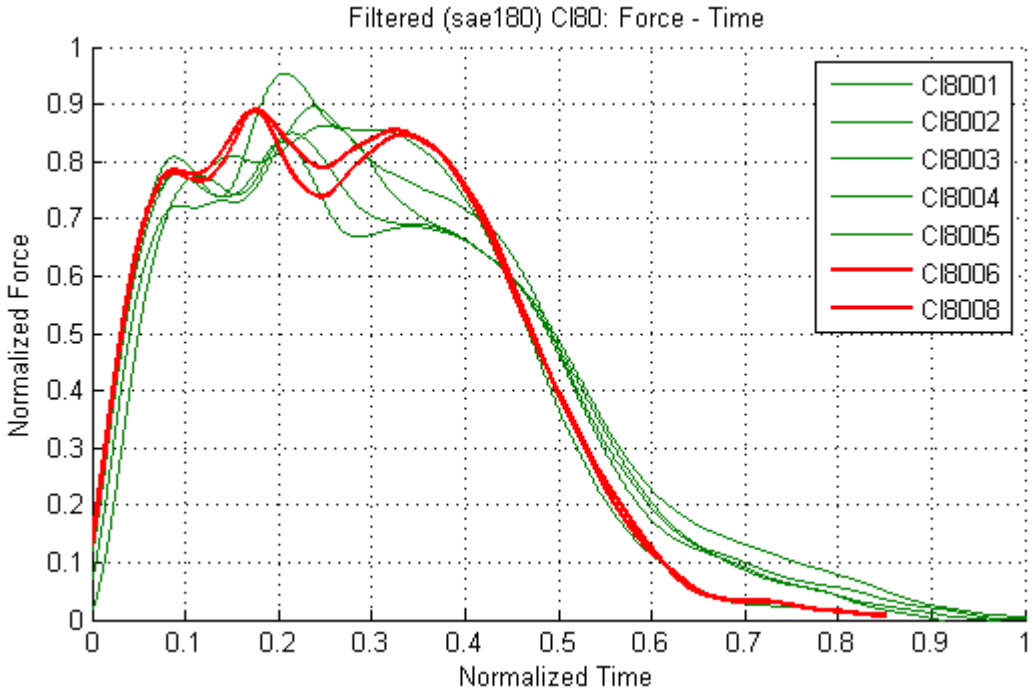

Figure 3-33: Normalized and filtered (sae180) FT curve for CI80

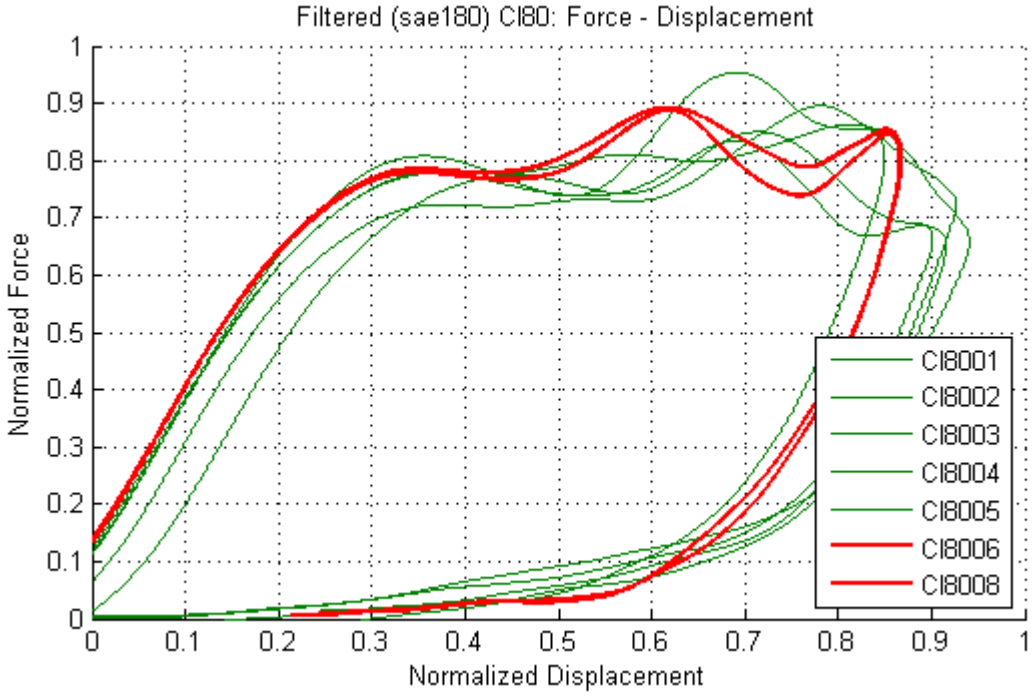

Figure 3-34: Normalized and filtered (sae180) FD curve for CI80

Test Variability

Filtering the results reveals the variance in test results. While the test videos confirms that it is the same events that are occurring, the timing of the events and the influence of the events vary for both CI45 and CI80. This test variance is attributed to the fixture setup discussed in chapter 3.2.2.3. With the second round of CI80 testing the variance in the fixture setup was controlled yielding two tests with similar response as seen in figure 3-33 and 3-34. In addition the fixtures for CI8006 and CI8008 were controlled with the updated numerical model in mind, making these two tests the basis for correlation.

Events

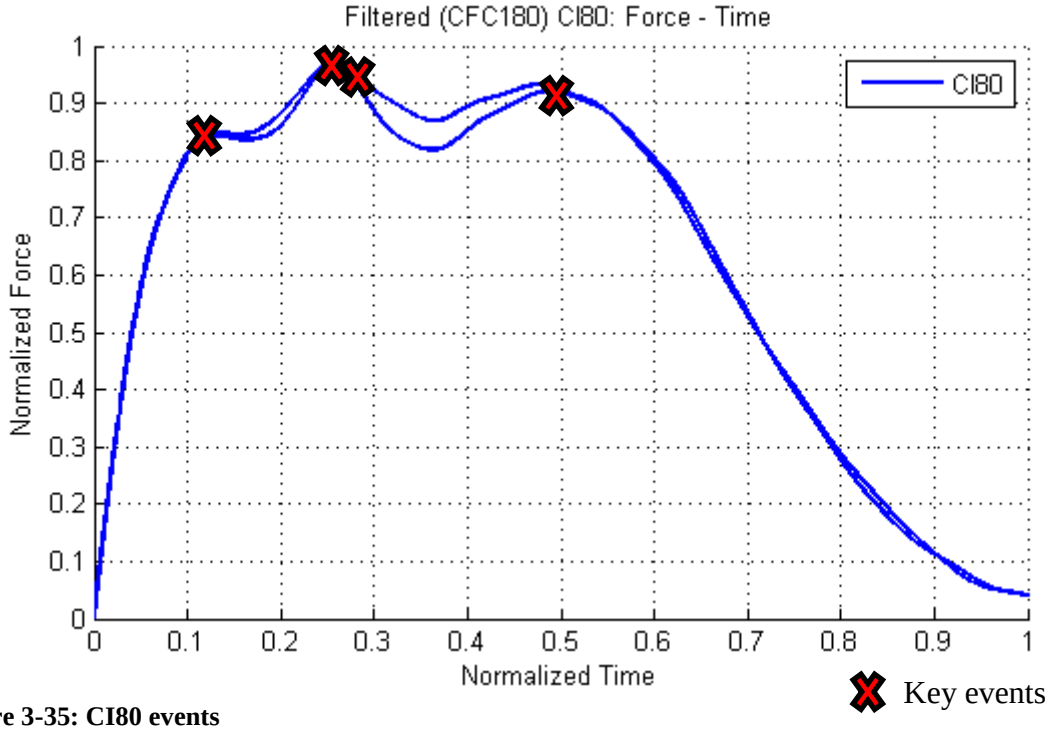

Figure 3-35: CI80 events

There are 4 key events occurring for the CI80 impacts. The first one is the initiation of the first local buckling pattern leading to the first plateau in response. There are two events occurring very close to the peak response, the first one of those are causing the actual peak response and it is an initiation of a second local buckling pattern. The event right after the peak response is a large fracture beneath rib +3 causing a significant drop in force. The last event is the start of the rebound, as confirmed for the Force-Displacement plot. Below are images of the three first events. The red lines in figure 3-36 and 3-37 represents buckling patterns, the circle highlight the fracture.

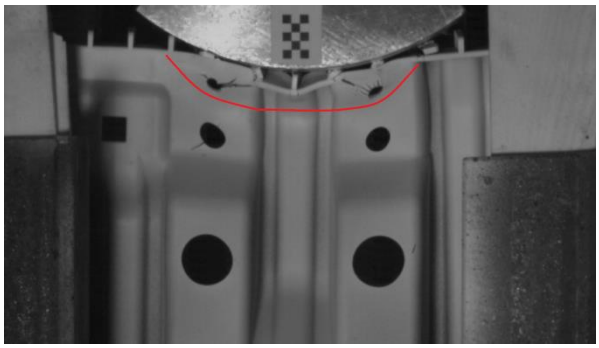

Figure 3-36: Initial buckling pattern

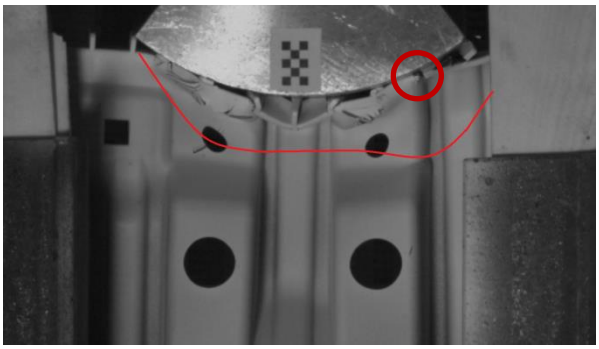

Figure 3-37: Secondary buckling pattern and fracture

3.2.3.3 Digital Image Correlation (DIC)

Point Tracking

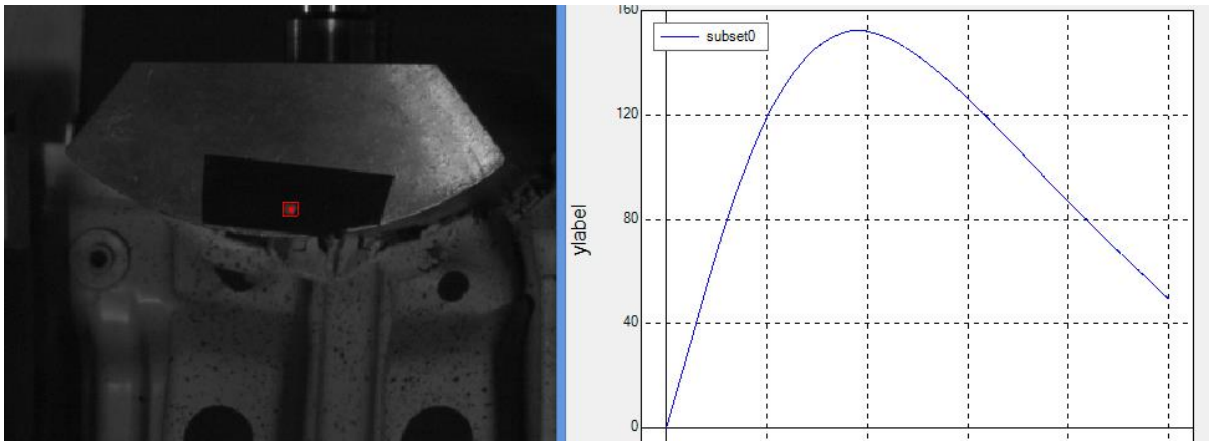

Figure 3-38: Point tracker

Point tracking was used during the laboratory sessions to verify the displacement calculated from the load cell coincided with the one seen in the images.

3D DIC

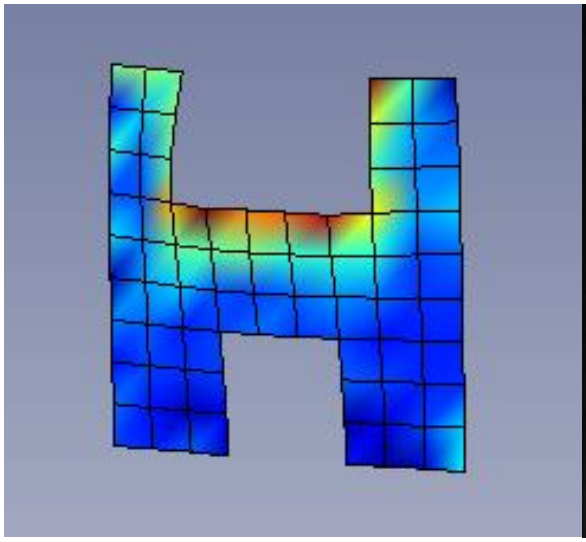

Figure 3-39: 3D DIC results

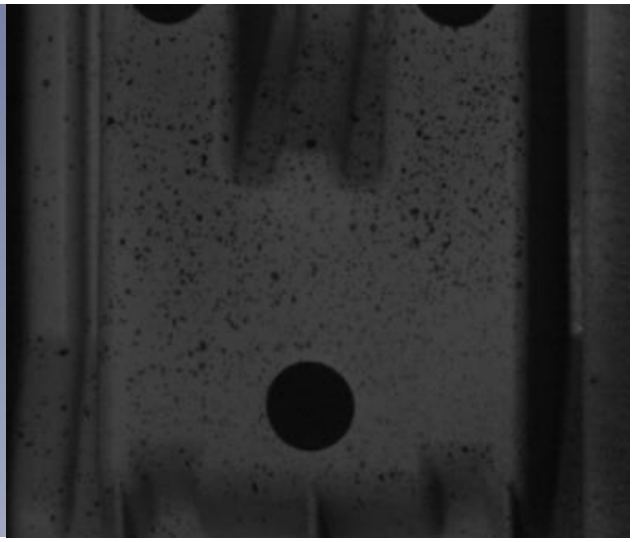

Figure 3-40: Area analysed by 3D DIC

The reason for using two primary cameras for the first round of testing was to perform 3D DIC on the impact location to obtain accurate surface strains, and have another way to monitor out of plane displacement. However with the setup used the accuracy was not sufficient to add any useful information.

There are two types of errors when performing 3D DIC, correlation error between images and discretization error due to rough FE mesh. To obtain good correlation the element size needs to be at least 20x20 pixels, although larger element sizes reduces correlation error. It is also important to ensure high image quality with good lighting, proper focus and a proper speckled pattern to ensure good correlation. To reduce discretization error a fine FE mesh is needed, which in turn gives higher correlation error. The end result is that the resolution of the videos needs to be high enough in the area of interest to have large enough elements for correlation but small enough to capture the strain field.

4 Numerical Study: Box

4.1 Introduction: Box Impact

The first part of the numerical study in this project is focused on the box study. The purpose of studying the boxes first is to obtain knowledge on this type of problems and the performance of the SPM such that it can be applied to the lower absorber study.

The majority of the time spent on this project has been spent on the numerical study of the boxes, the primary reason for this is the issues with the geometry. Even though the geometry is considered simple compared to a component like the lower absorber it is still complex enough to make it difficult to properly measure and capture all the details. This means that a several issues with the geometry were discovered over time leading to 4 iterations of the geometry covered in table 4-1.

Geometry	Material Model	Mesh Size	Impact Location	Overall Quality Before Fracture	Quality of Fracture
Initial geometry from supplier	SPM without viscoelasticity	5mm	CT/SW/CO	x	x
		2mm	CT/SW/CO	x	x
		Refined	CT/SW/CO	x	x
Altered initial geometry	SPM without viscoelasticity	5mm	CT/SW/CO	Δ	x
		2mm	CT/SW/CO	Δ	x
		Refined	CT/SW/CO	Δ	x
Initial CAD geometry	SPM without viscoelasticity	5mm	CT/SW/CO	Δ	x
		2mm	CT/SW/CO	Δ	x
		0.8mm solid	CT/SW/CO	Δ	Δ
Final improved CAD geometry	SPM without viscoelasticity	5mm	CT/SW/CO	Δ	x
		2mm	CT/SW/CO	Δ	x
	SPM with viscoelasticity	5mm	CT	○	-
			SW	○	-
			CO	○	x
		2mm	CT	○	-
			SW	s	-
			CO	s	x
		0.8mm solid	CT	○	-
			SW	s	-
			CO	s	○
		Refined solid	CO	s	○

Table 4-1: Simulation overview

Very good	s
Good	○
Poor	Δ
Very poor	x

Table 4-2: Simulation quality legend

This chapter will focus only on the final iteration of the geometry and only on the key observations and results. This is because the entire dataset is extremely large as it was run a total of 214 simulations for the box study alone, each with their own purpose and results.

4.2 Modelling

4.2.1 Reverse Engineered CAD geometry

The initial numerical model for the boxes was delivered by the supplier of the test boxes. There were several issues with that model as it had several major flaws in the geometry as well as no access to the CAD geometry. In response to a CAD geometry was reverse engineered from one of the test boxes and used as a basis for the simulations.

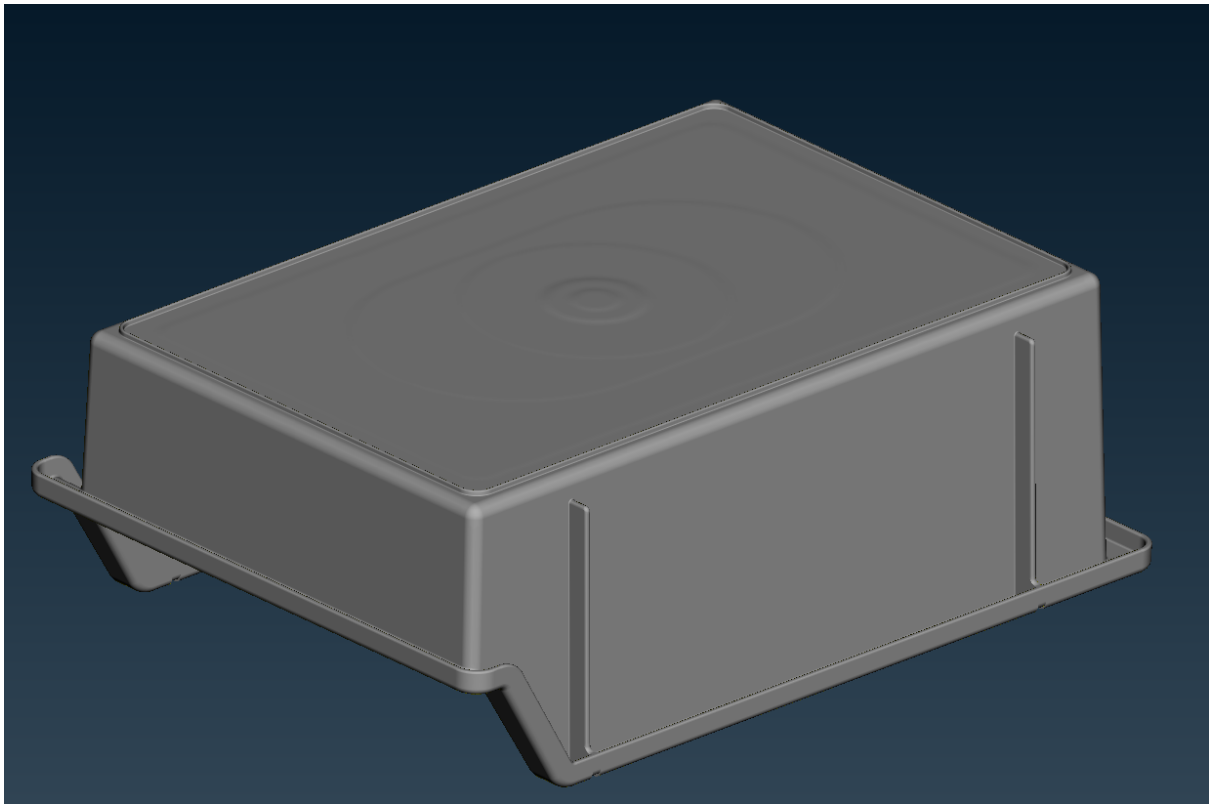

Figure 4-1: Box CAD geometry

The reverse engineered CAD geometry solves the major issues of the initial model. The large flaws in the initial geometry are fixed, but as it is reverse engineered there are some simplifications made that should not have a large influence. The main problem with the reverse engineered geometry is that the measurements on which is it based are not very accurate as it was measured with basic tools. Ideally a 3D scan of the object should have been performed to obtain an accurate geometry, even then it would not be a perfect representation of the boxes used in the tests due to damage from transport as mentioned in section 3.1.2.2. Thus the geometry remains a source of error which is difficult to quantify.

Shell Mesh

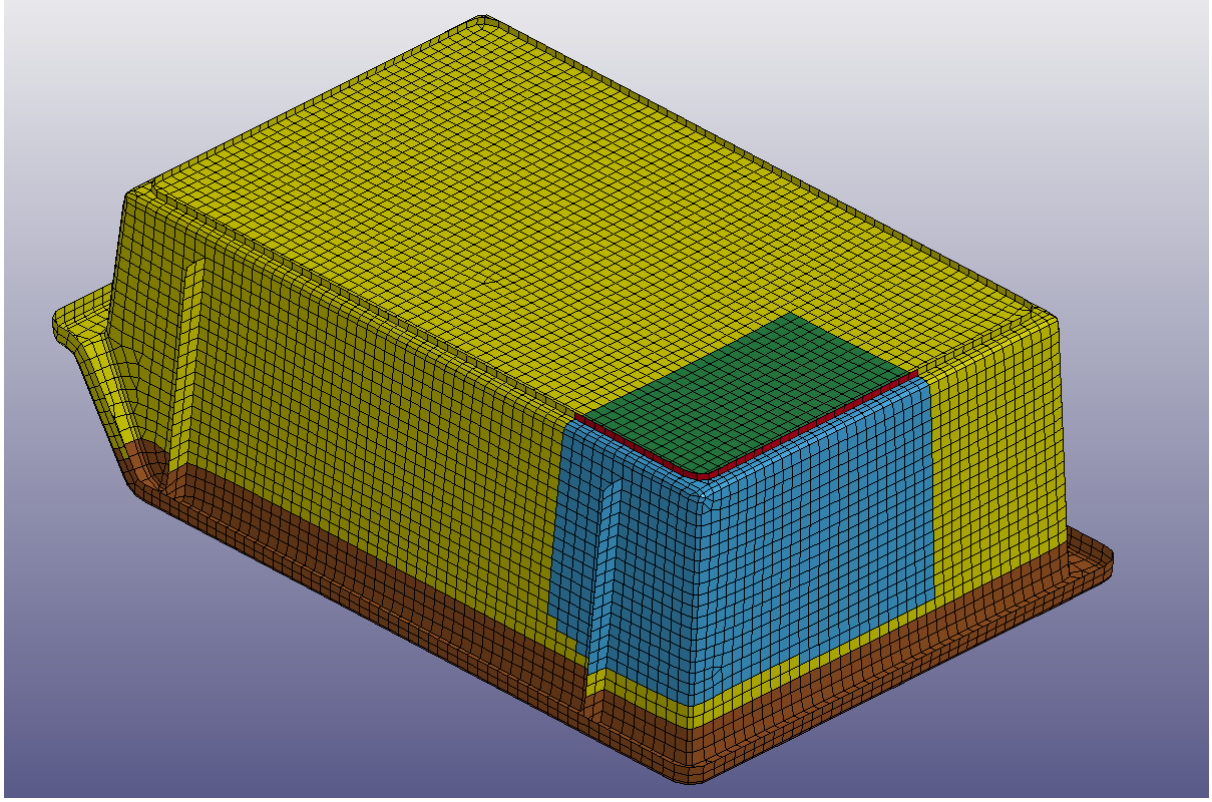

Figure 4-2: 5mm shell mesh: Corner impact

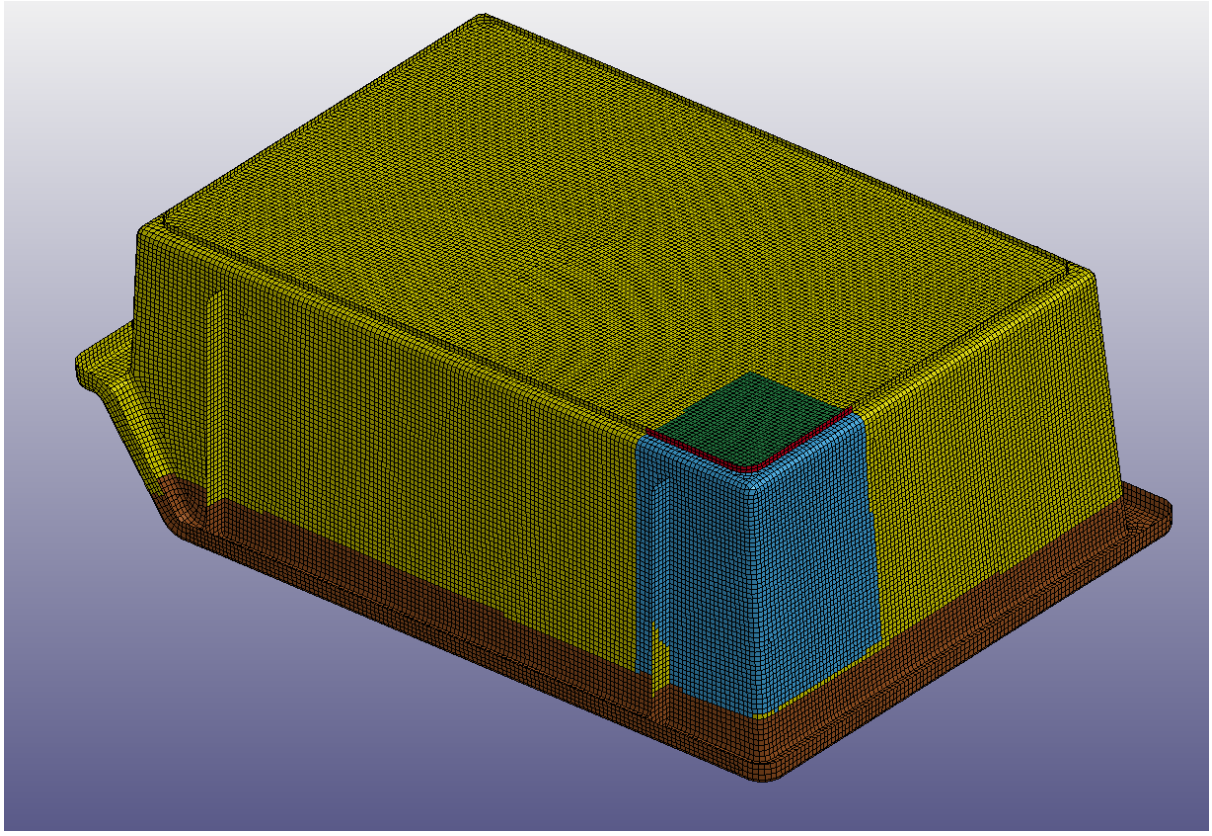

Figure 4-3: 2mm shell mesh: Corner impact

Figure 4-2 and 4-3 display the 5mm and 2mm shell mesh used for this project. The 5mm model consists of 7453 elements while the 2mm model consists of 49184 elements. The colours represent each part in the LS-Dyna model. As the CAD geometry was available an automatic thickness mapping has been used, where the thickness is applied to each node in the ELEMENT keyword which overrides the thickness defined in the SECTION keyword. Because of this the thickness mapping is significantly smoother and it removes the need for 12 different parts to define the thickness of each area.

As the pictures show, the shell model is still split into 5 different parts, this is done to reduce the CPU cost of the contact algorithms. The impact area (corner impact in figure 4-2 and 4-3) is split into 3 parts which are all in one contact definition, this is done to define force-transducers such that the response of each component can be monitored.

Solid Mesh

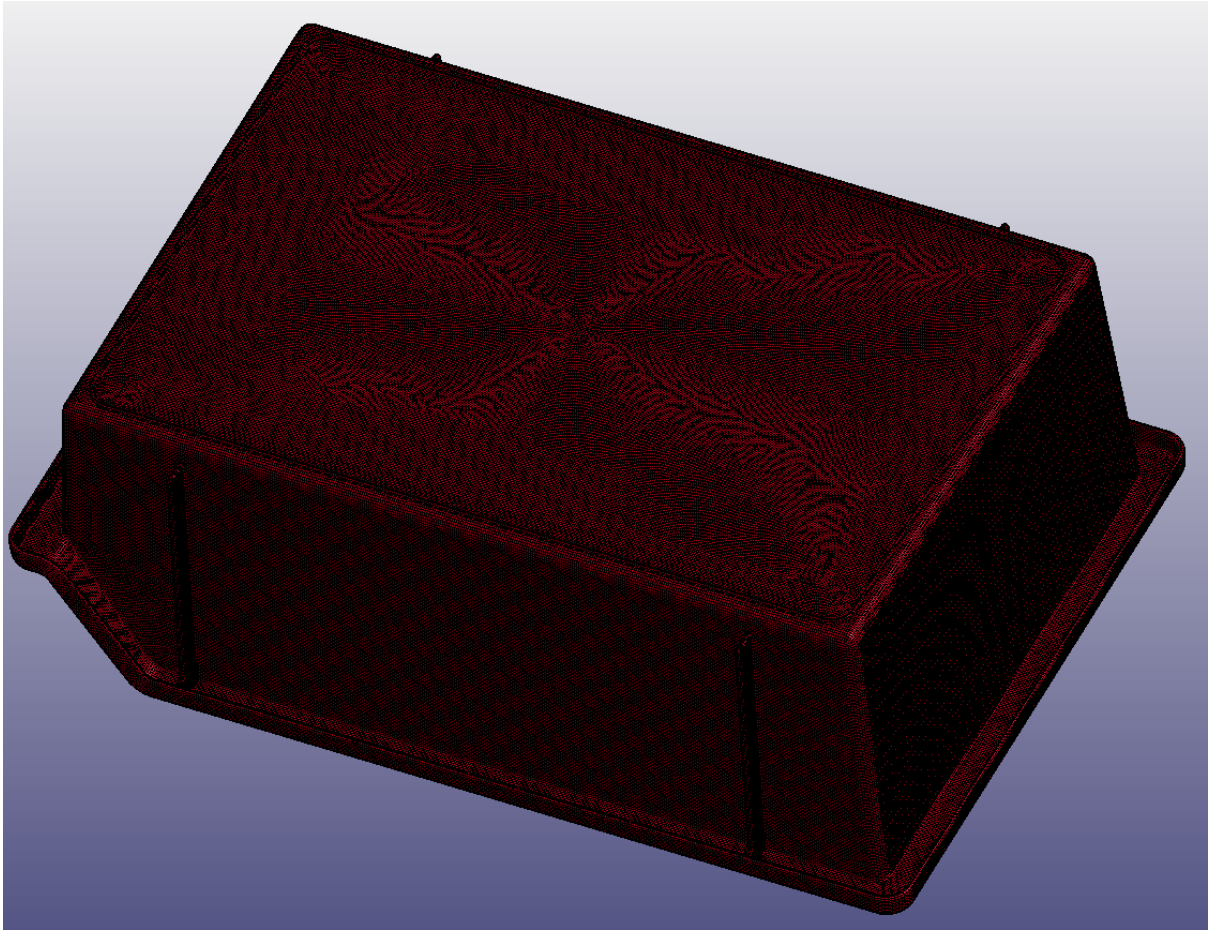

Figure 4-4: Overview solid mesh

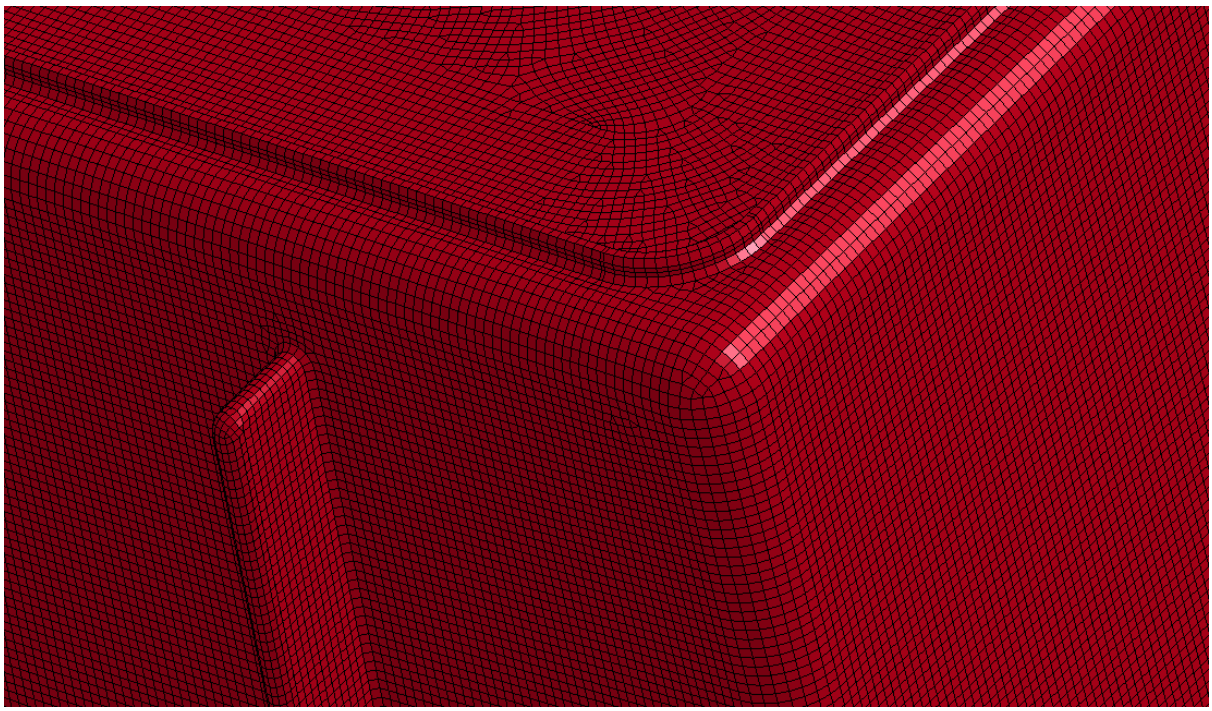

Figure 4-5: Solid model detail: Corner

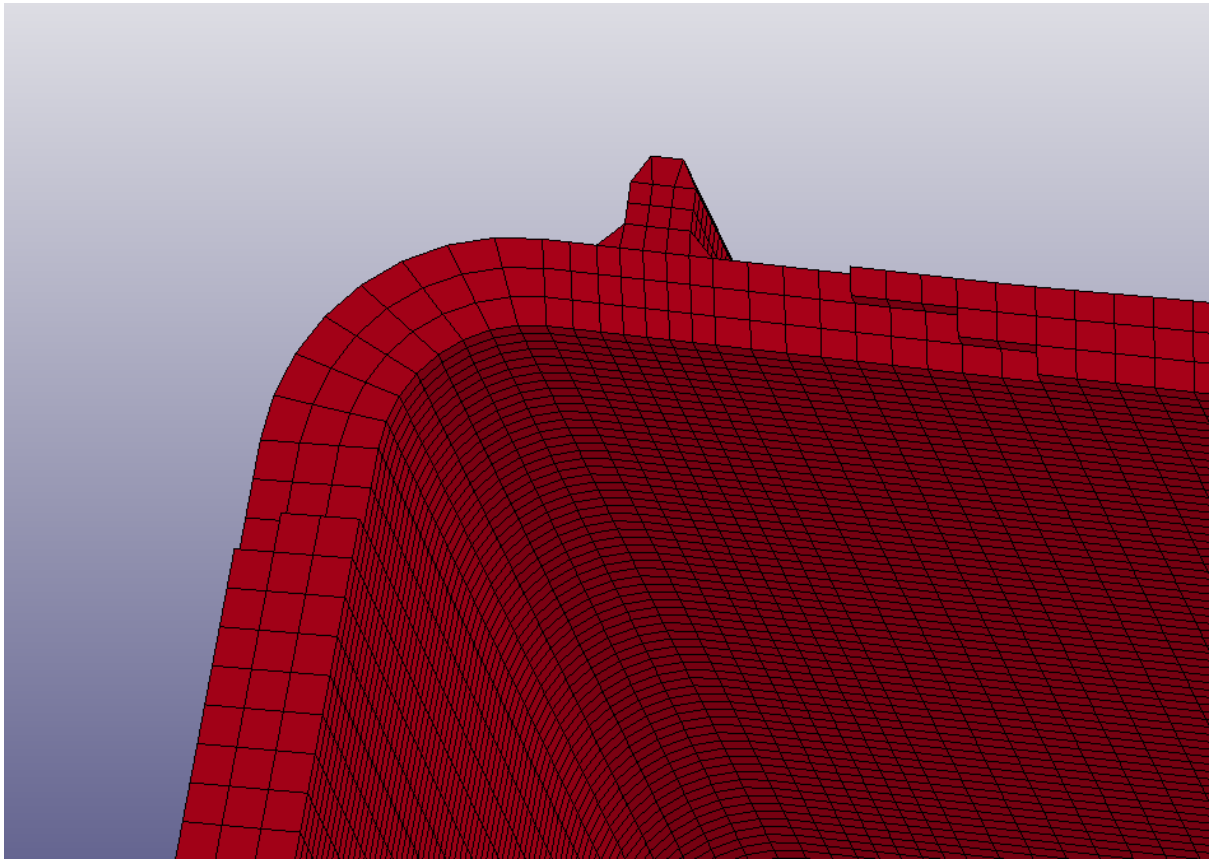

Figure 4-6: Solid model detail: Cross section

The primary solid model used for all impact locations is based on a 0.8mm mesh size which gives 3 elements through the thickness as seen in figure 4-6. The model has been generated using primarily mapped meshing ensuring a high quality mesh. Automatic tetra meshing has been used on a few insignificant features to complete the model. In total the model consists of 945 840 solid elements and a coating layer of 604 448 shell elements for the contact definitions.

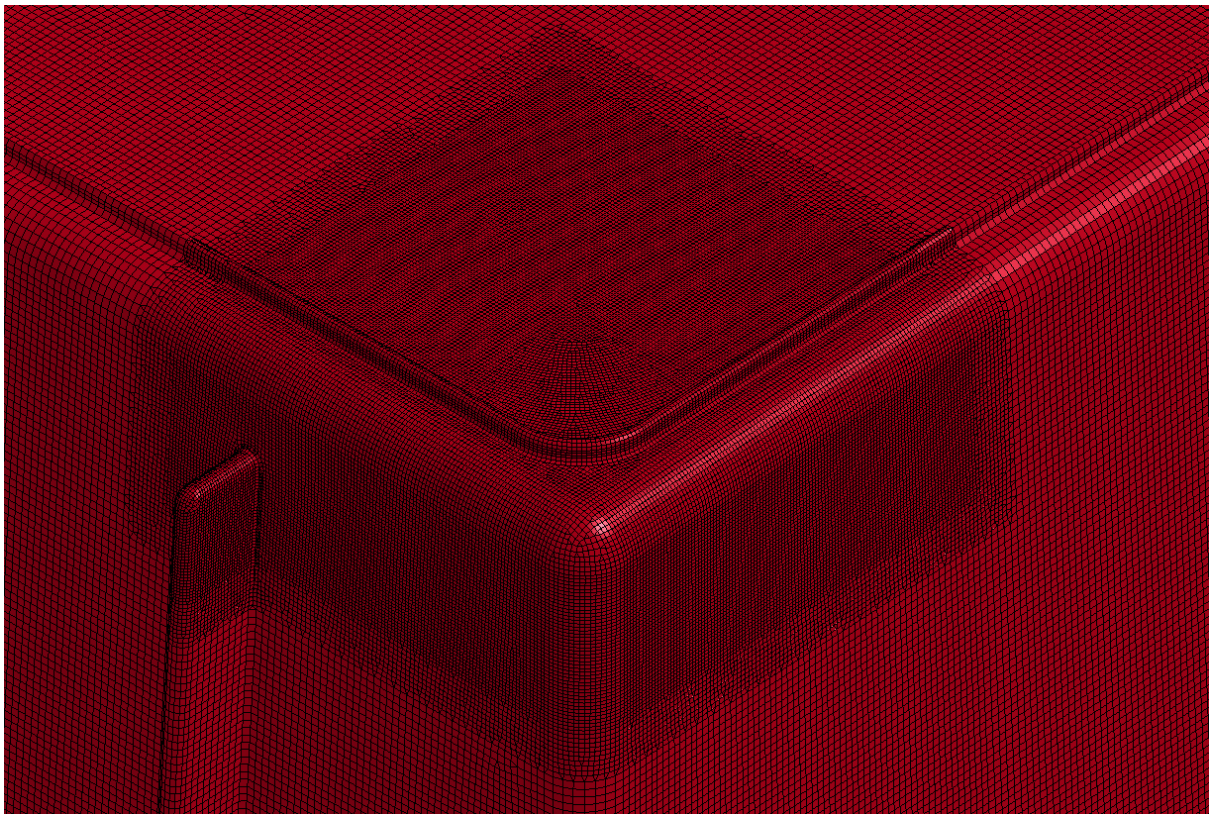

Figure 4-7: Refined solid model

A solid model refined in the corner was made for further study of the corner impact. The refined area has a general mesh size of 0.4mm ensuring 6 elements through the thickness. This refinement brings the total number of solid elements to 1 528 436 with 705 749 shell elements for the coating. The connection between the 0.4mm part and the 0.8mm part is done with an automatic tetra mesh such that the mesh quality is poor in the connection area.

4.2.2 Impactor and Fixture Model

Impactor model

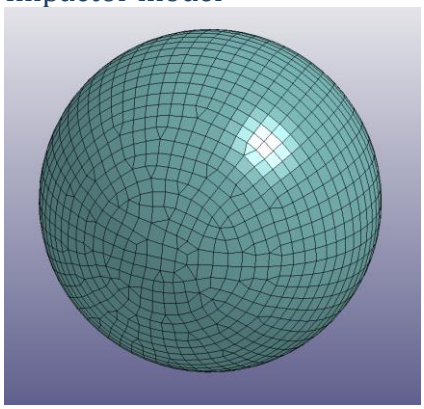

Figure 4-8: Box impactor

The impactor model is a sphere made to represent the spherical impactor nose. A general mesh size of 1mm was chosen to obtain a sufficient discretization of the geometry as the radius of the impactor is only 10mm. In total the impactor consist of 1858 elements. The material for the impactor is assumed rigid, using LS-Dyna MAT_RIGID.

Fixture model

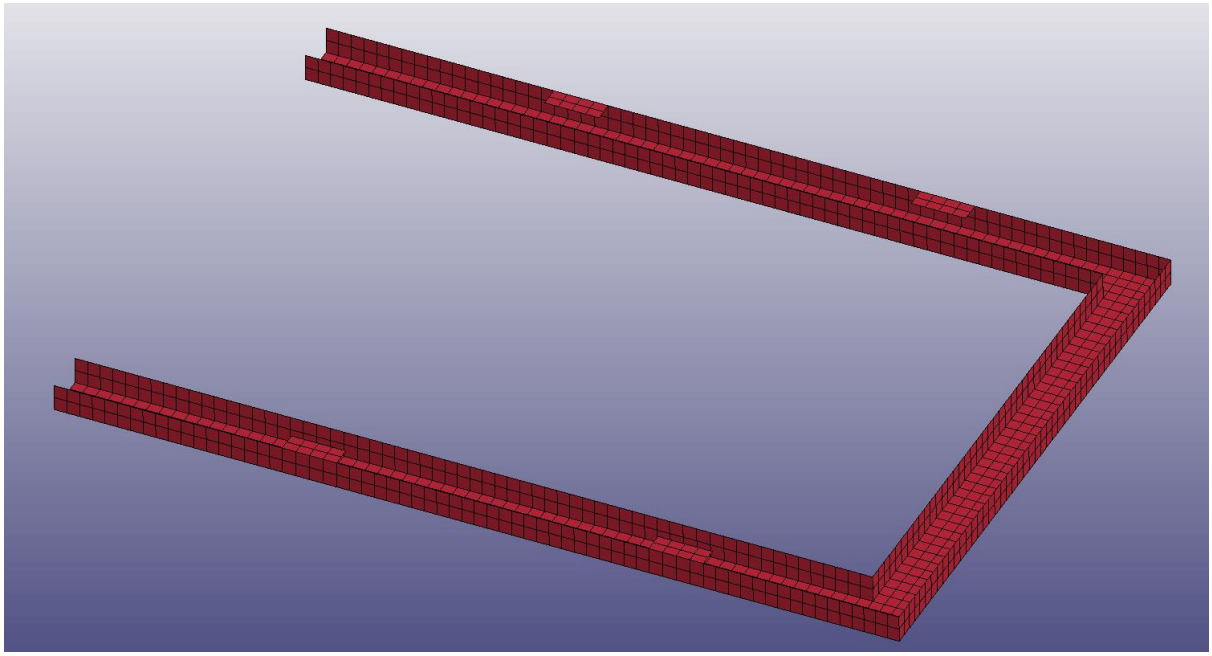

Figure 4-9: Box fixture

The fixture consists of 1424 elements with a general mesh size of 5mm. The geometry of the fixture is based on a tight fit with the numerical models mentioned in section 4.2.1 as geometry of the numerical models are not exact and that it was observed a tight fit in at the lab. The material for the fixture is assumed rigid, using LS-Dyna MAT_RIGID.

Contact

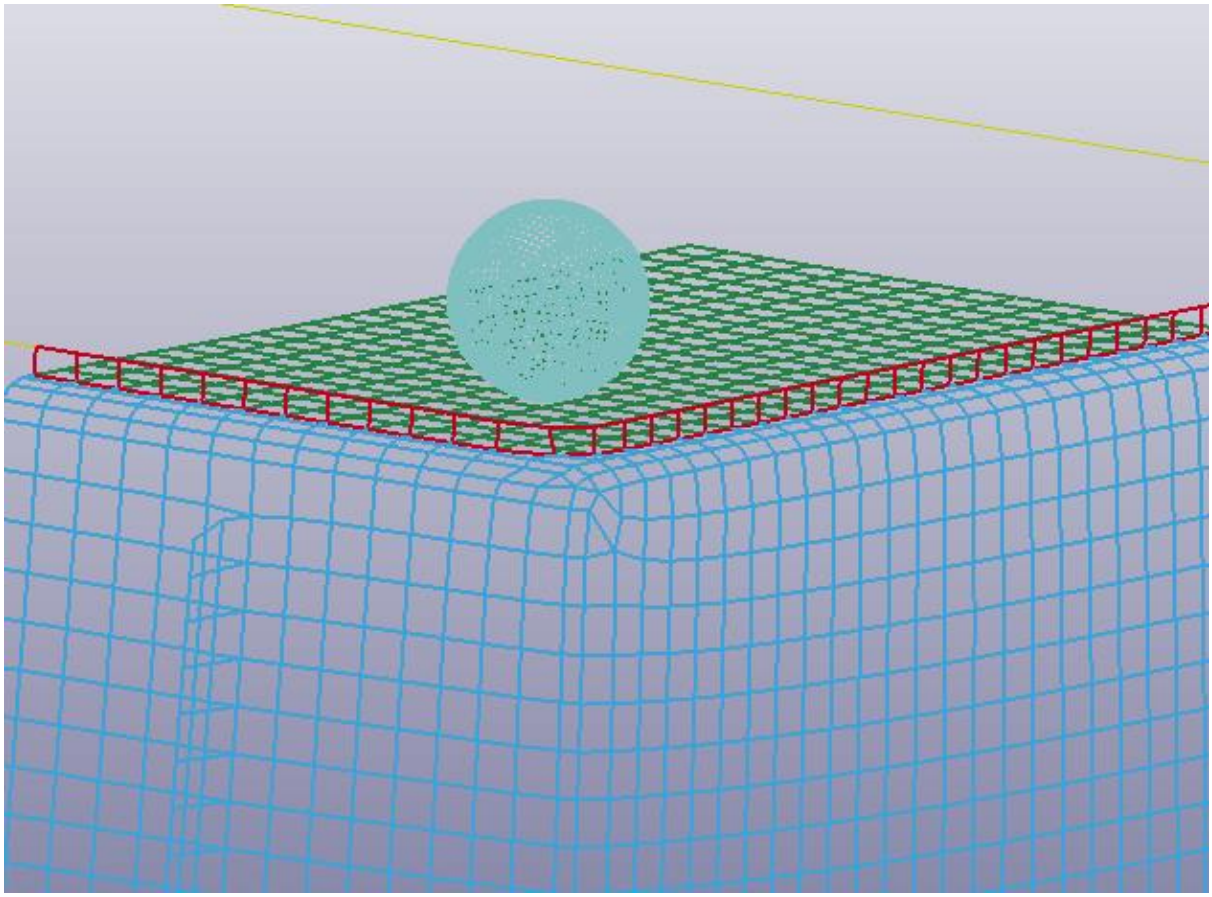

Figure 4-10: Corner impact contact

For the shell meshes the contact definitions are reduced by only defining them in the areas of interest as seen in figure 4-10. The contact definition used is CONTACT_AUTOMATIC_SURFACE_TO_SURFACE for the contact between the box and impactor as well as box and fixture. For contact parameters the standard values have been used except for the friction coefficients. Master and slave side have been chosen as to avoid penetration. The self-contact for the box is defined with CONTACT_AUTOMATIC_SINGLE_SURFACE with standard values as well.

4.3 Results

4.3.1 Centre Impact

Overview of Numerical Response

Below is a plot of the key response curves for the centre impact based on shell meshes. It has been chosen one representative test for comparison as figure 3-16 show that there is very little test variability.

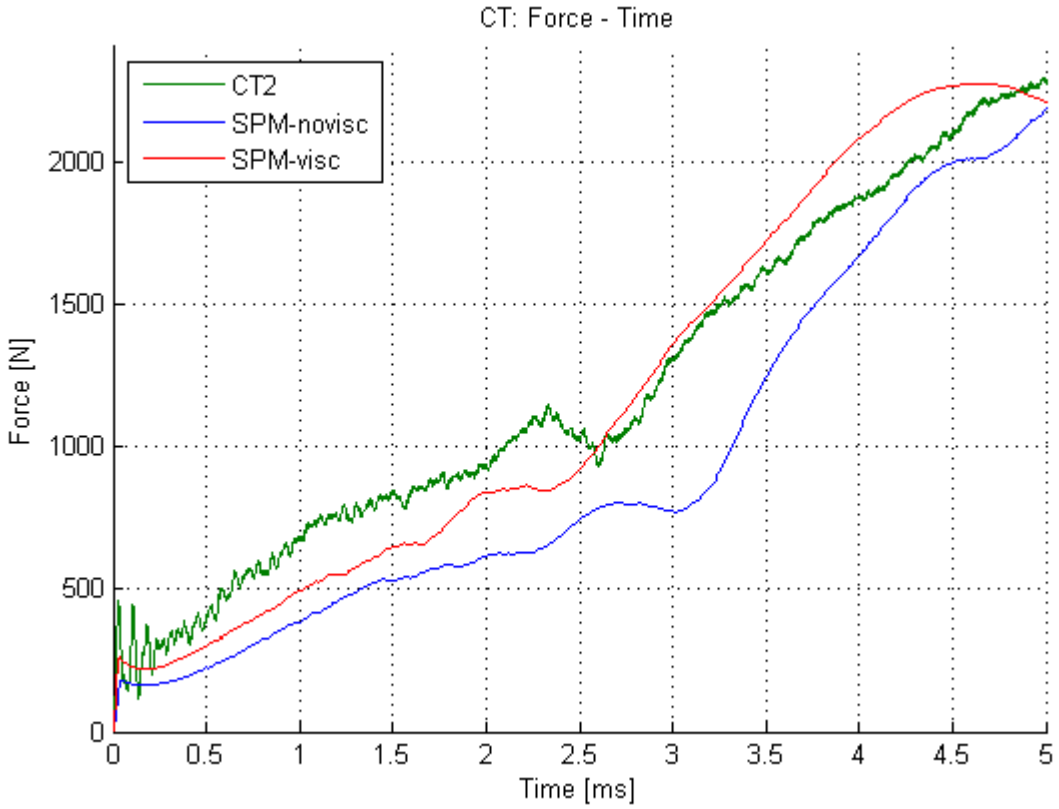

Figure 4-11: Overview of numerical response

Name	Material model	Model and Mesh
CT-SPM-novisc	SPM without viscoelasticity	Final CAD geometry - 2mm
CT-SPM-visc	SPM with viscoelasticity	Final CAD geometry - 2mm

Table 4-3: Numerical models used in figure 4-11

General Comments on the Response

For the centre impact there are two key phenomena that influence the results. The first event causing the bump between 20 and 25 mm displacement is cause by reflection of surface waves in the elastic region. This phenomenon is captured by all the numerical models, however the timing of the bump is highly influenced by both material model and geometry.

The second phenomenon is an initiation of a new deformation pattern caused by the corners folding in on themselves. As seen in figure 4-12 this phenomena is accurately captured by the numerical model, although the exact timing and at which response this event occurs varies again with both material model and geometry.

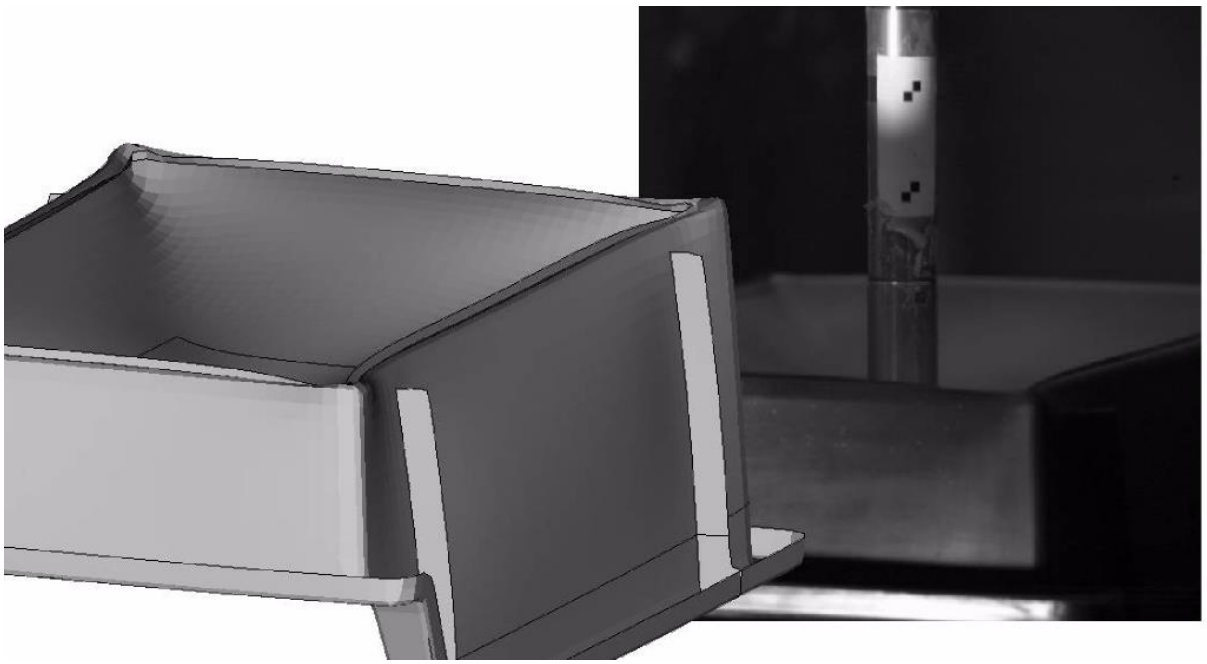

Figure 4-12: CT - Comparison: Numerical model and test

Focus: Viscoelasticity

As all the models capture the key phenomena present for this impact location the discrepancy observed is caused by the material model and the geometry. As the plot in figure 4-11 using a material model with viscoelasticity enabled significantly improves the overall response especially in the first 2.5ms, for which the test specimen is primarily in elastic region as seen in figure 4-13. This suggests that the material used for the boxes are highly viscoelastic which will be seen in the rest of the results as well.

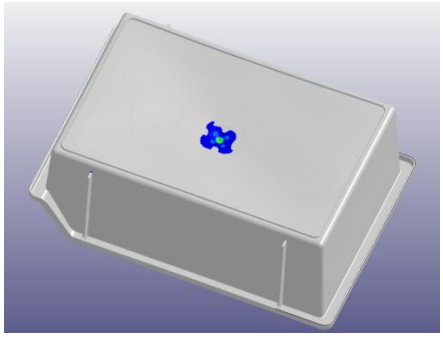

Figure 4-13: Plastic strain at time 2.35ms for centre impact

The centre impact also highlights how using a viscoelastic material model can significantly alter the timing of events and also how the events behave. In the case of the bump between 2.0ms and 2.5ms viscoelasticity causes the bump to occur earlier as it increases the stiffness in the elastic region making the surface wave travel faster. Also because the of this stiffness increase the amplitude of the surface wave is significantly reduced.

Using the SPM with viscoelasticity increases the CPU cost by a factor of roughly 3-5 times compared to the SPM without viscoelasticity. Exactly how much longer CPU time is problem dependent as it depends upon how large part of the model is in the plastic or elastic region.

4.3.2 Sidewall Impact

Overview of Numerical Response

Below is a plot of the key response curves for the sidewall impact based on shell meshes. As the sidewall impacts yield a significant test variability all 5 test results will be displayed in the overview of the numerical response compared to the test results.

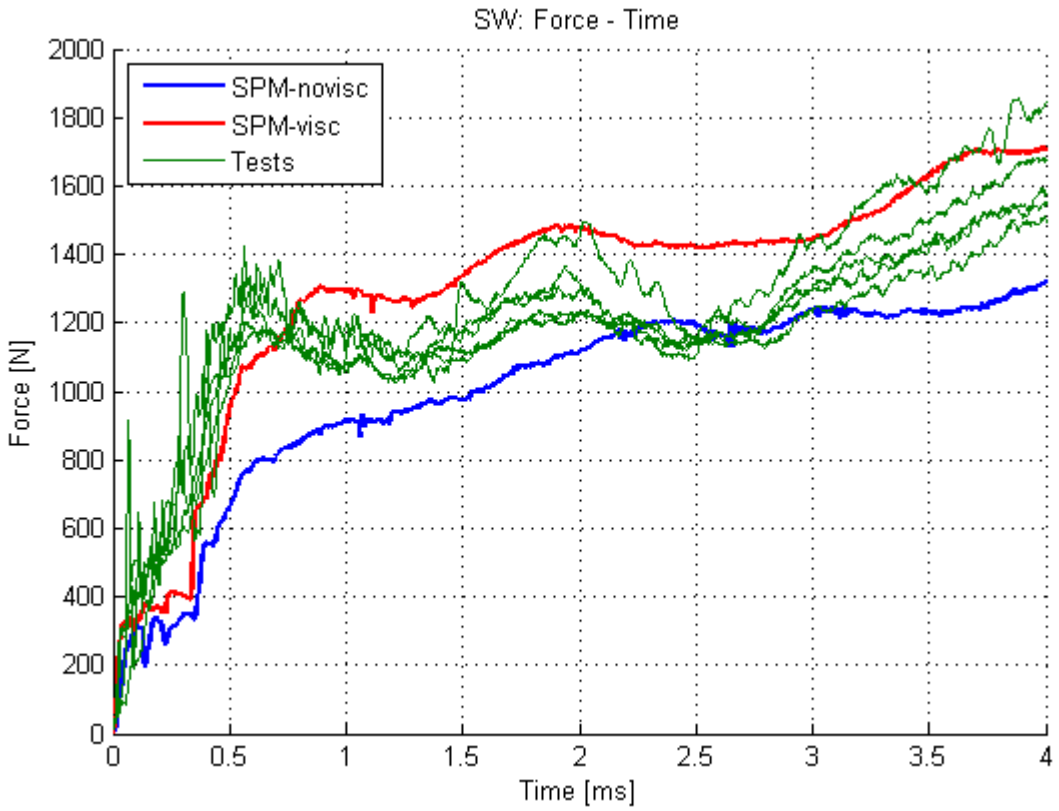

Figure 4-14: Overview of numerical response

Name	Material model	Model and Mesh
SW-SPM-novisc	SPM without viscoelasticity	Final CAD geometry - 2mm
SW-SPM-visc	SPM with viscoelasticity	Final CAD geometry - 2mm

Table 4-4: Numerical models used in figure 4-14

General Comments on the Response

There are two significant phenomena for the sidewall impact as well, both happening during the first millisecond after initial impact. The rest of the response is influenced by very subtle events like a change in the deformation pattern locally around the impactor. The first event occurring between 0.3ms and 0.4ms after impact is contact between the impactor nose and the sidewall. Initially the impactor is only in contact with the impact surface rib such that the total response comes only from the rib. Secondly the first peak is caused by buckling of the sidewall.

As the response curves show, viscoelasticity is essential to obtain good correlation both in terms of response and in terms of events for sidewall impact as well. The general deformation pattern as seen in figure 4-15 is similar for all the simulations.

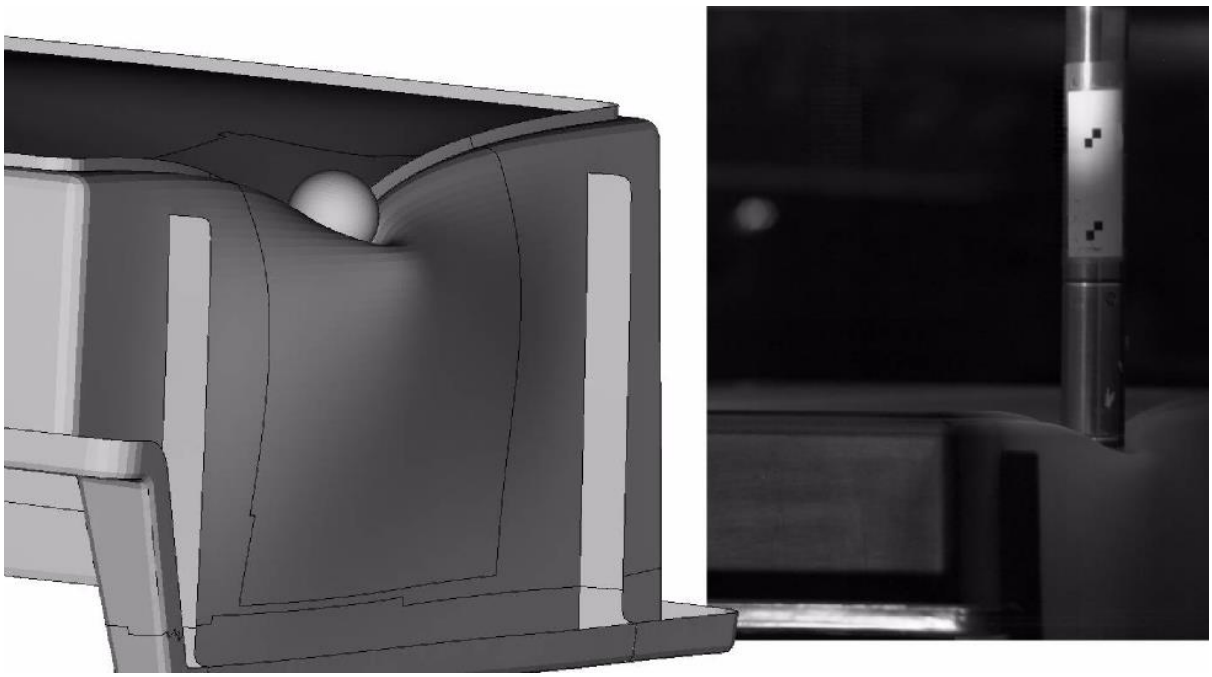

Figure 4-15: SW - Comparison: Numerical model and test

Focus: Geometry Influence

The initial behaviour is very dependent on way the impactor impacts the rib and the time between initial impact and contact with the outer surface. This makes the sidewall impact very sensitive to impact location and any flaws in the geometry, as will be discussed in further detail in this section.

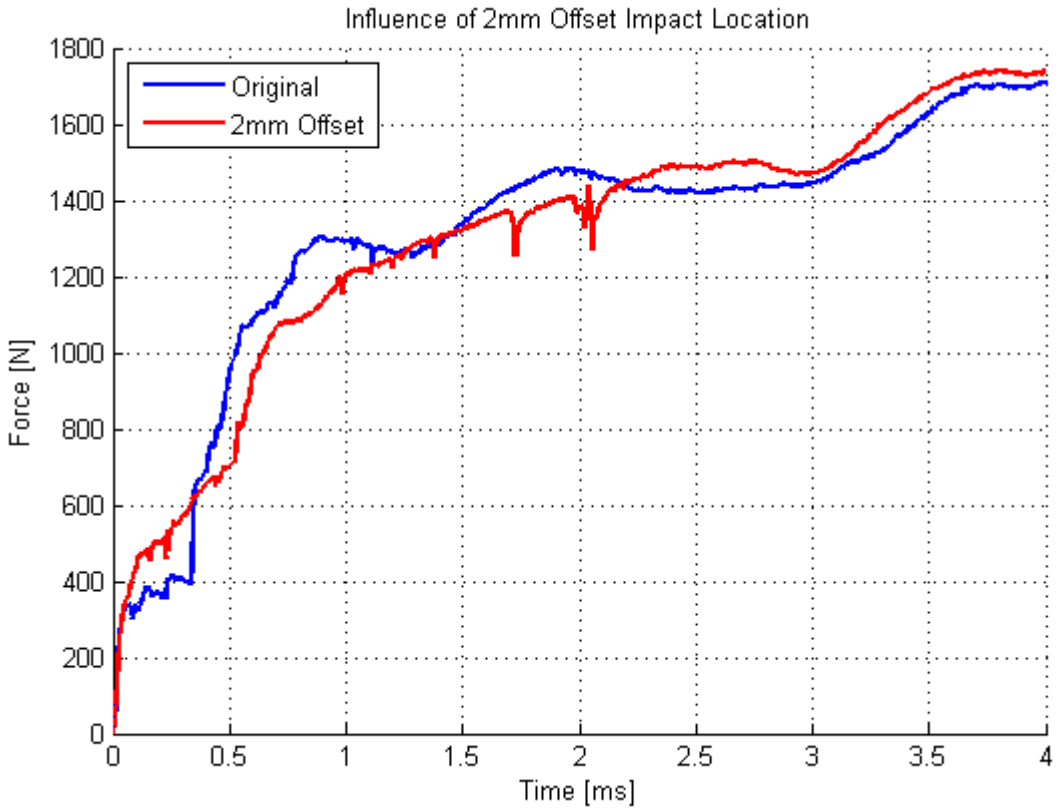

Figure 4-16: Influence of 2mm offset impact location

Comparing the response of the initial model with a model with 2mm offset impact location illustrates the sensitivity of the geometry for the SW impact. As figure 4-16 shows the initial response is different, the first event is delayed which further delays the buckling of the sidewall which in turn changes the behaviour for the rest of the simulation.

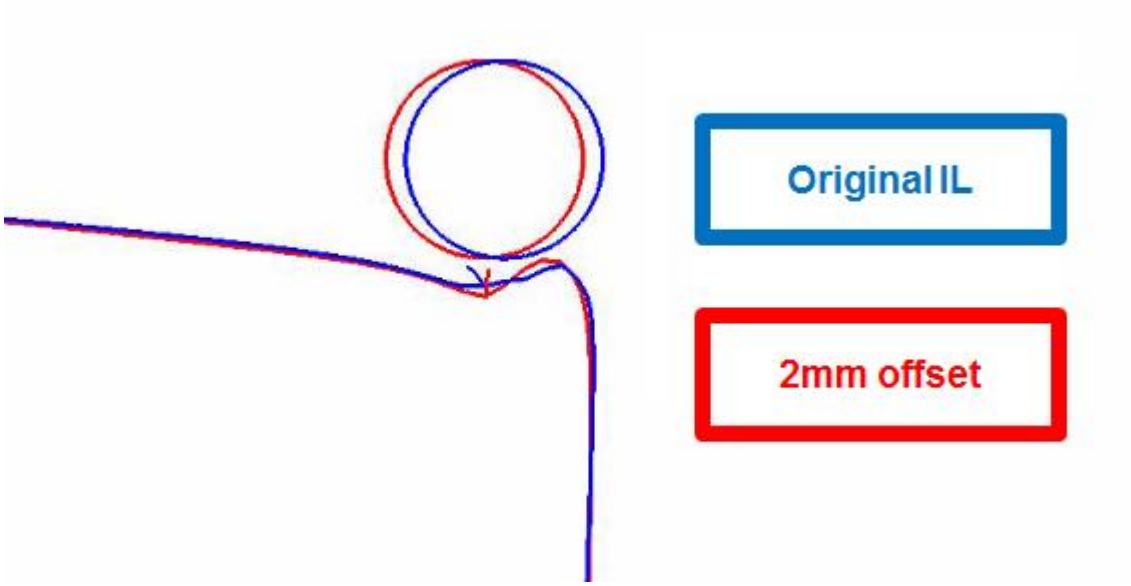

Figure 4-17: Cross section view of comparison original and 2mm offset impact location

The cross section view of these two cases shows how the rib is behaving differently. The original impact location which is further out gives a larger horizontal component to the response making the rib buckle earlier than for the 2mm offset. This changes the deformation pattern on top of the sidewall as can be seen in figure 4-17, which in turn change the conditions for buckling of the sidewall.

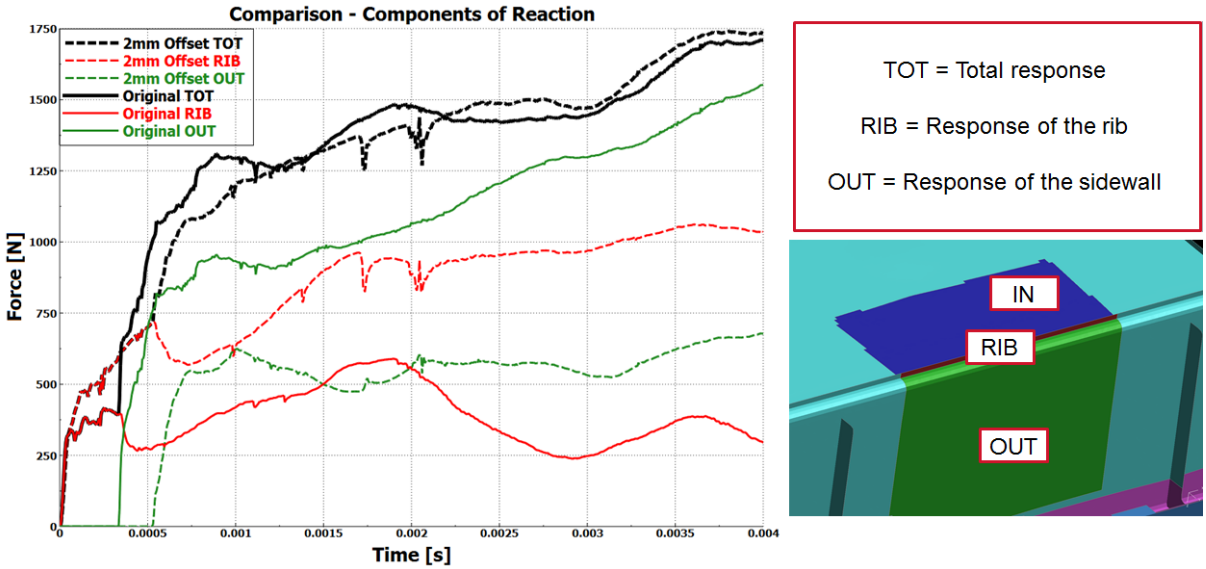

Figure 4-18: Response breakdown of SW impact location study

Breaking the response down to the components coming from the rib and the sidewall reveals how different the component responses are. This is especially critical for fracture events, as it would greatly influence both timing and location of fracture.

4.3.3 Corner Impact

Overview of Numerical Response

Ignoring the test that behaved completely different from the rest there is only a small amount of test variability for the sidewall impact. On that basis it is chosen to use one representative test with the least amount of noise for comparison.

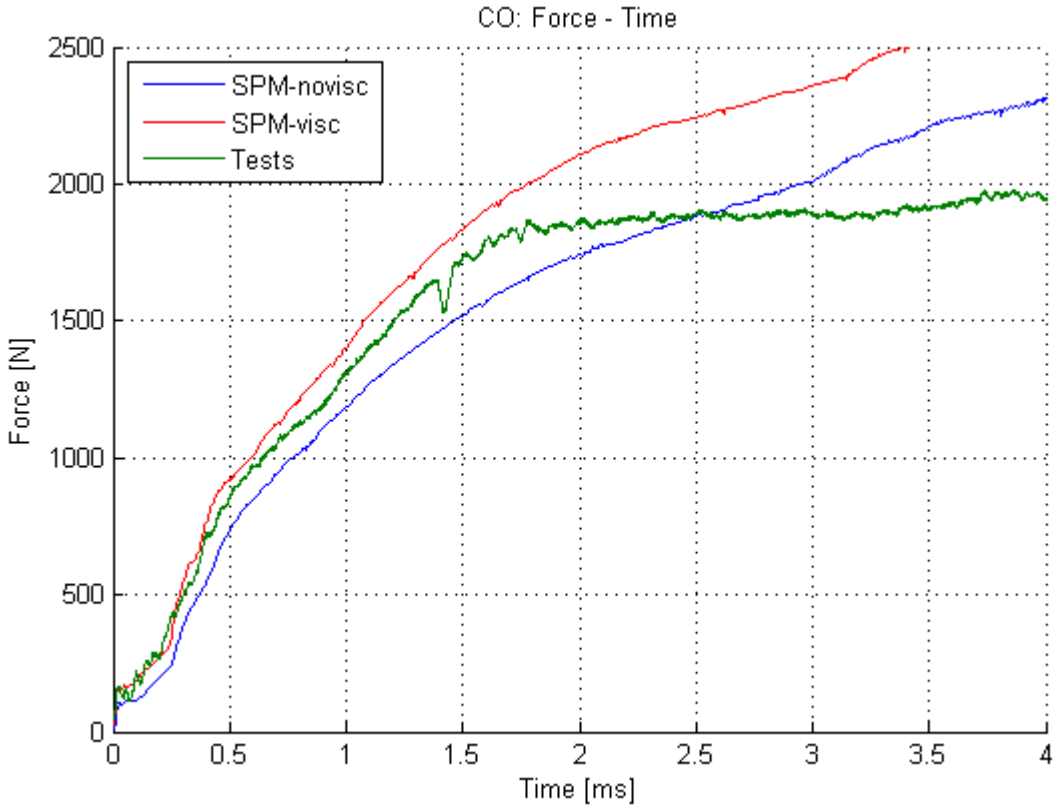

Figure 4-19: CO: Overview of numerical response

Name	Material model	Model and Mesh
CO-SPM-novisc	SPM without viscoelasticity	Final CAD geometry - 2mm
CO-SPM-visc	SPM with viscoelasticity	Final CAD geometry - 2mm

Table 4-5: Numerical models used in figure 4-19

General Comments on the Response

There are 3 key events to be captured for the corner impact. The sudden change of stiffness at roughly 2ms is caused by the impactor making contact with the impact surface rib, which is properly captured in all the simulations. The second event causing the first plateau in the response is likely cause by cracking on the inside of the corner. This cracking is not observed in the videos from the testing as the crack location is not visible, however there are some subtle indications to a sudden softening in the area. The next section will go more in detail on the numerical evidence that strongly suggest that this cracking is cause of the plateau in response. The third event is a fracture on the top of the sidewall rib, this fracture occurs at roughly 2.8ms. The top of the sidewall rib fracture has a negligible influence on the response initially, but it allows for a different deformation pattern further on. This last fracture is not captured using common shell mesh sizes as 5mm and 2mm, but a very refined shell mesh or a solid mesh is able to capture this event.

The response of the numerical model is until the cracking event almost exact using SPM with viscoelasticity. The deformation pattern is as well more or less identical until that point as figure 4-20 shows.

Figure 4-20: CO – Comparison: Numerical model and test

Focus: Fracture

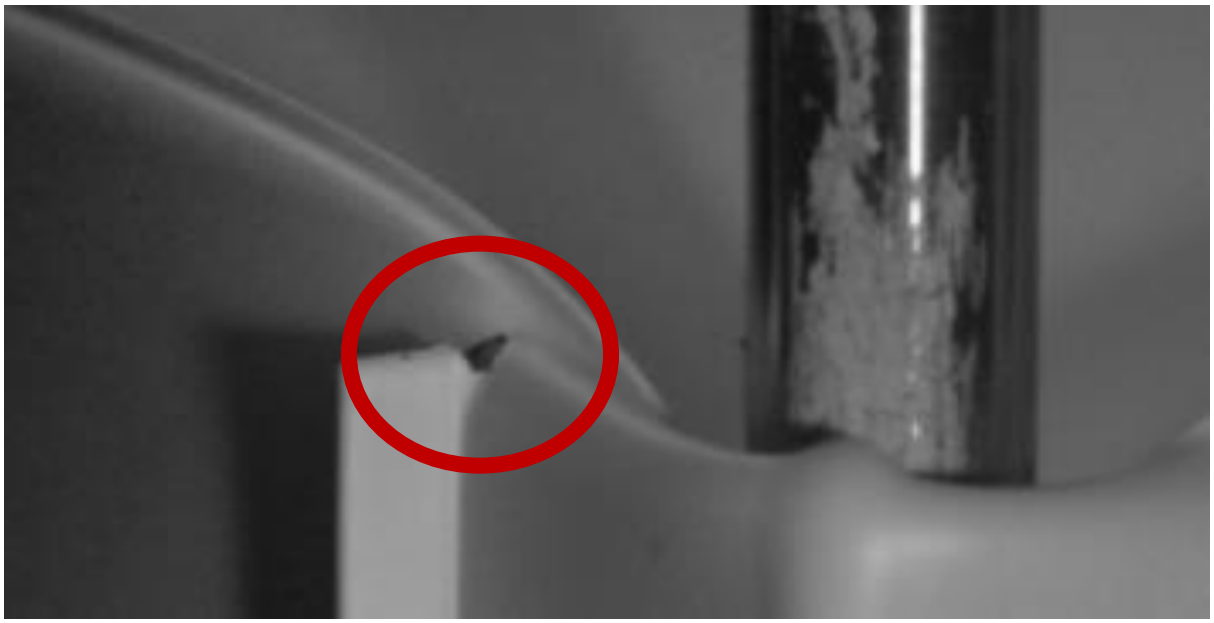

Figure 4-21: Top of sidewall rib fracture

The way fracture is currently implemented it deletes an element as soon as one of the integration points reaches a critical value in the selected fracture criteria. This means that for a shell element in bending where only the outer integration point in tension reach a critical value the whole element will be deleted. This means that with the current implementation it is impossible to properly represent cracking on one surface with shell elements. Shell elements should however be able to capture the fracture on top of the sidewall rib as depicted in figure 4-21.

The two fracture criteria implemented in the SPM are both based on the stress/strain state as mentioned in chapter 2.4, and the stress/strain state is in turn mesh dependent. This makes fracture mesh dependent, which will be studied next using the sidewall rib fracture.

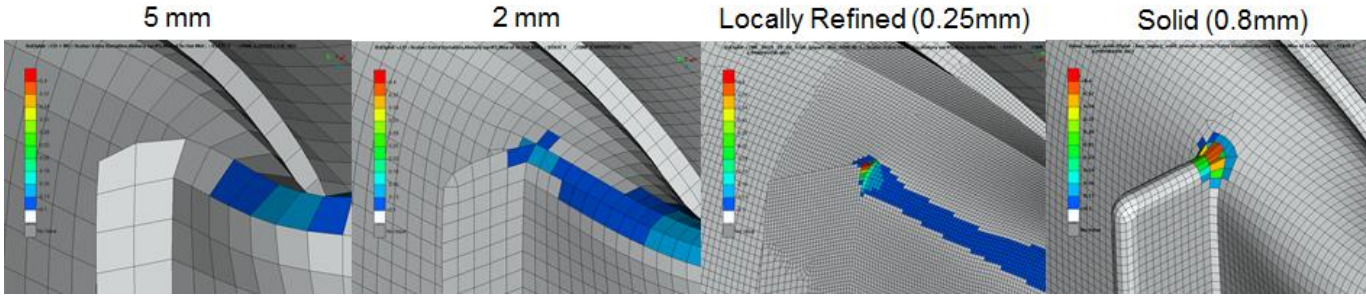

Figure 4-22: Mesh dependency of fracture 1

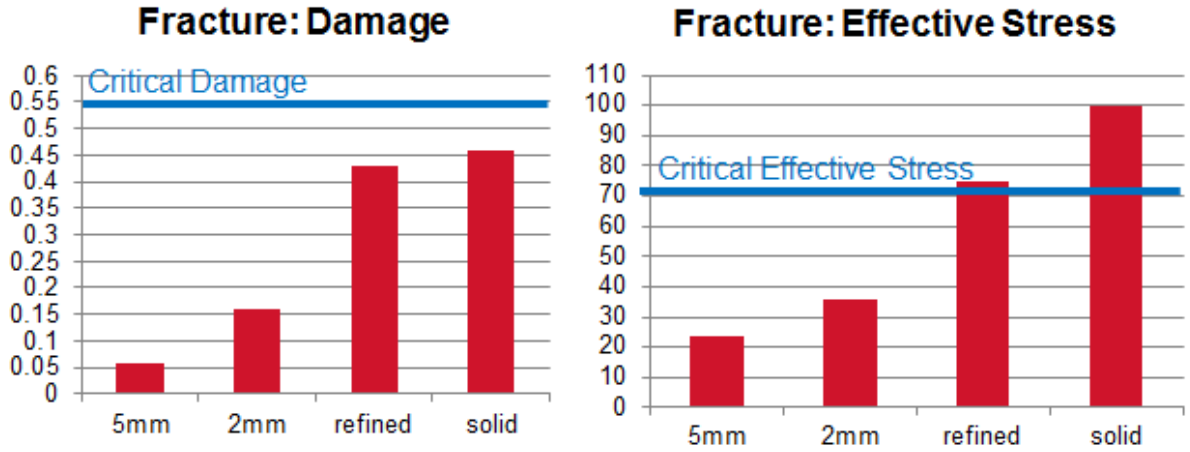

Figure 4-23: Mesh dependency of fracture 2

The fracture parameters displayed in the bar graph is based on the most critical integration point on top of the sidewall rib at a specific time.

The above figures show that the top of the sidewall rib fracture is highly mesh dependent. For the standard mesh sizes 5mm and 2mm the top of the rib is not even the most critical point in the area. Which means that for these meshes fracture will occur at a different location than the real one and at a completely different time. For this type of fracture it is required a very refined shell mesh to capture the fracture at the correct time and location. This is due to the fracture being caused by a stress concentration created by the discontinuous geometry causing large stress gradients which in turn require a very fine mesh to properly describe. Using a solid mesh instead of a shell mesh the actual geometry of the problem area is captured much better which in turn allows for a larger mesh size than with shell elements to capture the fracture.

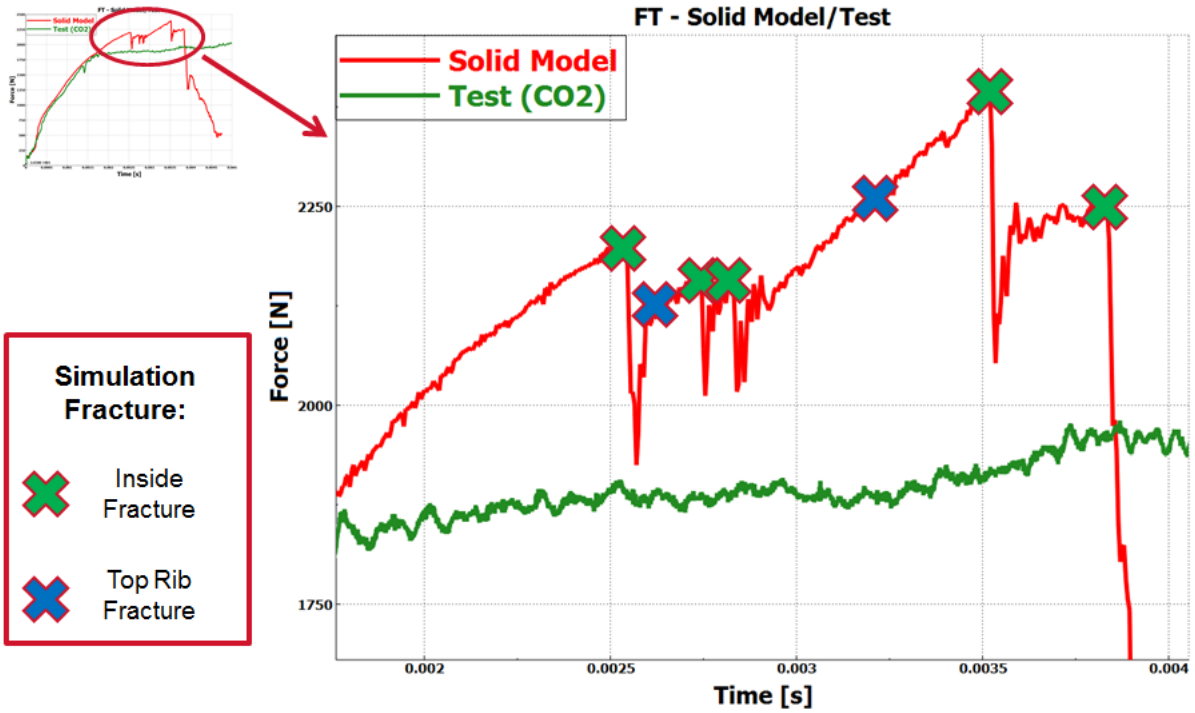

Figure 4-24: CO: Response of 0.8mm solid model

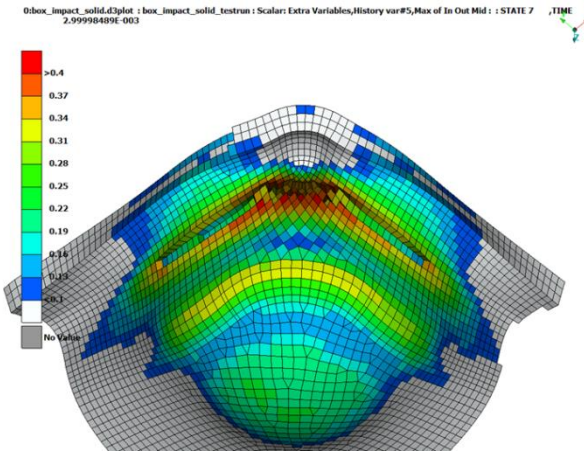

Figure 4-25: CO: Crack at t=2.3ms

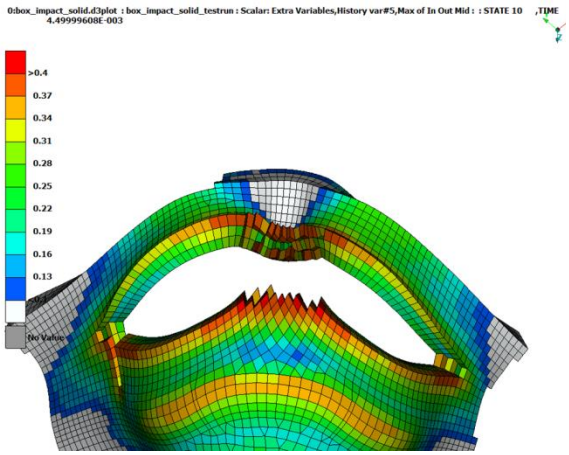

Figure 4-26: CO: Crack at t=4.3ms

Further analysis of the solid model gives a strong indication that the first plateau in the response is caused by cracking on the inside on the corner as the above figures show. As the figures show the inner layer of elements fracture emulating cracks, this makes the cross section transition from carrying in bending to pure tension. However as this model is based on 0.8mm solid mesh it is only 3 elements through the thickness each fracture causes a significant drop in response in addition to making the crack too deep. The end result is that the crack propagates through the cross section instead of stabilizing.

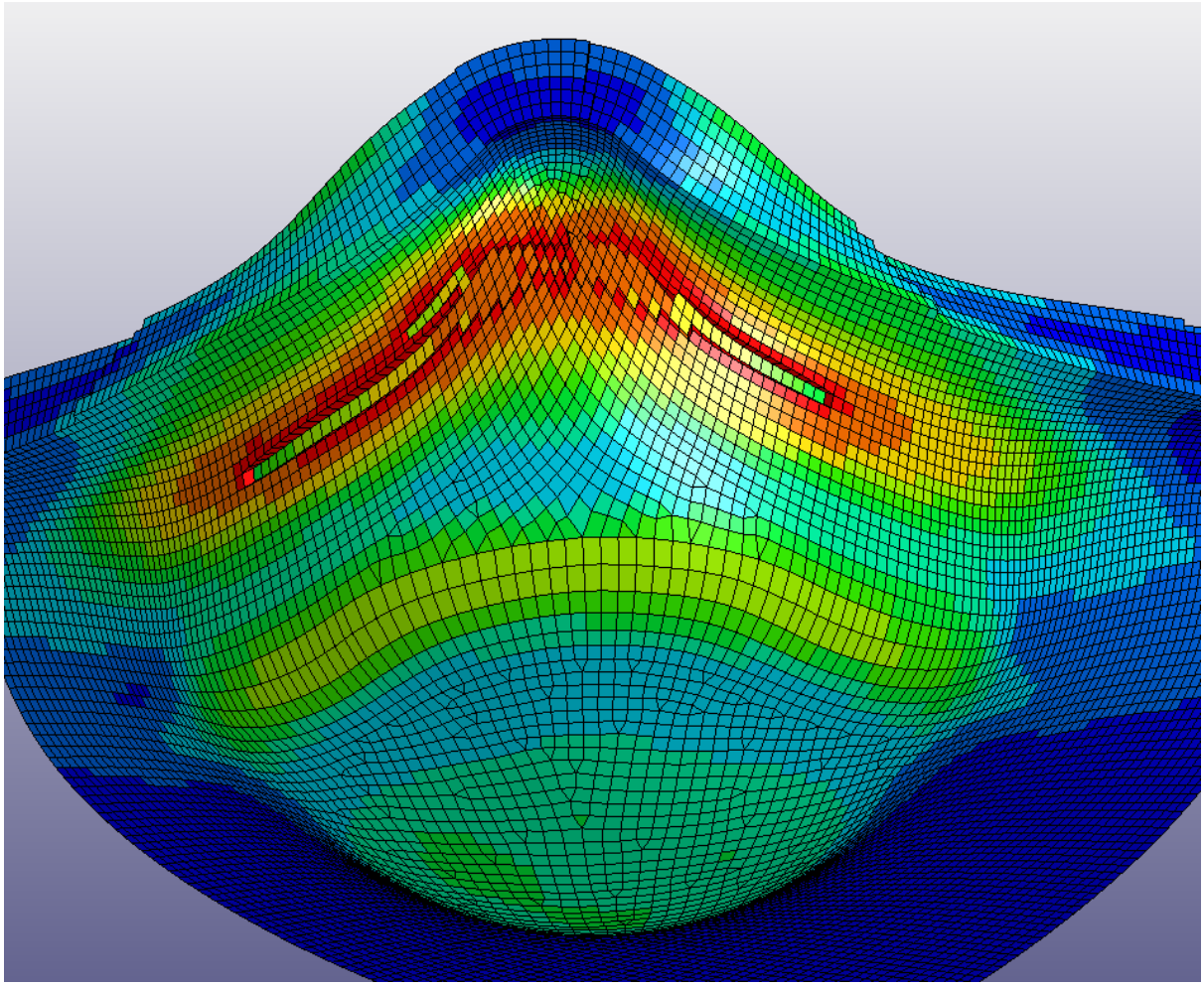

Figure 4-27: CO crack in 0.4mm solid mesh

Figure 4-27 display how a 0.4mm mesh is able to represent a shallow crack which leads to smaller drops in response compared to the 0.8mm mesh and thus better capturing the response of the tests. In general the critical damage calibrated has been too high to activate fracture as it does not take strain rate into account. The result is that the effective stress criterion has been the critical fracture parameter for all the simulations. A drawback with the effective stress criterion is that is very mesh dependent, using the effective stress criterion for this 0.4mm solid mesh makes the fracture propagate so fast that it completely fractures much earlier than the 0.8mm solid mesh. To create the crack seen in figure 4-27 it is used a damage based fracture criterion with a critical value adjusted to ensure initiation at the correct time.

In summary this section highlights some of the key problems with fracture in the current implementation of the SPM. It is in general very mesh dependent and the fracture model is too simple to properly capture strain rate sensitivity and stress state.

4.3.4 Sensitivity Study Summary

A short summary of the results from the several sensitivity studies performed on the box impacts is presented in the table 4-5.

Parameter	Comment
Mesh size	The influence of mesh size on fracture is covered in detail in section 4.3.3. Else refining the mesh generally softens the response and is necessary to capture subtle details depending on the complexity of the geometry. For this project the primary mesh sizes have been 5mm and 2mm, and the CPU cost of going from 5mm to 2mm has been roughly a factor of 6 using shell elements. In theory the CPU cost of halving the element size should lead to roughly 8 times increase in CPU time with shell elements as the number of elements is increased by a factor of 4 and the critical timestep is halved.
NIP	The effect of the number of integration points through thickness of shell elements (NIP) on the component response is negligible. Taking the skin-core effect [1] this might change. For elements that should fracture in bending the position of the integration point furthest from the centre line is critical. Thus using 5 instead of 3 NIP will significantly alter the timing of fracture for a given element. Going from 5 to 7 NIP makes a much smaller difference. In terms of CPU time, it is proportional to NIP when using the SPM.
Friction coefficient	The friction coefficient between the metal impactor and the plastic specimen and between the wooden fixture and the plastic specimen has been studied, and both of them have a negligible influence on the response.
Impact location	As section 4.3.2 covers in detail impact location can have a large impact on the response. This sensitivity towards impact location is also observed for the two other impact locations.
Element formulation (shell LS-Dyna)	The two element formulations investigated during this project is element formulation 2 and 16. El. form. 2 is a reduced integrated element with hourglass stabilization and el. form. 16 is fully integrated. When using the SPM with viscoelasticity it will generally give a too stiff solution, such that using el. form. 2 which softens the response will improve the result. Meaning in general using el. form. 2 is optimal unless significant hourglassing is observed.

Table 4-5: Summary of sensitivity study

4.4 Summary

Overall accuracy of the simulations considering the issues with geometry has been good. Looking at energy absorbed until fracture or until brakes are applied is roughly within 5 % using the SPM with viscoelasticity. Looking at the response of the corner impact (see section 4.3.3) until fracture occurs the response is almost exact, indicating that the potential accuracy for problems where fracture is not occurring is very high.

The box study shows that viscoelasticity is critical to obtain a good response for this material. It influence whether or not events occur and the behaviour of such events as covered more in detail in section 4.3.1. With the SPM the cost in terms CPU time using viscoelasticity is a factor of 3-5 depending on the problem.

It is also observed that this type of impact problem is sensitive to geometry. This is indicated by the sensitivity to impact location covered in section 4.3.2. However as mention in section 4.1 it has been run a plethora of simulations on multiple of iterations of the geometry which is not covered in detail. The overall results of these simulations show a large spread in results depending on the geometry.

Fracture is in its current implementation unreliable. As section 4.3.3 covers in detail a there is a strong mesh dependency, in addition to the fundamental limitation that a sufficiently accurate mesh is needed to properly capture the stress/strain state first. Some of the limitations of the simple fracture model are also observed in this study as fractures under different conditions are captured with different accuracy. One of the issues is that strain rate sensitivity to fracture is not taken into account for the damage based fracture and partly compensated for with the effective stress based fracture.

The sensitivity study shows that the response of the component is sensitive to mesh size, impact location and element formulation. If fracture is relevant to the problem the number of integration points through the thickness of shell elements become significant as well.

5 Numerical Study: Lower Absorber

5.1 Introduction

The purpose of the numerical study of the lower absorber is to perform a validation of the SPM on an industry relevant component with complex geometry and loading. The goal is to find the limitations, which phenomena can be represented with a standard shell mesh and what is necessary to get the full picture. In addition TME has an interest in quantifying the performance of SPM in terms of increased accuracy and cost compared to their currently implemented material model (MAT81 LS-Dyna).

Mesh	Material Model	Response		
		Initial Stiffness	Peak Load	Max. Disp.
5mm	SPMvisc	Δ	○	s
	SPMnovisc	Δ	○	○
	MAT81	x	Δ	Δ
2mm	SPMvisc	Δ	s	s
	SPMnovisc	Δ	○	Δ
	MAT81	x	Δ	x
Solid elements in impact area	SPMvisc	s	-	-
	MAT81	Δ	-	-

Table 5-1: Simulation overview

Very good	s
Good	○
Poor	Δ
Very poor	x

Table 5-2: Simulation legend

A total of 38 simulations were run of the lower absorber. Most of the simulations run were run to identify the reason behind the poor initial stiffness and to study the sensitivity of the response to changes in the fixtures. This chapter will focus on the key results obtained from the 2mm mesh size and the model with solid elements in the impact area. The results of the CI45 simulations are not presented due to the large test variability covered in section 3.2.3.2.

5.2 Modelling

5.2.1 Shell model

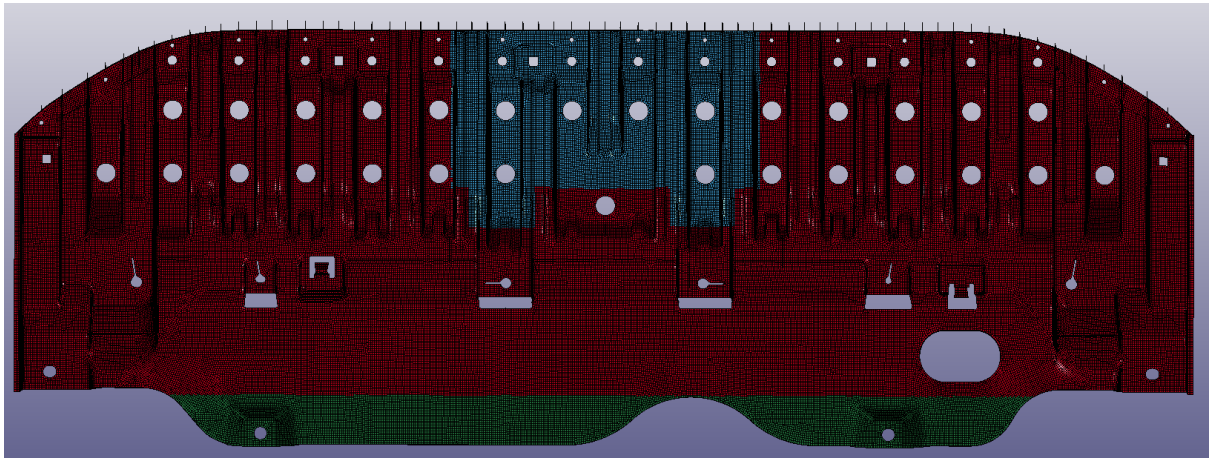

Figure 5-1: Overview of LA shell mesh

Figure 5-1 displays an overview of the 2mm shell model of the lower absorber. The LA is made of 202962 shell elements separated into 3 different parts. The 3 parts are separated as to reduce the CPU time on contact algorithms.

The shell mesh was made from scratch based on the CAD geometry during the course of this project as the initial 5mm mesh provided by TME was of poor quality. This has enabled an automatic thickness mapping where the thickness is defined for each node on each element. Some of the more complex parts of the geometry as seen in figure 5-2 had to be rebuilt manually and thus also thickness mapped manually which might not be the best representation of the real part.

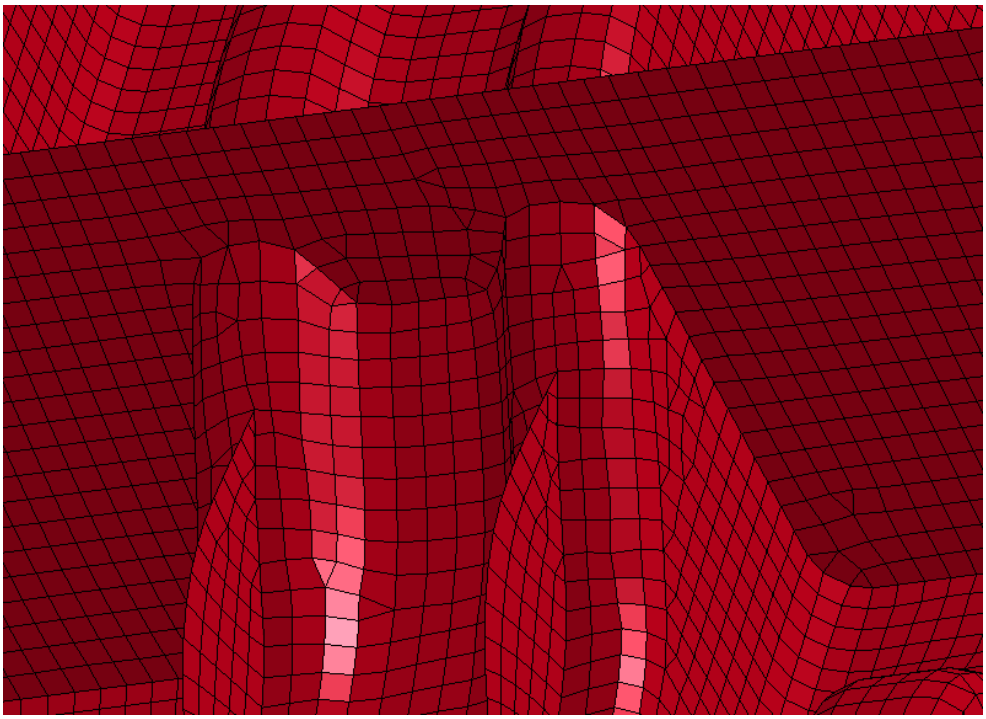

Figure 5-2: Manually rebuilt area.

5.2.2 Solid impact area model

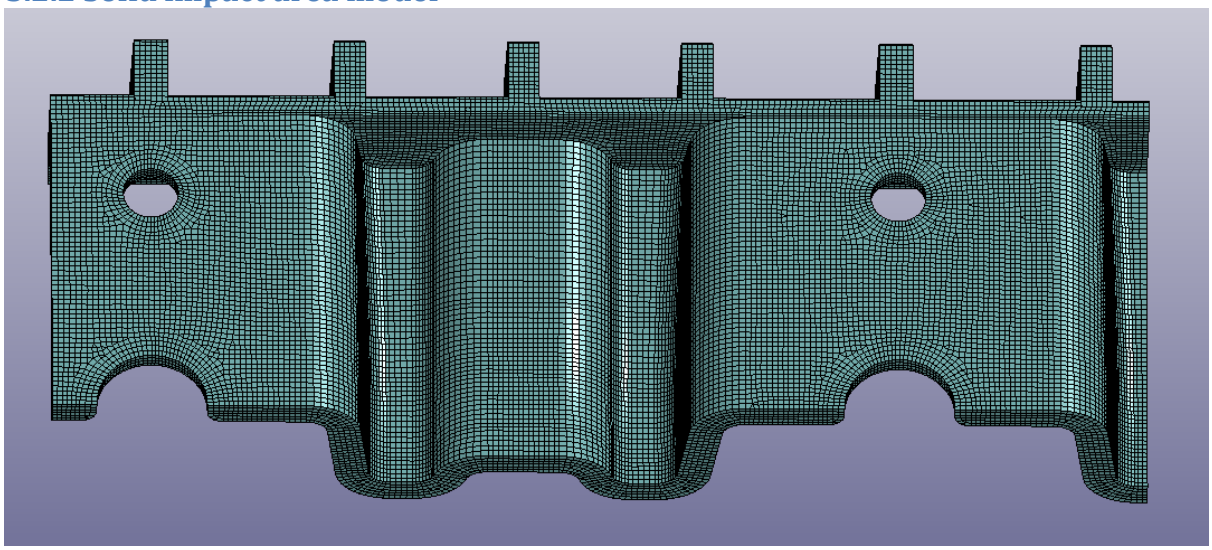

Figure 5-3: Solid elements in LA solid impact area model

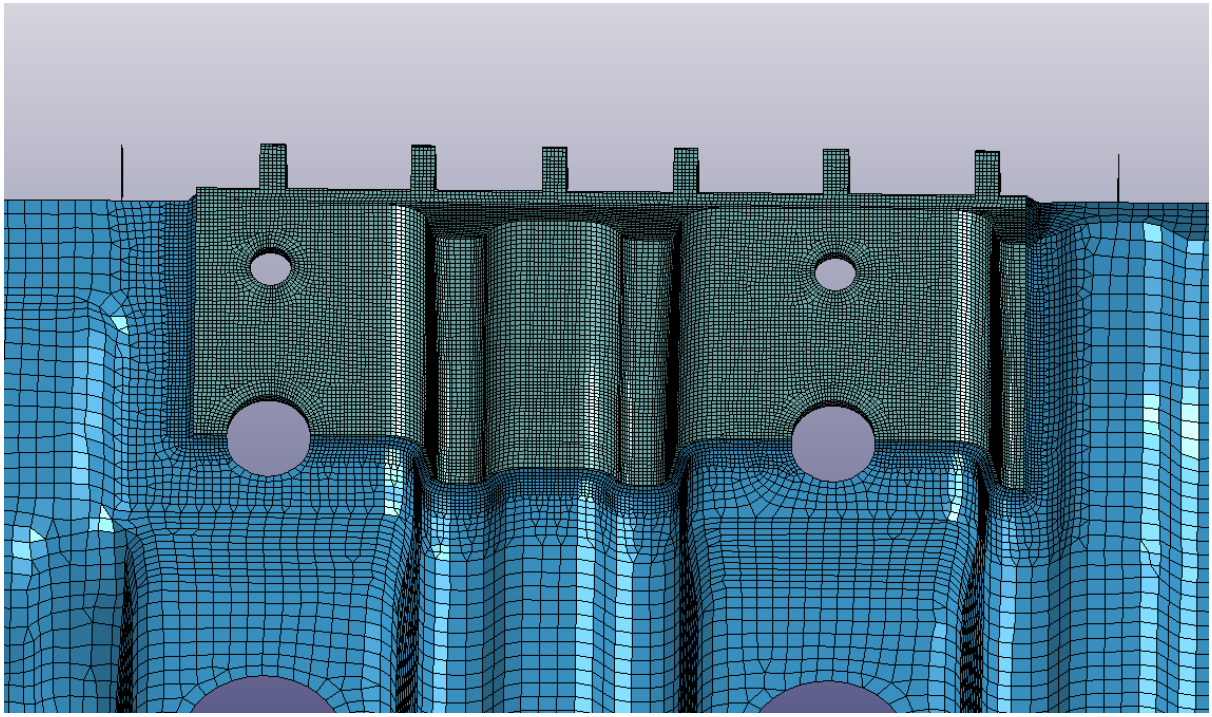

Figure 5-4: Solid elements connected to shell mesh

The solid part of the model as seen in figure 5-3 by itself consists of 212950 solid elements with a general mesh size of 5mm giving 6 elements through thickness. The solid part is covered in shell elements to define contact.

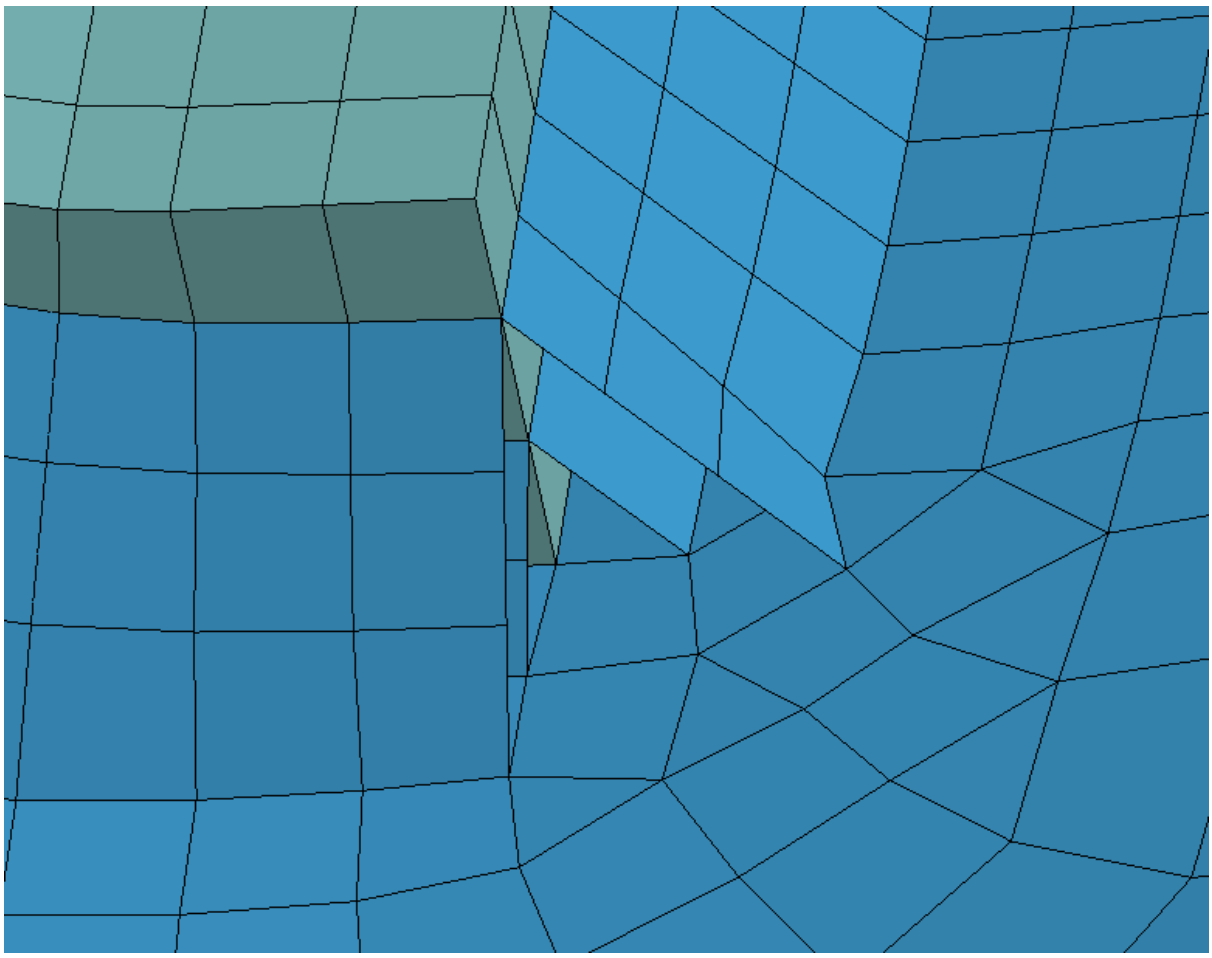

Figure 5-5: Connection between solid and shell elements

This model with solid elements in the impact area was done late in the project with very limited time with the only purpose of investigating the initial stiffness. Because of this a simplified connection between the shell and solid elements were used. This simplified connection as seen in figure 5-5 is overly stiff and do not properly transfer forces such that it generates fictional stress concentrations. However until it starts to deform significantly the results from this model should be reliable.

5.2.3 Fixtures

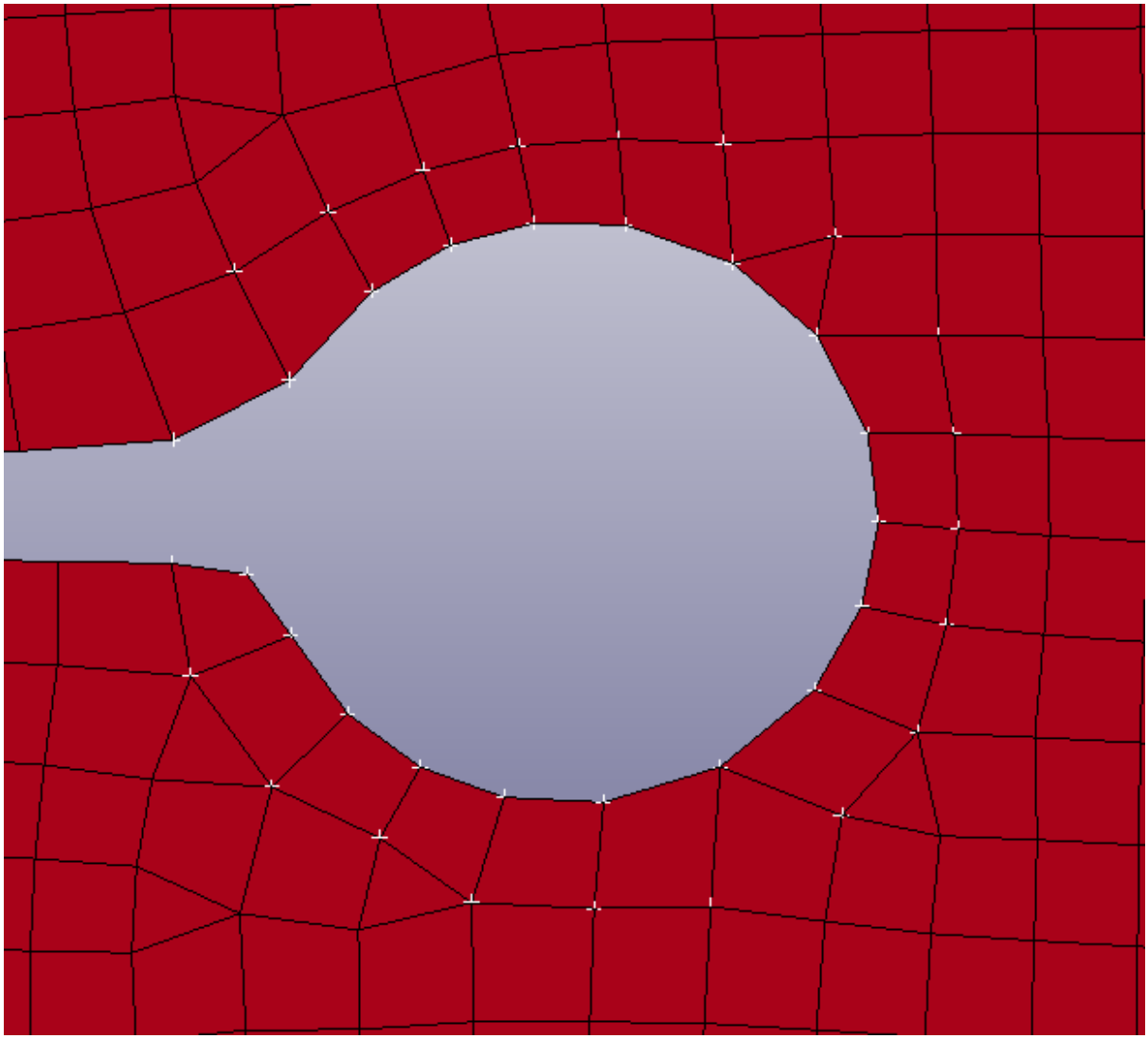

Figure 5-6: Bolt hole SPC boundary conditions

The bolts are represented with fixed boundary conditions that restrain translations and rotations in the nodes. Figure 5-6 displays which nodes around a bolt holes that are fixed.

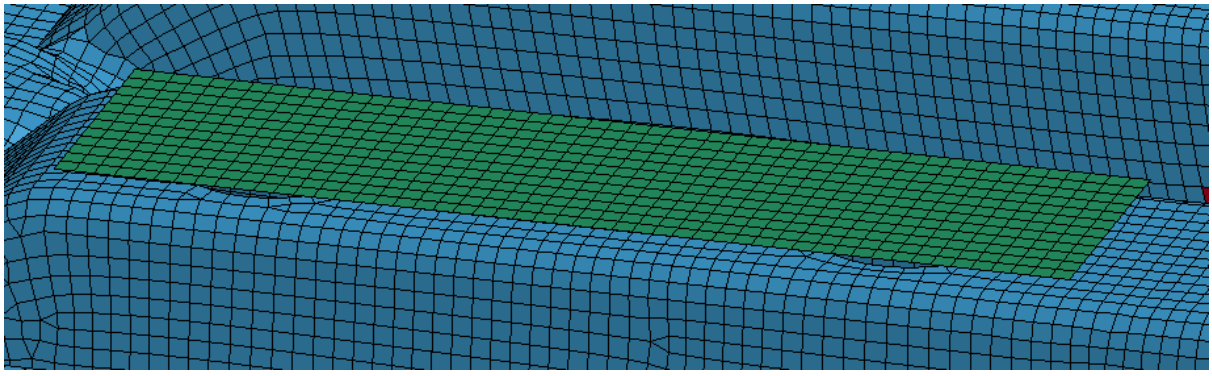

Figure 5-7: Front wooden fixture model

The front wooden fixtures are represented by a surface that is parallel to the LA as seen in figure 5-7. The general mesh size of the fixtures is 2mm to match the mesh size of the lower absorber. All the fixtures used are assumed rigid and modelled with MAT_RIGID. There were not observed any major deformations on the wooden fixture during the tests, such that a rigid assumption is valid, however they did move slightly in the last setup and this is not captured by the model.

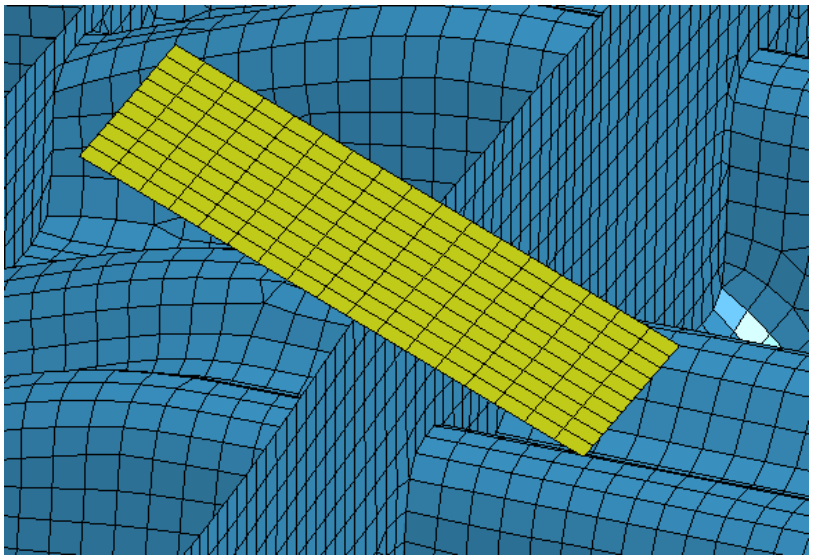

Figure 5-8: Back wooden fixture model

The back wooden fixtures are modelled in the same way as the front wooden fixtures as a rigid surface. The angle is the same as observed during tests. Using this angle it acts almost as a rigid boundary condition, however the way it is modelled allows for some displacement in the area which corresponds with the tests.

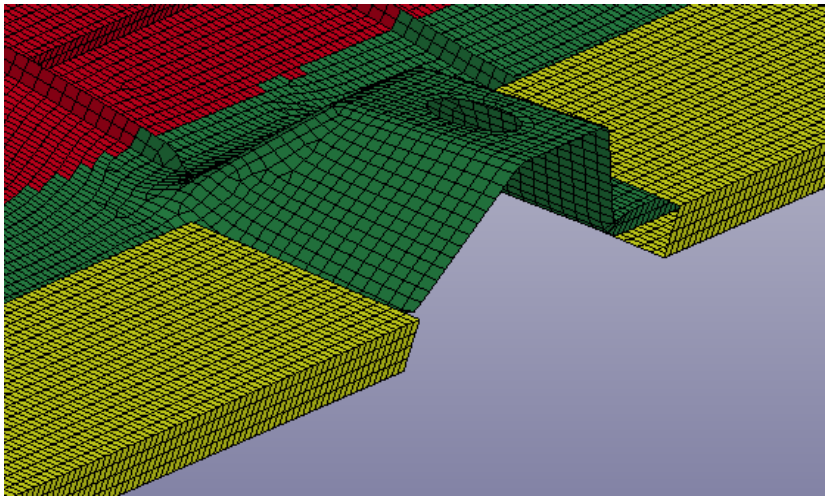

Figure 5-9: Bottom fixture

The bottom fixture is roughly modelled to have the same function as the bottom fixture in the tests, which is to restrict large vibration of the bottom part of the lower absorber. Else it is modelled the same as the wooden fixtures as rigid surfaces.

5.2.4 Impactor

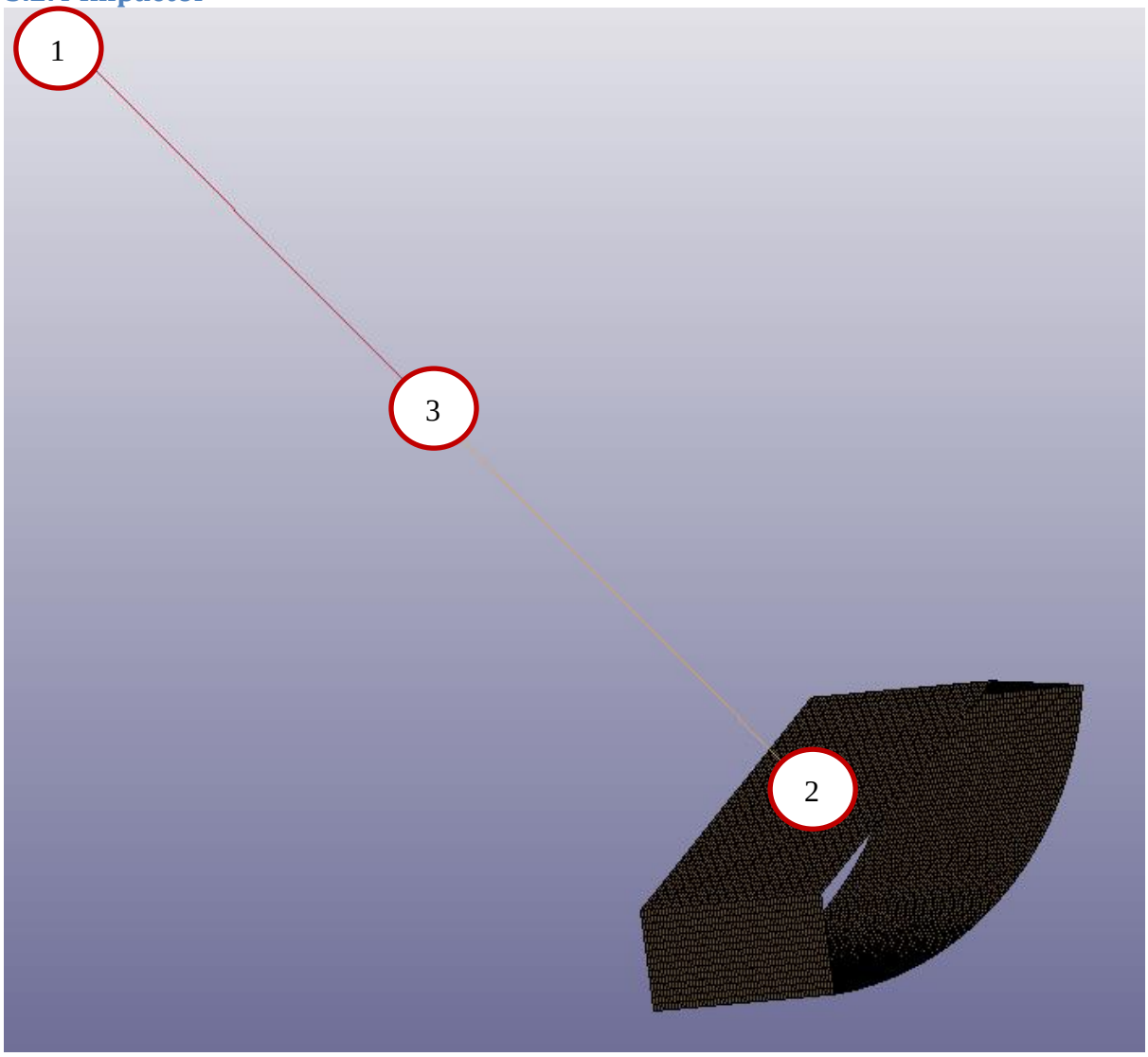

Figure 5-10: Full impactor model with key points marked

The impactor model for the lower absorber consists of both the impactor rod as described in section 3.1.2.3 and the lower absorber impactor nose. The upper part of the impactor is modelled as a mass element in point 1 on figure 5-10. The impactor rod itself is modelled as 2 beam elements with diameters 30mm and 20mm, using steel as material. There is also added a mass element in point 2 on the figure to adjust the total impactor weight to the correct one and to take the connection between impactor rod and nose into account.

The whole impactor model is only fixed in one point namely point 1 in figure 5-10. In this point it is restricted against out of plane displacements and rotations, however it is allowed to move in the impact direction and freely rotate around the impact direction axis. The nodal displacements and rotations are monitored at point 3 in the model to track vibrations of the impactor rod.

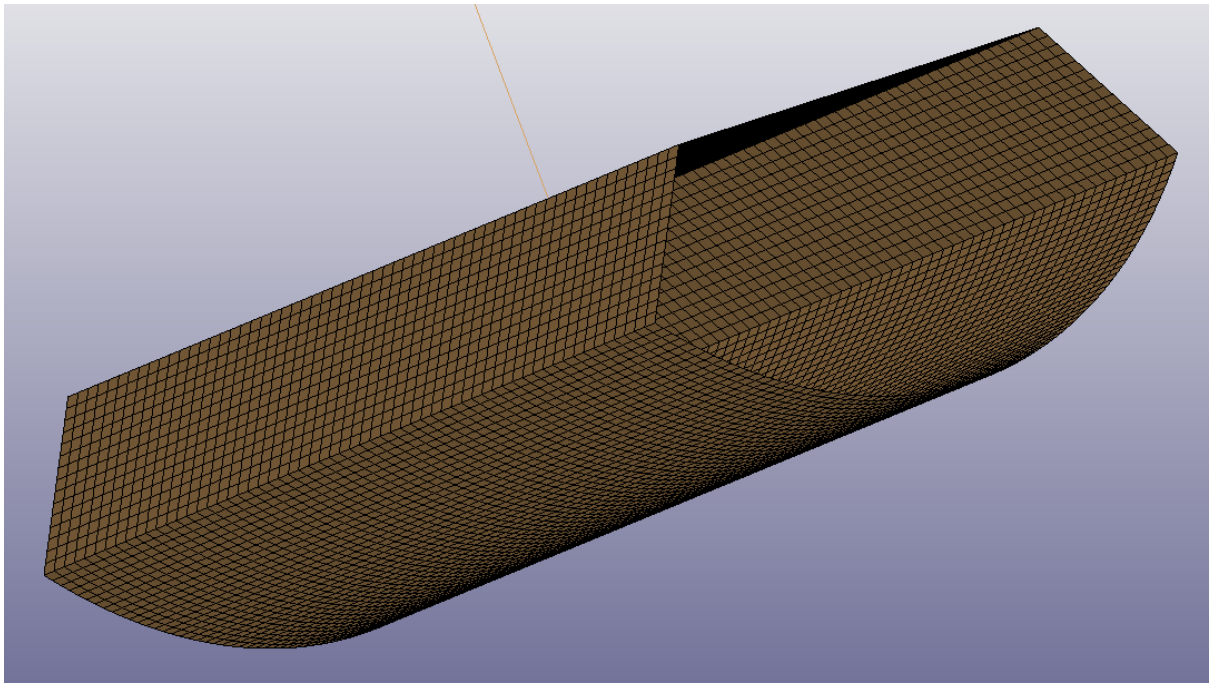

Figure 5-11: LA impactor nose

The impactor nose itself is modelled with a 2mm shell mesh using a rigid material MAT_RIGID. The impactor nose model consists of in total 9000 elements and the mass is adjusted to the correct mass as measured in the lab of 1.660kg.

5.2.5 Contact

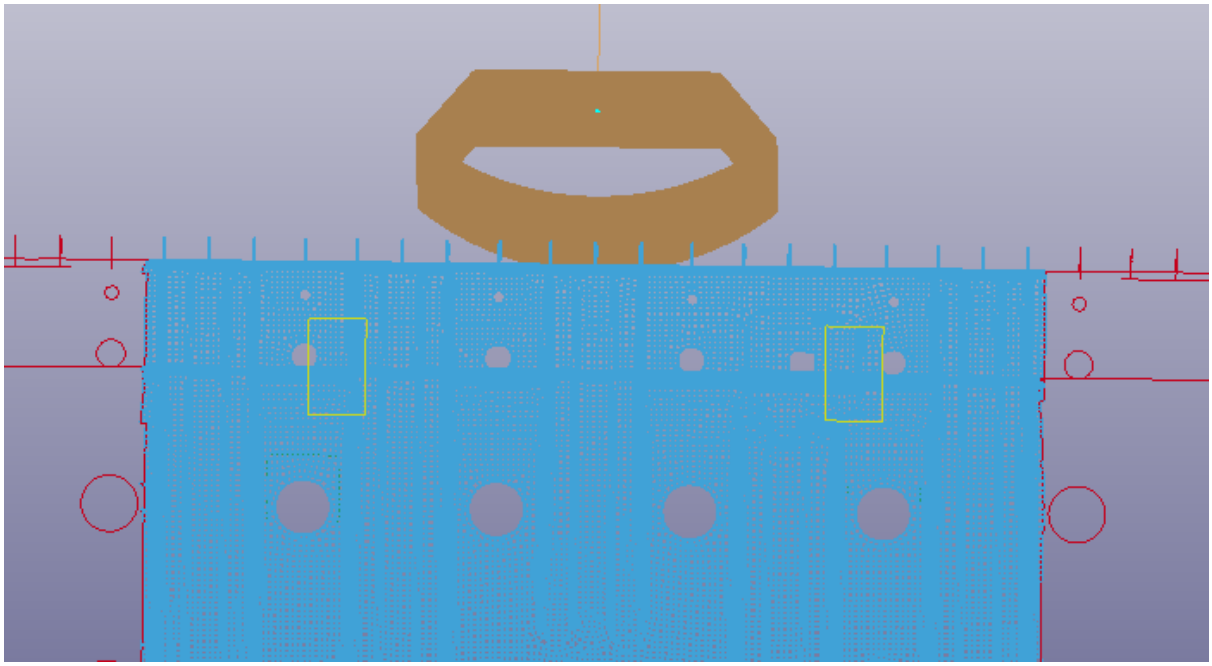

Figure 5-12: Contact area

The contacts are based on the parts as seen in figure 5-12. All contacts except for self-contact in the impact area are defined with CONTACT_AUTOMATIC_SURFACE_TO_SURFACE with standard values except for friction. The self-contact is defined with CONTACT_AUTOMATIC_SINGLE_SURFACE using standard values.

5.3 Results

5.3.1 Shell Mesh Response

Below is the filtered response of the key full shell element simulations performed on the lower absorber. The comparison is done with a CFC180 filter due to the oscillations observed in the test results, further details on this in section 3.2.3.1.

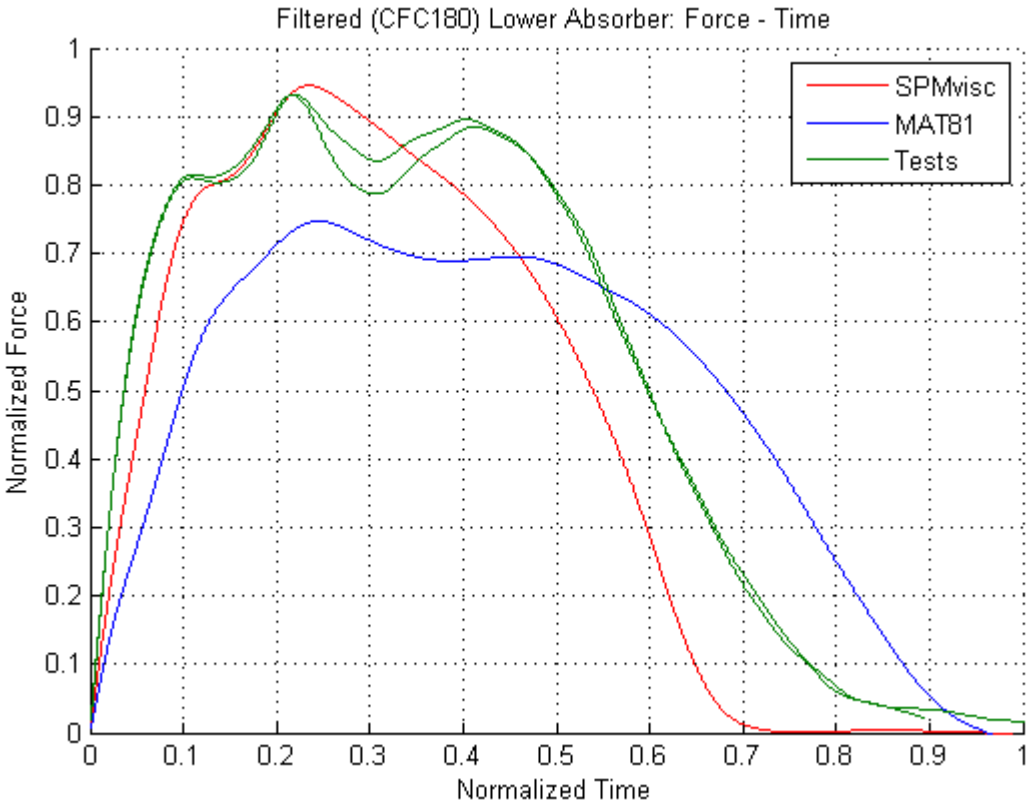

Figure 5-13: Filtered LA response – FT

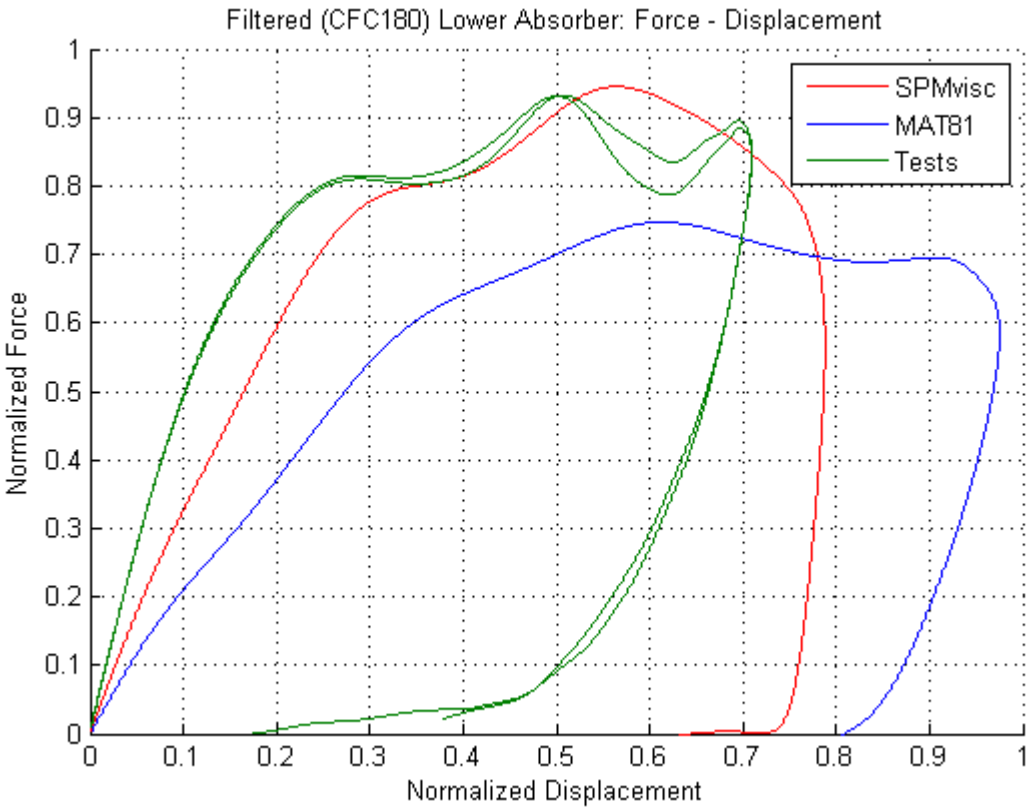

Figure 5-14: Filtered LA response - FD

The red curve represents the 2mm mesh seen in section 5.2.1 with element formulation 2 and 3NIP using the SPM with viscoelasticity. The blue curve is based on the exact same model but with a different material model, the one TME is currently using for their polymer parts. The material model in the blue curve is a standard LS-Dyna material MAT81 with tabulated damage and plasticity using a von Mises yield surface.

These results highlight the benefits with using a research based material model compared to a standard material model. The key parameters from an industry point of view namely initial stiffness, peak response and maximum displacement all show a large improvement in accuracy. However this increase in accuracy comes at a cost in terms of CPU, going from MAT81 to the SPM without viscoelasticity means an increase in CPU time by a factor of roughly 15, and going from MAT81 to the SPM with viscoelasticity is roughly a factor of 50.

Detailed Analysis of Events: Shell Model – Tests

This section will cover the key events occurring in the LA tests to see which events are captured by the shell model and which are not and how they influence the response.

First event, not covered in section 3.2.3.2, is the initial deformation of the front wall where the rib +1 and rib -1 are crushed into the front wall as seen in figure 5-16. This event is not captured by the shell mesh, instead of large deformations in the shell elements connected to the ribs the ribs buckle instead. This buckling significantly reduces the initial response as will be covered more in detail in section 5.3.2. The reason to why this event is not properly captured is that the shell model is not able to properly capture the complicated geometry in the area of interest.

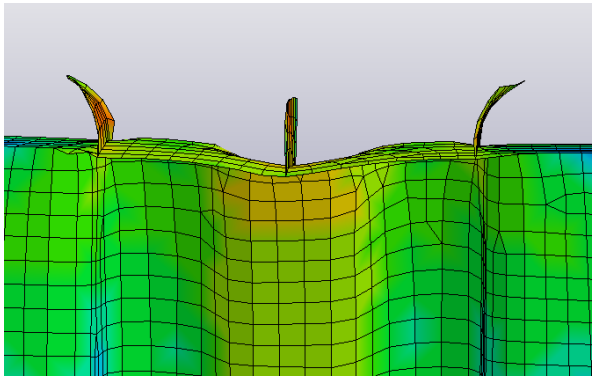

Figure 5-15: Rib buckling

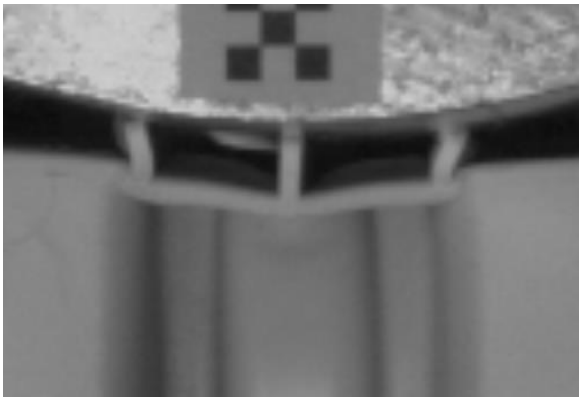

Figure 5-16: Initial crushing

The first peak which is caused by initiation of the first buckling pattern is captured in the shell model as seen in figure 5-17 and 5-18, however it is slightly delayed due to the reduced initial stiffness.

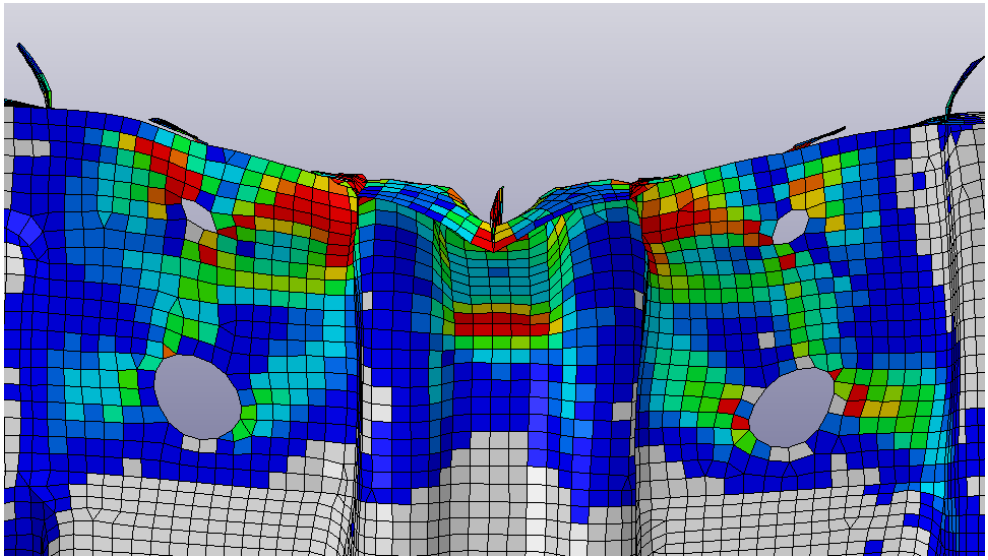

Figure 5-17: First buckling pattern – Numerical model

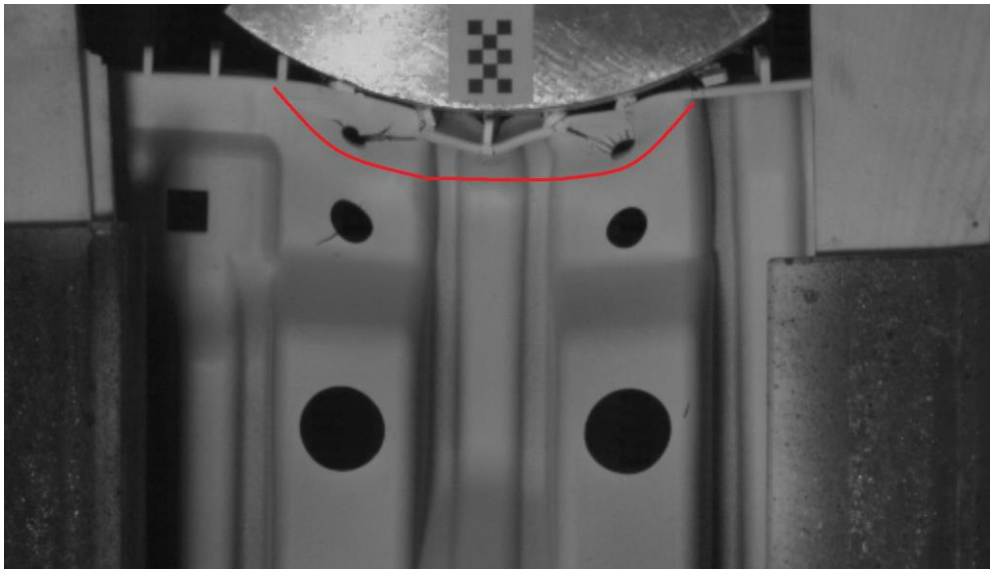

Figure 5-18: First buckling pattern - Tests

The maximum response is cause by the initiation of the second buckling pattern as seen in figure 5-20. This is captured by the shell model, it is not exactly the same buckling pattern as in the tests, but the difference is negligible such that the response is similar. The difference in buckling pattern is likely caused by inaccuracies due to discretization.

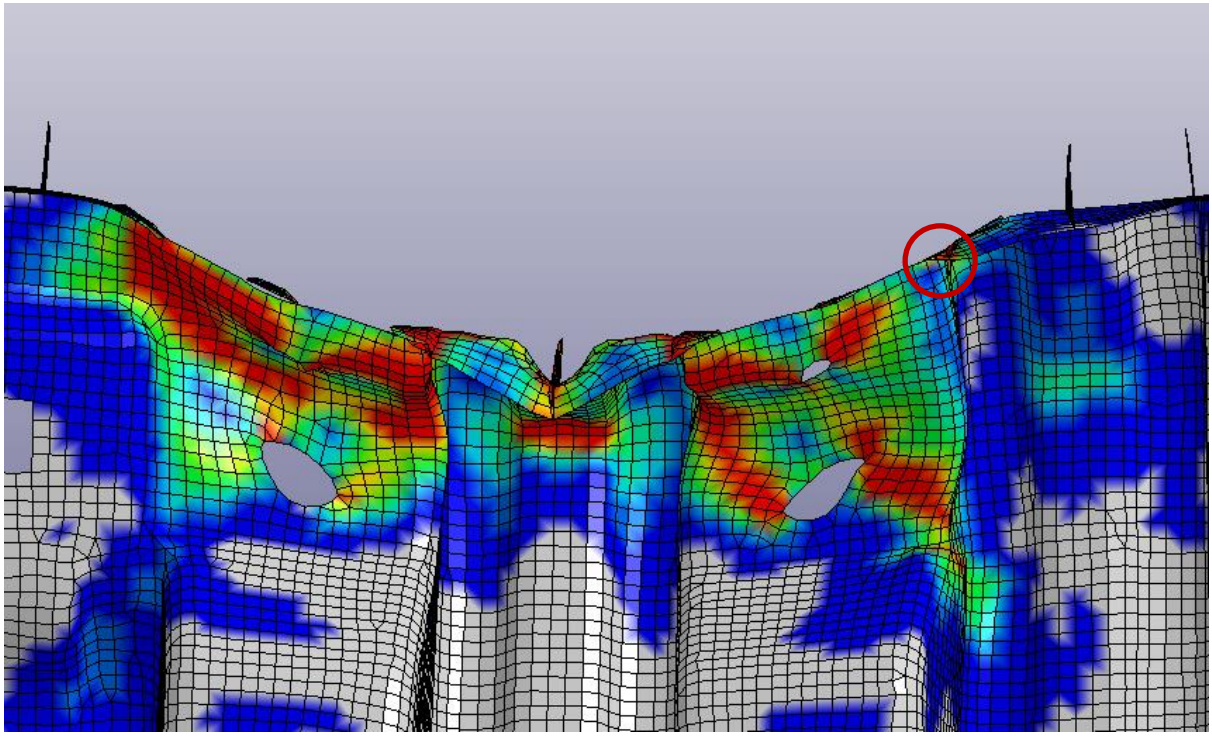

Figure 5-19: Second buckling pattern – Numerical model

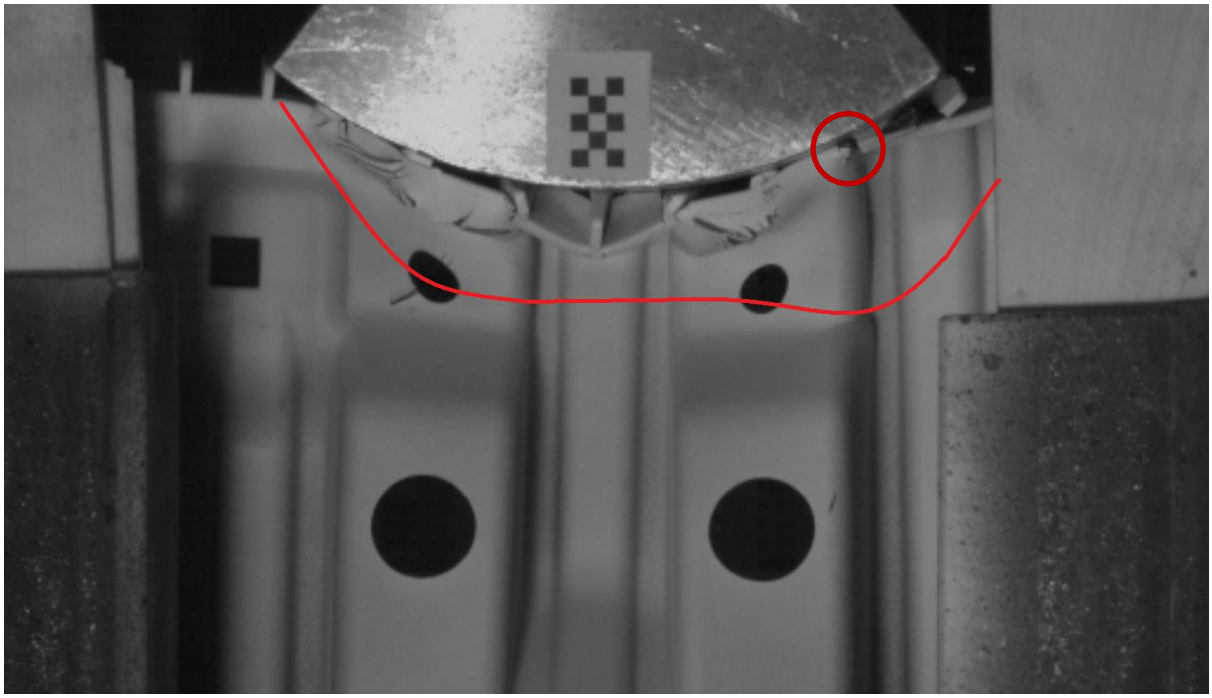

Figure 5-20: Second buckling pattern and fracture: Tests

There is a major fracture beneath rib +3 happening right after the maximum response is reached initiating a new deformation pattern which further softens the test response. This is not captured by the shell model. However in the shell model right after the second buckling pattern is initiated the stresses in the elements next to rib +3 increases rapidly as seen in figure 5-19. This indicates that with an improved discretization or a better fracture implementation would lead to a fracture in the right area at the right time.

The rebound is delayed in the shell model compared to the tests. This is both due to the problem with the initial stiffness and the missing major fracture causing a significantly different deformation pattern.

5.3.2 Solid Mesh Response

The model with solid elements in the impact area was generated specifically in investigate the first event not captured with the shell mesh as it was suspected to be the cause of the discrepancy in the initial stiffness. It was put a lot of effort into finding the source of the issue with the initial stiffness as it is one of the key parameters from an industry point of view.

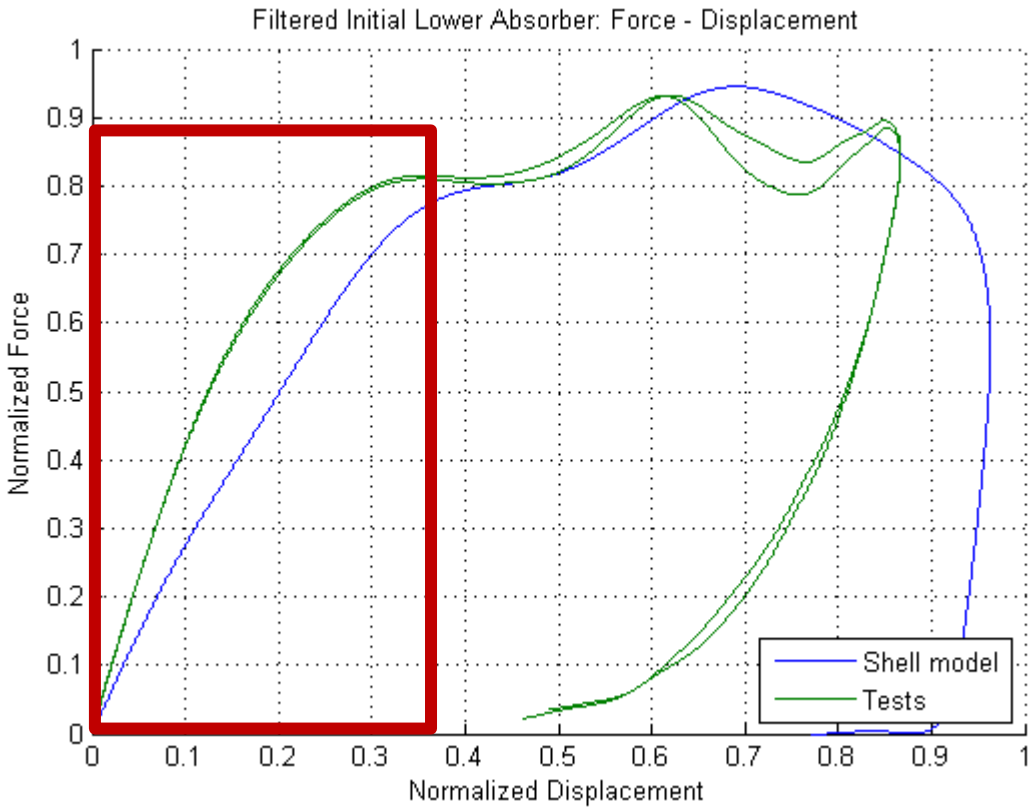

Figure 5-21: Filtered response – Problem area highlighted

Figure 5-22: Unfiltered response in problem area

The unfiltered response curves reveal that even before the oscillations starts to dominate the tests results there is a large discrepancy in response. The oscillation in the simulation result corresponds exactly with the buckling of rib +1 and rib -1 which does not occur in the tests.

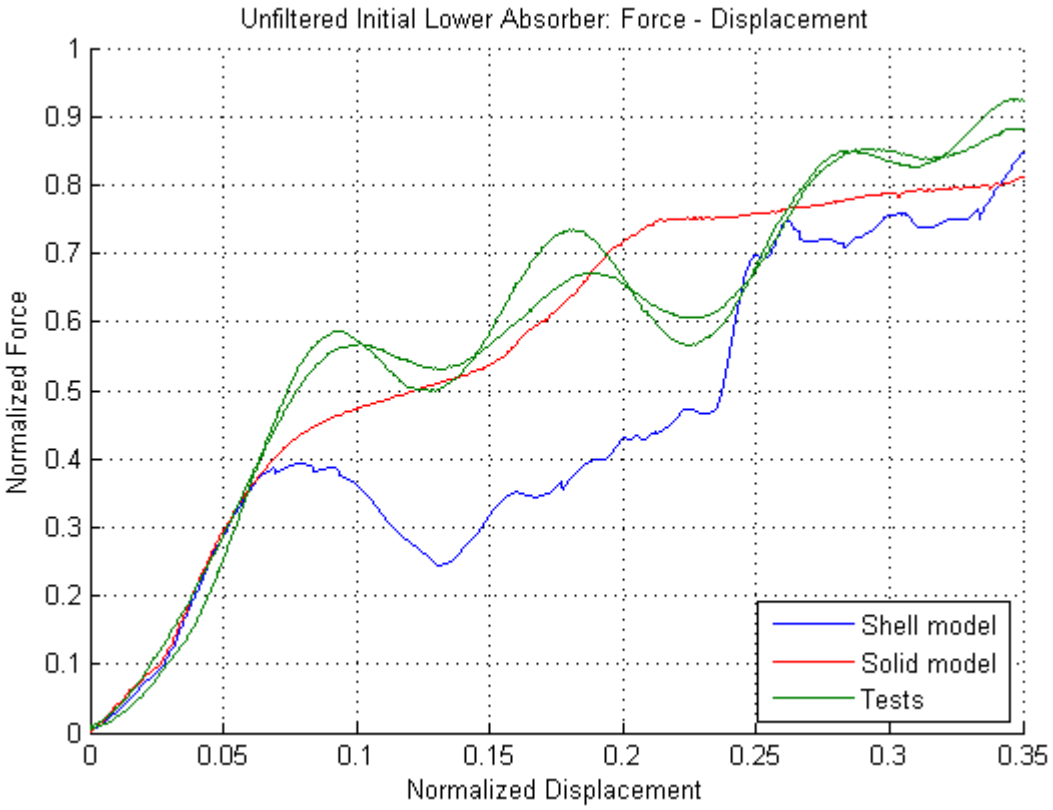

Figure 5-23: Unfiltered response in problem area with solid model

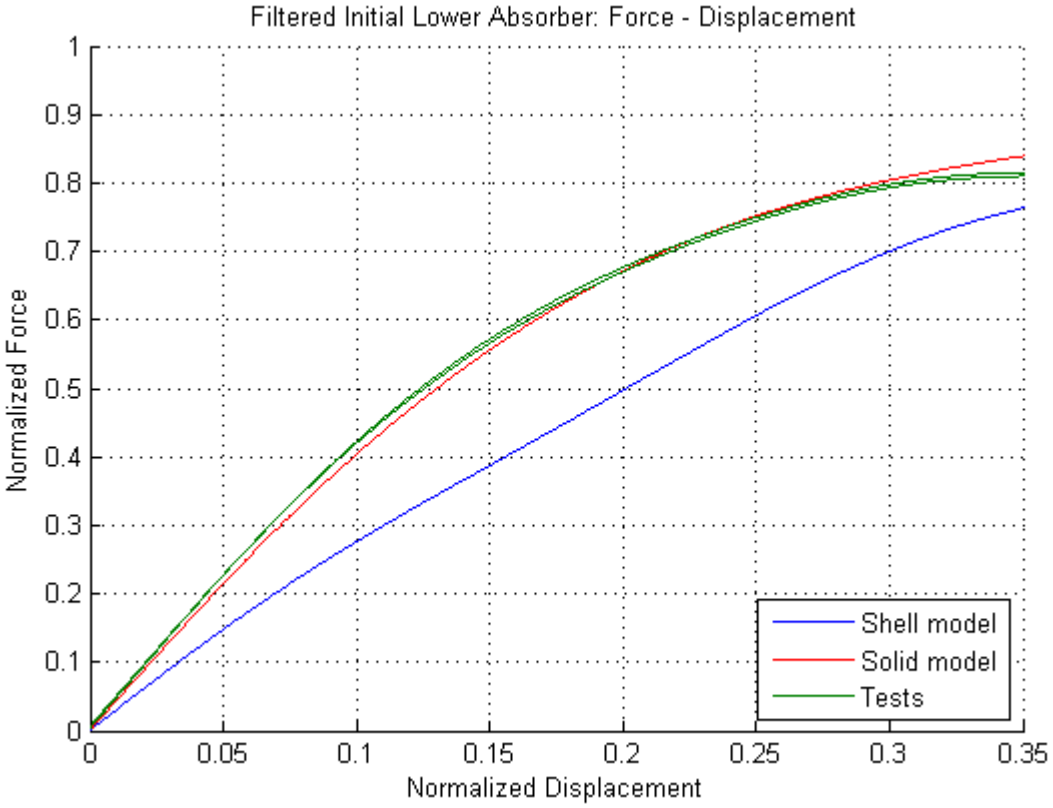

Figure 5-24: Filtered response in problem area with solid model

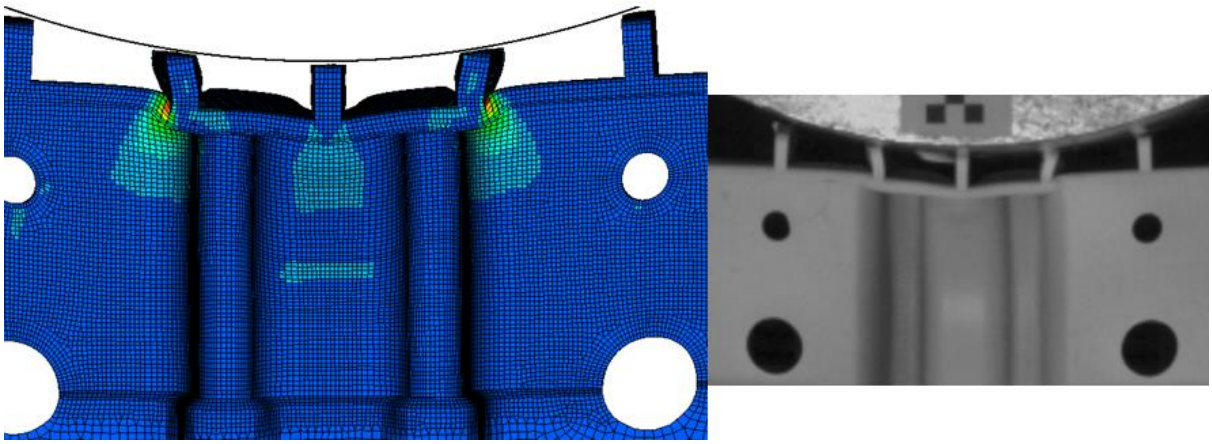

Figure 5-25: Comparison between solid model and tests

As figure 5-24 show the initial response is almost exact using solid elements in the impact area. The solid elements allow for the crushing observed in the impact area as seen in the tests thus recreating the exact deformation pattern which in turn yields a perfect response using the SPM with viscoelasticity.

The response of this model is only accurate the first 0.17-0.19 of normalized displacement as the connection between the shell mesh and solid mesh (see section 5.2.2) is overly stiff. As soon as this connection starts to deform significantly the response becomes overly stiff and it initiates large fractures which are not occurring in the tests.

5.3.3 Effect of Key Features in SPM

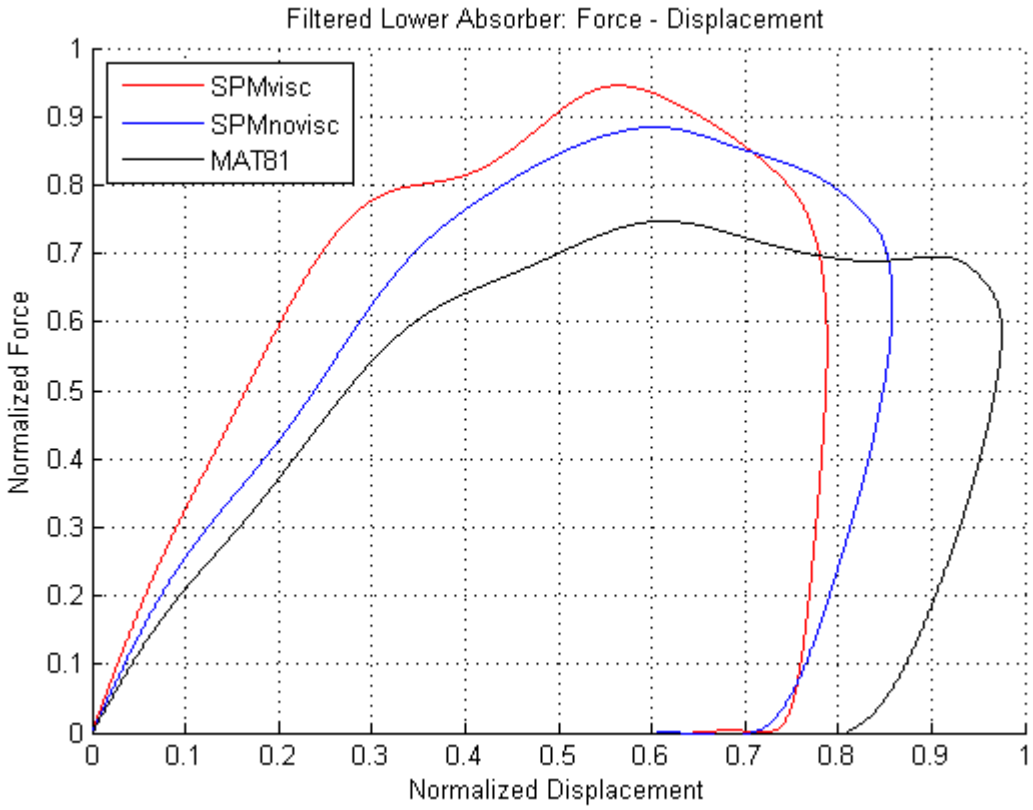

Figure 5-26: Comparison LA response – 3 different material models

The model used for the simulations in figure 5-26 are all based on the same model as before, only difference is which material model is used. The SPM with viscoelasticity is the red curve, while the blue curve is the SPM without viscoelasticity and the black curve is MAT81. Figure 5-26 display some of the effects covered in chapter 2 with the material model and how it influences the response. Going from MAT81 to the SPM without viscoelasticity there is one major difference. While the damage evolution is tabulated in MAT81 but calculated in the SPM they give roughly the same behaviour. However the yield function used for the SPM is a Raghava yield function while MAT81 is based on a von Mises yield function (see chapter 2 for details). This difference makes the SPM pressure sensitive such that it yields faster in tension than in compression, while MAT81 behaves the same in both tension and compression. And this is what causes the difference between the black and blue curve, as the lower absorber is deforming mainly in compression a pressure sensitive material gives a stiffer response.

Going from the blue curve to the red curve is purely the effect of viscoelasticity. As already observed with the boxes viscoelasticity makes the response significantly stiffer. This increase in stiffness makes the simulation response stiffer than the test results such that refining the mesh makes the simulation response converge towards the test result. It is also evident from figure 5-26 that the influence of viscoelasticity is largest initially and then drop off as plasticity becomes more and more dominant. Viscoelasticity also significantly changes the rebound as it is a dissipative effect. This means that energy is dissipated instead of stored as elastic energy, and it is the elastic energy which drives the rebound. A plasticity formulation with backstress would improve the rebound, however there might be some nonlinear elasticity driving the rebound as well.

5.4 Summary of Key Observations and Results

The results clearly show that going from a standard material model like MAT81 to the research based material model like the SPM there is a significant increase in accuracy. The physical properties of ductile polypropylene material like pressure sensitivity and viscoelasticity are crucial for the response of a component made of that material. The increase in accuracy using the SPM is because the SPM is able to properly describe these physical properties unlike a simpler material model. This comes at a computational cost, during this project it is observed an increase in CPU time by a factor of roughly 50 when going from MAT81 to the SPM with viscoelasticity.

A typical industry component like the lower absorber has a much more complex geometry than typical test specimens. As the solid impact area model displayed that with these complex geometries a much heavier and complex model is needed to capture all the events crucial to the response of the component. A shell mesh is sufficient to capture the response dominated by nonlocal deformation patterns. This highlights that when using a proper material model the limitation in accuracy is likely to be caused by poor discretization or geometry.

6 Conclusions

The goal of the thesis has been to observe the performance and behaviour of the SPM for the two validation cases, and use that to evaluate whether or not the model is ready for implementation in the industry. While there is no definite answer to whether or not the SPM is ready for the industry in this thesis there have been made several key observations regarding its performance and behaviour.

The simulation results for the box specimens with the simple geometry show that it is possible to obtain very accurate response prior to fracture using the SPM with viscoelasticity and a standard size shell mesh. Also for the lower absorber with a complex geometry it is possible to obtain high accuracy on a key parameter like peak load using only a standard size shell mesh. Comparing the results to the material model currently in use for ductile polymers at TME there is observed for all simulations a large improvement in accuracy.

The primary reason to this good accuracy is that the simulations are able to capture the key events. These events are in most cases captured by both the standard material model and the SPM, however with the SPM the response of the event is accurately described as well yielding the accurate response.

The SPM is able to better describe the behaviour of the events is because it is able to capture physical properties evident in the ductile polypropylene material studied during this project. One of these key properties is the pressure sensitivity which the SPM is able to capture with using a different yield function in the form of Raghava's yield function. Another effect that is prominent in this material is viscoelasticity which is also captured by the SPM.

This improvement comes at a cost in CPU. Going from a standard material model in MAT81 to the SPM without viscoelasticity is alone an increase in CPU time by a factor of 10-15, while going from MAT81 to the SPM with viscoelasticity is roughly a factor of 50.

The box study showed that these types of problems are very sensitive to geometry, such that both an accurate geometry and a sufficiently good discretization of the geometry is necessary to obtain good results as the material model is no longer the limiting factor. The lower absorber study showed that with the complexity of a typical industry component it will in some cases be necessary to use a solid mesh of the component to fully capture the critical events.

The current implementation of fracture in the SPM is unreliable. It is seen during both the box study and the lower absorber study that fracture is heavily mesh dependent. In addition, several of the fractures in the tests require a very fine mesh or a solid mesh to become critical points for fracture. The critical fracture parameters are calibrated from a single uniaxial tensile test, and due to its simple implementation it does not properly take into account different stress states and strain rates as observed during this project.

7 Recommendations for Further Work

This thesis has been primarily done from a pedestrian protection point of view, and even for the studies performed here fracture has been seen to be critical. Going to full crash simulation, fracture will be much more important. Such that finding solutions to make fracture more reliable should be a top priority. Setting up standard calibration procedures for a given mesh size and fracture type is one way to make certain types of fracture more reliable. Other than that it should be spent more resources on gaining a better understanding of fracture in ductile polymers enabling a better fracture implementation in the future.

The SPM is in its current state too costly in terms of CPU to be fully implemented, it should only be used on crucial components or parts of components. A general optimization of the code should be performed in addition to making separate tailored versions to reduce CPU cost.

The test components studied in this thesis have had issues with either inaccurate CAD geometry or too complex geometry such that error in geometry has not been possible to fully eliminate. To find the limitations of the SPM there should be performed validation on simple well defined geometry with complex loading conditions.

8 Bibliography

[1] SIMLab, NTNU. Theory Manual – SIMLab Polymer Model (Spring 2014). NTNU

[2] Heine Havneraas Røstum. Behaviour and Modeling of injection Molded PP. Master thesis, NTNU 2014

[3] John Fredrick Berntsen. Mechanical Behaviour of a PP Material Applied in the Automotive Industry. Project, NTNU 2014